UNIVERSITY OF CALIFORNIA
IRVINE

Early-life exercise engages neural epigenetic mechanisms to enable hippocampal memory.

DISSERTATION

submitted in partial satisfaction of the requirements
for the degree of

DOCTOR OF PHILOSPHY

in Biomedical Sciences

by

Anthony Mark Raus

Dissertation Committee:
Assistant Professor Autumn Skye Ivy, Chair
Professor Marcelo Wood
Associate Professor Qin Yang
Professor Marian L. Waterman

2022

Dedication

To my parents, my brother and my fiancé.

For their love and support.

To my friends and family

Without whom I would not be who I am today.

Table of Contents

List of Figures

Acknowledgements

To my dissertation committee members: Dr. Marcelo Wood, who has provided excellent mentorship and is always pushing me to question my assumptions, Dr. Qin Yang, who's encouragement and honest assessment of my work has pushed me to think more critically about my epigenetic data whenever possible, and Dr. Marian Waterman, who's mentorship and perspectives on regulation of gene expression have been critical to my progress in my graduate studies.

To Dr. Autumn Ivy who has been an incredible mentor and teacher during one of the hardest societal challenges in history. You have held me to a standard of excellence and encouraged my professional development even during the worst of the COVID-19 pandemic. I am honored to work with you and to call myself your first graduate.

Funding: This work was supported by the National Institute of Neurological Disorders and Stroke of the National Institutes of Health, under award number K12NS098482, the Conte Center @ UCI Seed Grant, UC Irvine Institute for Clinical and Translational Sciences Pilot Award, and the Robert Wood Johnson Foundation Amos Medical Faculty Development Program (awarded to Autumn S. Ivy), and the Lorna Carlin Professional Development Award (awarded to Anthony M. Raus). We thank the UC Irvine School of Medicine, Departments of Pediatrics for support. We would also like to thank Dr. Marcelo Wood for scientific discussions and critical input on the project, and Drs. Melanie Oakes and Jenny Wu of the UC Irvine Genomics High Throughput Sequencing Facility for next generation sequencing experiments support.

Publications: I'd like to thank Wiley Periodicals LLC, and Bio-Protocol LLC for allowing me, through their policies of publication and printing, to include material in my dissertation.

Author Contributions: For Chapters 1, 2, 3 and 4, Anthony M. Raus, Tyson D. Fuller, Nellie E. Nelson and Autumn S. Ivy designed the studies and interpreted the results. Anthony M. Raus, Tyson D. Fuller, and Autumn S. Ivy performed INTACT and TRAP studies. Anthony M. Raus built libraries for RNA- and TRAP-sequencing. Nellie E. Nelson performed CUT&RUN-seq experiments and built libraries for sequencing. Nellie E. Nelson and Autumn S. Ivy performed flow cytometry experiments. Anthony M. Raus and Autumn S. Ivy performed immunostainings and immunofluorescent imaging. David A. Valientes and Anita Bayat built exercise cages and monitored running behavior. Anthony M. Raus performed all bioinformatic analysis of sequencing data. Anthony M. Raus and Nellie E. Nelson analyzed sequencing data, performed GO, GSEA and IPA analyses, and all other downstream analyses except where noted. Autumn S. Ivy performed behavioral studies. Tyson D. Fuller performed Spearman's correlations and gene length by fold change analysis. Tyson D. Fuller performed qPCR. Nellie E. Nelson designed the figures. Anthony M. Raus, Tyson D. Fuller, and Autumn S. Ivy wrote and edited the material from or based on the manuscript "Early life exercise primes the neural epigenome to facilitate gene expression and hippocampal memory consolidation"[1], with Nellie E. Nelson providing edits to that material. Anthony M. Raus adapted this material for this dissertation.

For Chapter 2, the detailed methods and understanding the results section was written by Anthony M. Raus with optimization from Nellie E. Nelson and edits from Nellie E. Nelson and Autumn S. Ivy. Anthony M. Raus adapted this material for this dissertation.

For Chapter 5, the method was designed by David A. Valientes. The software was designed, developed, and written by Anthony M. Raus. The data was collected and analyzed by David A. Valientes and Anthony M. Raus. The written material in that section was based on or originally written by material written by David A. Valientes and Autumn S. Ivy with contributions and edits from Anthony M. Raus. Anthony M. Raus adapted this material for this dissertation.

For Chapter 6, some segments are based on or incorporated from "Early life exercise primes the neural epigenome to facilitate gene expression and hippocampal memory consolidation"[1] (see the first paragraph in this section for author information about those segments). Anthony M. Raus adapted this material for this dissertation. The rest of the chapter was written solely by Anthony M. Raus with edits and revisions by Autumn S. Ivy.

To Dr. Devon Lawson, who's participation on my advancement committee provided useful insights into ways of thinking about sequencing data.

To Dr. Ilhem Messaoudi-Powers and to Dr. Suhas Sureshchandra who's mentorship during my rotations allowed me to acquire the bioinformatics skills that have been critical to the preparation of this dissertation.

To my colleagues in the Ivy Laboratory: Dr. Tyson Fuller, Nellie Nelson, David Valientes, Sijia Yang, Tim Yu, Anita Bayat, Sonia Parievsky, Ijeoma Chikezie, Brian Gomringer, Muhammad Shahbaz, Parmida Abdoli, Fred Sohn, Alison Mogul, Jazmine Moore, Sandra Sandria, Emmanuella Bassey, Brooke Waechtler, Irene Baghdasaryan, Suraay Verma, Aisha Malik, Raven James, August Owusu Agyemang, and Abraham Albedrop. This journey would not be the same without you and I could not have completed this work without your contributions.

To Nellie Nelson, who has been an amazing colleague. Your contributions, support and guidance have been essential to my graduate work and career. It has been a pleasure working with you.

To my brother Luke Raus who helped me master my informatics skills and who has always been there for me when I have needed it most. I would not be the person I am today without you. It is an honor to have you as a brother.

To my Parents Anita and Mark Raus who's generosity and sacrifice has given me the opportunity to pursue my dreams. You have been amazing role models and parents. I am eternally grateful and honored to be your son.

Finally, Kelly Hatfield. You are the love of my life and have held me up during some of the hardest times of my graduate studies. Your support and love mean the world to me. From the bottom of my heart: Thank you. I cannot wait to marry you.

Thank you.

Vita

Education

University of California, Irvine *Irvine, CA*

Ph.D. Biomedical Sciences 2022 GPA: 3.983
Research – Transcriptomics and Epigenomics of Memory and Development
Advanced to Candidacy – September 2021

M.S. Biomedical Sciences 2021 GPA: 3.983
Department – Physiology and Biophysics

B.S. Biology 2017 GPA: 3.718

Research Experience

University of California, Irvine – Graduate Student Researcher
Ph.D. Candidate as of September 2021

Professor Autumn Ivy – Bioinformatics and Data Science of Memory May 2019-Current

As the senior graduate student in the lab, I lead laboratory meetings. I also lead a large project coordinating 3 other researchers which is leading to the publication: "Early life exercise primes the neural epigenome to facilitate gene expression and hippocampal memory consolidation." I am investigating the effects of early-life exercise on the epigenetic regulation of genes implicated in hippocampus-dependent learning and memory. Using biological and transgenic mouse models, I am performing Chromatin Immunoprecipitation (ChIP), RT-qPCR, CUT&RUN-seq and RNA-seq experiments. I computationally and bioinformatically analyze the data for large datasets in the lab to address my and other hypotheses. I also developed software with a graphical user interface for: "An improved method for individual tracking of voluntary wheel running in pair-housed juvenile mice."

Professor Klemens Hertel – Molecular Biology of RNA Splicing Apr 2018-Jun 2018

I analyzed alternative mRNA splice patterns of colon cancer cells to identify potential treatment targets.

Professor Yongsheng Shi – Biochemistry of RNA Processing Dec 2017-Mar 2018

I analyzed the connection between pumilio proteins, alternative polyadenylation, and neuron development by differentiating NTera2 cells into neurons. The knowledge could aid in the differentiation of neurons in the future.

Professor Ilhem Messaoudi – Bioinformatics and Immunology Sep 2017-Dec 2017

I investigated the effect of alcohol on the immune system of *Rhesus macaques* using RNA-seq and Luminex. I also investigated the effect of HIV on micro-RNA levels in the human immune system. My work led to the publication: "Dose-dependent effects of chronic alcohol drinking on peripheral immune responses".

Professor Young Jik Kwon – Nanoparticle Gene and Drug Delivery Systems Jan 2015-Mar 2017

I worked on developing drug and gene delivery systems using acid degradable polymers, monomers, and extracellular vesicles.

Publications

ORCID: 0000-0003-1688-2135

Early life exercise primes the neural epigenome to facilitate gene expression and hippocampal memory consolidation. (In review at *Communications Biology*) **Anthony M. Raus***, Tyson Fuller*, Nellie E. Nelson*, Samuel David Amio Valientes, Anita Bayat, Autumn S. Ivy. (*co-first author). Preprint: https://doi.org/10.1101/2021.12.23.473936

SIT with Emx1-NuTRAP mice to isolate juvenile hippocampal excitatory neural mRNA and nuclei from the same sample. *Current Protocols in Neuroscience* (Accepted) **Anthony M. Raus**, Nellie E. Nelson, Tyson Fuller, Autumn S. Ivy.

An improved method for individual tracking of voluntary wheel running in pair-housed juvenile mice. *Bio-Protocol* Volume 11 Issue 13, (2021). S David Valientes, **Anthony M. Raus,** and Autumn S. Ivy. https://doi.org/10.21769/BioProtoc.4071

Dose-dependent effects of chronic alcohol drinking on peripheral immune responses. *Scientific Reports. 9*, (2019). Suhas Sureshchandra, **Anthony Raus**, Allen Jankeel, Brian Jin Kee Ligh, Nicole A. R. Walter, Natali Newman, Kathleen A. Grant, Ilhem Messaoudi. https://www.nature.com/articles/s41598-019-44302-3/

Teaching Experience

2022 – Mentor – UC Irvine Center for the Neurobiology of Learning and Memory
Summer Institute in Neuroscience

I am mentoring an undergraduate student from Louisiana. I am teaching the basics of a career in research in a laboratory setting. The program is dedicated to exposing underserved and minority communities to a career in neuroscience research.

2021 – Mentor – UC Irvine Center for the Neurobiology of Learning and Memory

Irvine Interdisciplinary Internship in Neuroscience Program

I mentored a student as they researched a part of my work on the effect of early-life exercise on gene expression. I taught bioinformatic analysis of sequencing data and guided the student through the application of those techniques on sequencing data which our lab will present in future papers. I also helped guide her in presenting her work at an academic conference hosted by the UC Irvine Center for the Neurobiology of Learning and Memory.

2021 – Graduate Teaching Assistant - Remote Teaching During Covid

Biology M116L – Molecular Biology Laboratory

I taught and organized 2 laboratory groups of 6-7 students each. I taught computational analysis of molecular biology data from publicly available databases of sequencing experiments. I was responsible for organizing group projects, directing experimental design, and troubleshooting errors. I graded and reviewed assignments and provided constructive feedback for improvement.

Biology 99 – Molecular Biology

I lead discussions on molecular biology related to the regulation of gene expression and the computational analysis of related data.

2020-2021 – Graduate Student Mentor – UCI Cellular and Molecular Biosciences

I mentored a graduate student new to the UCI Cellular and Molecular Biosciences Program.

2013 – Jesuit High School Sacramento

High School Chemistry.

I taught and mentored students after school helping with their coursework and questions. The tutoring was organized by Victoria Cerati.

Presentations

International-Advisor Invited to Speak - Anthony M. Raus, Tyson Fuller, Nellie Nelson, Samuel David Valientes, Anita Bayat, Autumn S. Ivy, An in vivo, neuron-specific approach for pairing translational and epigenetic signatures of early-life exercise. Glasgow Scotland, International Behavioral Neuroscience Society June 2022, Poster

Invited to speak - Anthony M. Raus, Tyson Fuller, Nellie Nelson, Samuel David Valientes, Anita Bayat, Autumn S. Ivy, A Neuron-Specific Approach Reveals Transcriptomic and Epigenomic Signatures of Early-Life Exercise, University of California, Progress in Neurobiology Seminar January 2022, Slideshow

Autumn S. Ivy, Nellie Nelson, Anthony M. Raus, Tyson Fuller, Samuel David Valientes, Anita Bayat, Parmida Abdoli, Brian Gomringer, Neural Epigenetic Signatures of Early-Life Adversity and Exercise Underlying Hippocampal Memory in Adulthood, American College of Neuropsychopharmacology Meeting, December 2021, Slideshow and Poster

International - Anthony M. Raus, Sijia Yang, Tyson Fuller, Nellie Nelson, Samuel David Valientes, Emmanuella Bassey, Autumn S. Ivy, Histone post-translational modifications underlying the persistent effects of early-life exercise on hippocampal memory, Society for Neuroscience Annual Meeting, November 2021, Slideshow and Poster

Anthony M. Raus, Tyson Fuller, Nellie Nelson, Samuel David Valientes, Anita Bayat, Autumn S. Ivy, The role of epigenetic modifications in enabled hippocampal memory after early-life exercise, University of California Irvine School of Medicine, Graduate Day October 2021, Poster

International - Autumn S. Ivy, Anthony M. Raus, Tyson Fuller, Nellie Nelson, Samuel David Valientes, Anita Bayat, Autumn S. Ivy, Paired genomic and epigenetic sequencing reveals neuronal signatures of early-life exercise, Society for Neuroscience Annual Meeting, November 2021, Slideshow and Poster

Anthony M. Raus, Tyson Fuller, Nellie Nelson, Samuel David Valientes, Sijia Yang, Autumn S. Ivy, Stable Epigenetic Signatures of Early-Life Exercise and Memory Function May Persist Into Adulthood, University of California, Irvine Conte Center Symposium March 2021, Slideshow

Anthony M. Raus, "Exercise in Early Life Enables Learning and Memory Into Adolescence via Stable Epigenetic Modification" Research In Progress Talk, Department of Physiology and Biophysics, February 2021, Slideshow

Anthony M. Raus, Sijia Yang, Samuel Valientes, Autumn Ivy, Early-life Exercise Increases the Occupancy of Histone 4 Lysine 8 Acetylation at Memory Associated Genes, CHOC Research, Go Beyond – Advancing Pediatric Research During the COVID-19 Pandemic, November 2020, Poster

Anthony M. Raus, Sijia Yang, Samuel Valientes, Autumn Ivy, Early-life Exercise Increases the Occupancy of Histone 4 Lysine 8 Acetylation at Memory Associated Genes, University of California, Irvine School of Medicine, Graduate Research Day, October 2020, Slideshow

Anthony M. Raus, Sijia Yang, Samuel Valientes, Autumn Ivy, Early-life Exercise Increases the Occupancy of Histone 4 Lysine 8 Acetylation at Memory Associated Genes, University of California, Irvine Conte Center Symposium February 2020, Poster

Anthony M. Raus, Sijia Yang, Samuel Valientes, Autumn Ivy, Early-life Exercise Increases the Occupancy of Histone 4 Lysine 8 Acetylation at Memory Associated Genes, University of California, Irvine Research and Education in Memory Impairments and Neurological Disorders Symposium February 2020, Poster

Academic Awards

University of California, Irvine

Merck Award – 2015-school award given annually to an undergraduate who excels in organic chemistry.

Fellowships And Grants Awarded

Lorna Carlin Excellence in Research Award. $10,000 total support for promising translational research
.

Robert and Sylvia Mapel Research Innovation Award. Project title: "Early-life Exercise Modulates the Neuronal Chromatin Landscape to Enable Memory Performance." (To graduate student / PI pair, Anthony M. Raus and Autumn S. Ivy) 2021- 2022; $20,000

University of California, Irvine Summer Undergraduate Research Program Fellowship **-** $1200

Scholarships Awarded

California Grocers Association Scholarship (2014- $1000) – Awarded for academic excellence

Joyce Raley Teel Scholarship (2015-$2500) – Awarded for academic excellence

Professional Affiliations

Society For Neuroscience – Member since January 2020

UCI Graduate Professional Success for Ph.D. Students and Postdocs in Science, Technology, Engineering, and Mathematics – Member since January 2020

Extra Circular Activities and Volunteer Work

Graduate Professional Success for Ph.D. Students and Postdocs in Science, Technology, Mathematics, and Engineering – Bioinformatics and Data Science Networking Organizer since 2022– An organization for professional development of Ph.D. students. I organize, moderate, and host bioinformatics networking events for the organization.

ReachOut to TeachOut – Member 2021-2022 – An outreach group dedicated to the support of science in high schools. Groups of graduate students and post-doctoral scholars mentor high school students for their science fair projects.

Scientific Public Speaking Course – Student Participant Fall 2020 – A course on public speaking offered through UCI Graduate Professional Success for PhD students and Postdocs in Science, Technology, Engineering, and Mathematics. I improved my public speaking skills in scientific communication with an emphasis on audiences outside my field as well as the general public.

Ballroom and Swing Dancing – Active in various clubs, lessons, and venues since Fall 2016 – One of my favorite ways of socializing, expressing myself, and exercising all at once. I have a passion for dance.

Abstract of the Dissertation

Early-life exercise engages neural epigenetic mechanisms to enable hippocampal memory and neural function.

by

Anthony Mark Raus

Doctor of Philosophy in Biomedical Sciences

University of California, Irvine School of Medicine, 2022

Assistant Professor Autumn Skye Ivy, Chair

Aerobic exercise is well know to promote neuroplasticity and hippocampal memory. More recent studies suggest that early-life exercise (EX) can lead to lasting improvements in hippocampal function; however, the molecular mechanisms of this phenomenon are not understood. Histone post translational modifications (HPTMs) are strong candidates for bridging the gap between environmental experiences and altered gene expression. Epigenetic mechanisms such as HPTMs can be persistent or transient and can have lasting influences on neuronal function. This dissertation investigates epigenetic mechanisms a possible explanation for the effect of EX on memory and develops tools for that investigation. In chapter 2 we develop a mouse model and a novel method for coupling epigenetic information and translating mRNA in hippocampal neurons. A Emx1-Cre[2] mouse was crossed with a NuTRAP[3] mouse to produce a transgenic line we call Emx1-NuTRAP. This mouse expresses a cassette in hippocampal neurons which labels both the nucleus and ribosomes in a way that allowed us to develop a novel method we call “SIT” (simultaneous isolation of nuclei in targeted cell types (INTACT) and translating

ribosomal purification (TRAP)) to isolate both translating mRNA and intact nuclei from the same set of cells. We applied our lab's EX model to the Emx1-NuTRAP mouse, followed by the SIT method from hippocampal tissue to identify an epigenetic and translational signature of EX as it relates to improved memory (Chapter 3). These data revealed activation of neuroplasticity genes engaged by EX, and implicated critical upstream regulators. Chapter 4 demonstrates that EX-induced epigenetic changes correlate with altered gene expression during consolidation that may underly EX-induced enabled memory. We discovered a distinct set of genes that had new histone PTMs after EX that have altered expression during memory consolidation. This suggests that neuronal chromatin in hippocampus may be "primed" by EX-induced new histone PTMs Finally, Chapter 5 describes a novel method for tracking the individual running of group housed juvenile mice. We constructed an RFID tracking system and correlate it with running using a software we developed in-house. This technique could be used to identify a threshold dose of EX for enabling of memory. Taken together, we lay the foundations for the study of epigenetics as a key underlying mechanism of EX enabled memory and identify candidate mechanisms with novel techniques.

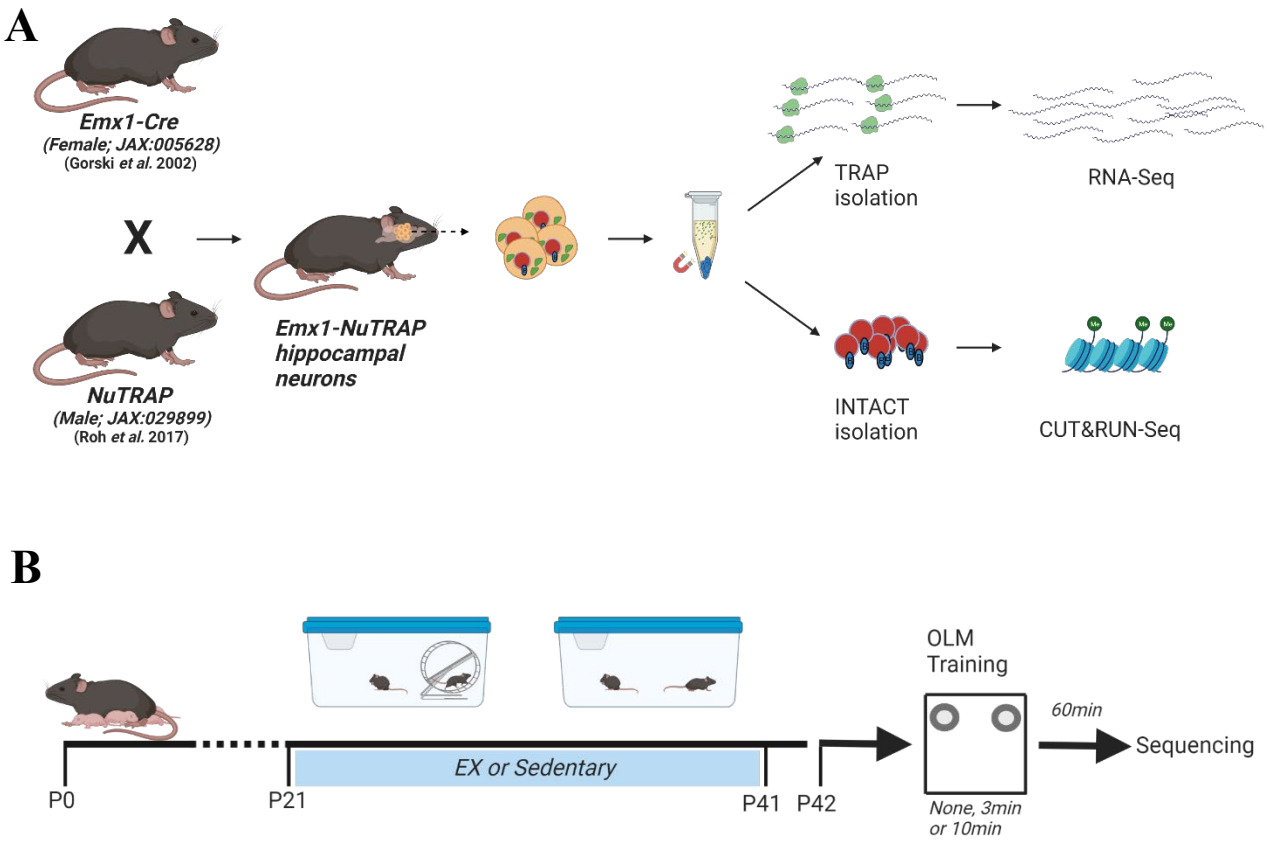

Figure 1: Experimental overview: (A) Diagram of the Emx1-NuTRAP mouse and the SIT protocol: Female Emx1-Cre[2] mice were crossed with male NuTRAP[3] mice to produce Emx1-NuTRAP mice. Their hippocampi were dissected and processed using SIT[1] which isolated both neuronal nuclei (using streptavidin coated beads) and mRNA bound to eGFP fused ribosomes (using TRAP) from the same lysate. (B) EX and OLM: Mice were allowed voluntary access to a running wheel P21-41 and sacrificed on P42 either 60 minutes after OLM training or without OLM training. Then their hippocampi were extracted and processed for sequencing.

Chapter 1: Introduction

Significance: The need for research into positive, potentially long term, early environmental influences on memory.

Early-life disorders of learning and memory are heterogeneous and are often comorbid with childhood neurological dysfunction[4-7]. Additionally, they have profound negative consequences for individual social, personal, and emotional development as well as integration into adult society. With regard to neurological disorders of childhood, there is significant cognitive comorbidity that is underappreciated when addressing neurological conditions. Further, there are even less studies attempting to address this problem in accessible ways. These cognitive problems often have significant emotional impacts. The economic cost is also substantial Learning disabilities in Canada were projected in 2002 to cost the country 700 billion CAD for all people with a learning disability at the time from birth to death[8]. My research addresses the cognitive impacts of early-life neurological disorders by understanding mechanistic targets and may ultimately improve cognition and lower emotional burden. Understanding how memory can be improved could greatly ease this burden. Positive environmental experiences like exercise, problem solving, and novelty are known to be able to improve memory in adult humans[9]. Enriched environment and exercise have improved memory in adult rodents[10,11], suggesting that the impacts of exercise on improving cognition are found across species. Recently exercise has been shown to improve memory in juvenile mice for a longer duration than in adults[12]. Understanding the mechanisms of memory improvement during early-life could lead to identification of therapeutic targets and recommendations for therapeutic intervention. This

could offset the negative environmental influences and aid the treatment of memory and other cognitive disorders in childhood.

Early environmental experiences have persistent impact on cognitive functions. Negative environmental influences, such as early-life stress, have been extensively studied[13-17]. These studies show environmental influences can have a long-term negative impact on memory. However, studies of early-life experiences with positive consequences for memory have been more sparse[12,18,19]. Exercise represents a useful positive influence for study. It is non-pharmacological, generally easily accessible, and can be used to reveal potential mechanisms for therapeutic strategies.

Epigenetics: A molecular link between the environment and memory function.

Epigenetic mechanisms (such as DNA methylation and histone modifications) have been found to play a significant role in long-term memory[20,21]. These mechanisms influence memory related synaptic and transcriptional changes[22-25]. Exercise is a powerful regulator of hippocampal memory and synaptic plasticity via epigenetic mechanisms; however, most of the work has been carried out in adult mice[26-28]. Although a number of studies in adult mice show that exercise improves hippocampal memory[29] the benefits of adult exercise on hippocampal memory are short lived[11]. On the other hand, pups of exercised pregnant mice show persistent increases in histone 4 acetylation and improved memory[30]. Recent research in the Ivy Lab has demonstrated that aerobic early exercise (EX) enables long-term object location memory[12]. Specifically, one week of exercise during postnatal day (P) 21-27 can persist for two weeks after the cessation of exercise, which is distinct from the 2 weeks needed in adult mice to achieve the same

result[11,12,31]. With my experiments, I aimed to identify target mechanisms promoting the facilitation of learning and memory as a result of EX.

Postnatal hippocampal development: A sensitive period to environmental influences.

The difference in the response to environmental stimuli may result from the hippocampus undergoing an extended period of postnatal development. For example, rodent hippocampal neurons may be more sensitive to the environmental influence of stress in part because of the increased corticotropin-releasing hormone (CRH) receptors during the first two postnatal weeks[32]. Another contributing mechanism could be that significant synaptic maturation is occurring during the fourth postnatal week in rodents[32]. This is supported further by hippocampal neuronal gene expression examined during this period of development, which demonstrates increased expression of plasticity related genes[33]. Synaptic maturation and synaptic plasticity are directly connected. Synapse maturation involves excitatory synapses being strengthened by an increased ratio of AMPA to NMDA receptors[34]. Other synaptic protein compositions are also changed during synaptic maturation[34]. Additionally, the peak of synapse addition occurs at p14-28 in rodents and during the second year of life in humans[34]. Therefore, most of the aims of my research should be most correlative with 2-5 years of postnatal human development though some synaptogenesis can continue into adolescence in humans[33,35]. Enriched environment in these developmental periods has previously increased cortical thickness, synaptic density and improved performance on memory tasks[35]. The molecular mechanisms that drive these developmental periods and increase their sensitivity to environmental stimuli are still being elucidated. However, since BDNF can regulate synaptic maturation[35] and exercise can increase levels of BDNF[11], exercise may have a strong influence on this developmental time period.

Some evidence points to epigenetic mechanisms being more readily manipulated and having greater stability when acquired during development. For example, Rett syndrome, a human disease characterized by intellectual disability, autism, epilepsy, and impaired motor functions, presents between 6-18 months of life[36,37]. A mutation in Methyl-CpG binding protein 2 (MECP2) alters the epigenetic landscape and causes Rett Syndrome[21]. MECP2, a critical epigenetic regulator, is necessary for normal brain development during a specific postnatal window when non-CpG methylation is reaching mature levels[37]. This evidence indicates that the developing brain is more sensitive to epigenetic change and the consequences of unusual epigenetic change during this period of development. Additionally, maternal exercise in embryonic development increases offspring histone acetylation and improves memory function into adulthood[30] providing evidence that these marks are stable and have lasting functional impacts. Changes in the epigenetic landscape could act as molecular memory of early environmental exposures, which can in turn inform subsequent brain function. Histone post translational modification (HPTM) changes are an important candidate epigenetic mechanism linking exercise to its effect on memory. H4K8ac is increased at memory associated genes by exercise in adult mice, and is correlated with enabled memory performance[20]. Further, using a histone deacetylase (HDAC) inhibitor during consolidation enables memory in the absence of exercise[20]. Taken together, these results provide support for a role of epigenetic modifications for facilitated memory performance a result of aerobic EX.

<u>Experimental overview: Develop and implement tools to identify epigenetic and transcriptional signatures of early life exercise as they impact memory.</u>

My dissertation accomplishes 3 major goals: identify an epigenetic and translational signature of EX, identify how this signature alters memory associated gene expression during memory consolidation to implicate epigenetic mechanisms, and develop the tools to accomplish these goals. In order to better understand the link between epigenetic and transcriptional changes made by EX, I helped develop the Emx1-Nutrap mouse and a corresponding protocol: simultaneous INTACT[38] (isolation of nuclei in targeted cell types) and TRAP[39] (translating ribosome affinity purification) (together: SIT).. This model and method allow for the simultaneous isolation of nuclei and translating mRNA specifically from excitatory neurons in the hippocampus (using a single homogenate), allowing for better correlation between epigenetic and translational mechanisms. I used these tools to identify a correlated epigenetic and translational signature of EX by allowing these mice access to running wheels from P21-41 and sacrificing them on P42 using SIT to isolate their chromatin and mRNA for CUT&RUN-seq[40] and RNA-seq. I compared this data with hippocampal RNA-seq data from mice exercised during the same window but exposed to a learning event, OLM (object location memory) training, on P42. I found that the epigenetic signature induced by EX appears to "prime" gene expression that correlates with EX facilitated enabled memory. So that future experiments may identify a dose of EX necessary for these phenomena, I also helped develop a method to individually track group housed juvenile mice using radio frequency identification (RFID) tracking and running wheel metrics. I developed a software to correlate these data sets allowing an experimenter to determine precisely how much voluntary aerobic exercise each animal performs, without the stress associated with social isolation or invasive implantation of tracking devices. This research paves the way for the field to investigate neural-epigenetic mechanisms of EX's influence on

memory in a neuron-specific and dose-specific manner. We also identify likely candidate regulators for these effects.

Chapter 2: Developing a novel transgenic mouse and protocol for understanding early exercises' influence on regulating neuronal gene expression.

Introduction:

The need for simultaneous analysis of both the transcriptome and epigenome

Epigenetic mechanisms are likely key to the study of environmental adaptation of neurons to improve memory[22,41-43]. The field of neuro-epigenetics has a significant gap in neuron-specific transcriptomic and epigenomic analysis of the effects of exercise, especially in early life, on the hippocampus. Some transcriptomic analysis of whole hippocampal tissue has been done to some success after exercise in adult mice[44]. New translating ribosome affinity purification (TRAP) approaches have allowed some to study mouse interneuron-specific transcriptomes[45-47]. I helped develop an experimental approach and mouse model to simultaneously analyze the neural-specific transcriptomic and epigenetic profiles specifically from hippocampal excitatory neurons[1]. I used this model and technique to contribute needed transcriptomic and epigenomic profiling of the effects of EX to the field.

Ivy *et al.* 2020 previously identified changes in synaptic function that correlated with enabled memory after EX[12]. Enhanced LTP (long term potentiation) was demonstrated after juv-adol EX(P21-41). This data suggests the enabling of memory due to EX may be a result of enhanced synaptic plasticity. Since gene expression may alter the ability of the cell to engage synaptic mechanisms, the regulation of neuron specific gene expression may be critical to understanding the mechanisms of enabled memory after EX. However, cell specific techniques

that currently exist to study both differential gene expression and underlying histone PTMs have certain drawbacks that may complicate the study of EX enabled memory. FACS can isolate neurons specifically, but it requires that cells be kept alive for long periods of time and undergo mechanical processing, factors which may compromise gene expression [48]. Much of the gene expression after learning is time specific with different genes being expressed rapidly at specific intervals during consolidation[49]. Few of these timepoints could be reliably captured with this method. Single cell sequencing presents an attractive alternative; however, many cells other than neurons would be sequenced, limiting the number of neurons that can be studied per sequencing experiment. This limitation can impair the detection of lowly expressed genes in the population of neurons that is detected[50]. In addition, it can be cost prohibitive when considering the large numbers of animals required for the study of multiple exercise timepoints. Preparing samples for the single cell sequencing also requires the cells remain intact for longer periods of time, resulting in changes in gene expression and difficulty capturing timepoint specific gene expression.

With the generation of the NuTRAP mouse[3], it became possible to isolate translating mRNA and nuclei from select cells labeling with a promoter specific Cre driver. However, an animal expressing this cassette specifically in hippocampal excitatory neurons had yet to be generated. Our goal was to interrogate the interaction between epigenetic regulation and translation in memory processes[1]; so we developed a mouse and a method to investigate these connected regulatory networks simultaneously. By crossing an Emx1-Cre mouse[2] with the NuTRAP mouse[3], we generated a transgenic mouse line that labels excitatory neurons in the hippocampus with both nuclear (mCherry and biotin) and ribosomal (GFP) tags. We crossed male NuTRAP reporter mice[3] with female Emx1-Cre[2,51] mouse lines to generate Emx1-Cre;

NuTRAP transgenic progeny for this study (Figure 1). Emx1-expressing neurons are predominately excitatory[2] and are necessary for hippocampal neurogenesis and motor skill learning[52]. In the presence of a *loxP* site-flanked sequence, Emx1-Cre facilitates recombination in approximately 88% of neurons in the neocortex and hippocampus, and in less than 2% of GABAergic inhibitory interneurons in these regions[2]. Emx1-Cre also targets neural progenitor cells and can be expressed in mature astrocytes in striatum[53]. Of note, we exclusively used Emx1-Cre female mice in our breeding schemes given that the Cre-recombinase has been reported to be expressed in a subset of male germline cells[54].

We then used this transgenic animal model to address, with a novel method, the problems of previous cell-type specific methods of investigating correlated epigenetic and transcriptional changes. Our method performs both isolation of nuclei tagged in specific cell types (INTACT) and translating ribosome affinity purification (TRAP) on excitatory hippocampal neurons from the same set of cells. We call this method "SIT" for Simultaneous INTACT and TRAP. Ultimately, the method isolates translating mRNA and nuclei from the same set of cells labeled for cell type specificity by the NuTRAP mouse model. Previous methods had been limited by performing TRAP and INTACT on separate tissue samples[3]. Brain regions are highly heterogeneous and small differences in cell type within the region could have large differences in function, even among neurons. Our method allows the translatome and epigenome to be studied in concert, from the same set of cells, to allow for better correlation of translating mRNA with epigenetic regulation. The isolated TRAP mRNA and nuclei can be used in downstream molecular analysis applications such as RNA-seq, CHIP-seq, CUT&RUN-seq, and ATAC-seq. Any cell type labeled with the NuTRAP cassette could use this method to isolate information from the same set of cells. This enables information to be gathered from the same sample (which

has the potential to reduce the number of samples needed in a given study) and to overcome population heterogeneity problems associated with using cells from separate regions in the analysis.

This chapter focuses on the SIT protocol and the generation of the Emx1-NuTRAP mouse model that enables SIT to isolate excitatory neurons in the hippocampus. We demonstrate the effectiveness of the Emx1-NuTRAP mouse for labeling excitatory hippocampal neurons specifically, and the SIT protocol for isolating high-quality chromatin and mRNA from the same cell homogenate.

Materials and Methods

Animals

Emx1-IRES-*Cre* knock-in mice (Jackson Laboratory Stock No: 005628), NuTRAP mice (Jackson Laboratory Stock No: 029899), and C57Bl6/J (Jackson Laboratory Stock No: 000664) wild type mice were obtained from Jackson Laboratories. Female Emx1-IRES-*Cre* and male NuTRAP mice were crossed to generate the Emx1-NuTRAP mice used for this study. Mice were given free access to food and water, and lights were maintained on a standard 12-hour light/dark cycle. On postnatal day (P) 21, mice were weaned and pair-housed in either standard bedding cages or cages equipped with a running wheel. Only male mice were used for the studies performed. Experiments were conducted according to US National Institutes of Health guidelines for animal care and use and were approved by the Institutional Animal Care and Use Committee of the University of California, Irvine.

Exercise Paradigm

After weaning on P21, male mice from the same litters were randomly divided and pair-housed in either standard cages without a wheel or cages equipped with a stainless-steel running wheel similar to methods already described[12]. Animals housed with running wheels had free access to the wheels from P21–41. Real-time data acquisition (Vital View Software) was used to track distance ran recorded by magnetic sensors that detect wheel revolutions. Each monitored wheel tracked running distance for the entire cage (two mice per cage). Revolutions were quantified for every minute daily for the duration of the exercise period and converted to

distance ran per cage (km). Exercised mice that underwent OLM training were individually tracked as described in Valientes et al. 2021[55].

Simultaneous INTACT and TRAP ("SIT")

On P42 bothEXand sedentary control (n=4/group) Emx1-NuTRAP mice were sacrificed by rapid cervical dislocation and both hemispheres of the hippocampus were dissected out and collected for tissue processing. Hippocampal tissue samples were mechanically homogenized in 1mL of nuclear preparation buffer (NPB) (10mM HEPES (pH7.5); 1.5mM MgCl2; 10mM KCl; 250mM sucrose; 0.1% IGEPAL CA-630; 0.2mM DTT; 100µg/mL cycloheximide; 1x Complete EDTA-free protease inhibitor (Roche)) by razor blade. Samples were then triturated with an 18G needle and syringe 50x on ice.

Homogenized tissue samples were pipetted slowly onto 100µm cell strainer caps on 5mL tubes and centrifuged at 1,000rcf for 10 minutes at 4ºC. Cell pellets were resuspended, and samples were pipetted onto 40µm cell strainer caps on 5mL tubes and centrifuged at 1,000rcf for 10 minutes at 4ºC. For nuclear isolation, 100µL of Streptavidin-coated Dynabeads were washed twice with 1mL NPB and resuspended with 100µL NPB. Cell pellets were resuspended and added to washed Streptavidin-coated Dynabeads. Samples were briefly pipetted to thoroughly suspend the beads and incubated on ice for 20 minutes. Samples were placed on a magnetic stand to pull down nuclei bound to the beads. The supernatant from each sample was slowly pipetted off the beads and transferred to new 1.5mL tubes for RNA isolation (described later). Nuclei-bound beads were washed twice with 1mL INTACT buffer (10mM HEPES (pH7.5); 1.5mM MgCl2; 10mM KCl; 250mM sucrose; 0.1% IGEPAL CA-630; 1x Complete EDTA-free protease inhibitor (Roche)) and resuspended in 100µL INTACT buffer. Bead-bound nuclei were flash

frozen on dry ice and stored at -80ºC until ready for CUT&RUN chromatin digestion and DNA purification.

For RNA isolation, 100µL of concentrated TRAP isolation buffer (10mM HEPES (pH 7.5); 117mM MgCl2; 1M KCl; 10% IGEPAL CA-630; 100µg/mL cycloheximide; 11mg/mL sodium heparin; 20mM DTT; 2.2units/µL Rnasin; 1x Complete EDTA-free protease inhibitor (Roche)) was added to each sample (supernatant above). Samples were mixed by gentle pipetting and centrifuged at 16,000rcf for 10 minutes at 4ºC. The supernatant from each sample was transferred to new 1.5mL tubes and 50µL of protein-G Dynabeads was added to each sample. (To bind anti-GFP, 100µL of protein-G Dynabeads were washed twice with 500µL NPB and resuspended to a final 100µL volume. 2µL anti-GFP antibody (Sigma-Aldrich, G6539, Lot:128M4867V) was added to each tube and incubated for 1 hour on a rotating nutator at 4ºC. Excess anti-GFP was washed off with 200µL NPB and beads were resuspended in a final 100µL volume.) Samples were incubated for 3 hours on a rotating nutator at 4ºC. Beads were washed 3x in 1mL high salt wash buffer (HSWB) (50mM Tris (pH 7.5); 12mM MgCl2; 300mM KCl; 1% IGEPAL CA-630; 2mM DTT; 100µg/mL cycloheximide) at 4ºC. After the third wash the beads were slowly resuspended in 350µL RLT buffer (from Qiagen RNeasy Mini kit #74004) by slowly pipetting up and down and incubated on a rotating nutator for 30 minutes at room temperature. Samples were placed on a magnetic stand to pull down the beads, and the supernatant from each were transferred to new 1.5mL tubes and stored at -80ºC until ready for RNA purification.

Separate TRAP RNA Isolation

On P42, mice (n=3 mice/group) were sacrificed and the hippocampus was dissected out as described above. Either the left or right brain hemisphere of the hippocampus was processed for TRAP RNA isolation using methods similar to those previously described[3,56] and the other hemisphere was processed for INTACT nuclear isolation (see below). Hippocampal tissue was homogenized with a motorized pestle in 1ml of TRAP homogenization buffer (50mM Tris, (pH 7.5); 12mM $MgCl_2$; 100mM KCl; 1% NP-40; 100µg/ml cycloheximide; 1mg/ml sodium heparin; 2mM DTT; 0.2units/µl RNasin; 1x Complete EDTA-free protease inhibitor (Roche)). Samples were centrifuged at 16,000rcf for 10 minutes at 4ºC. The supernatant from each sample was collected and incubated with 50µL of protein G Dynabeads (washed twice in 1mL TRAP homogenization buffer without RNasin or protease inhibitor and resuspended in 50µL of the same buffer). Samples were incubated for 30 minutes on a rotating nutator at 4ºC. Following the incubation, 100µL of anti-GFP bound protein-G Dynabeads was added to each sample. (To bind anti-GFP, 100µL of protein-G Dynabeads were washed twice with 500µL TRAP homogenization buffer without RNasin or protease inhibitor and resuspended to a final 100µL volume. 2µL anti-GFP antibody (Sigma-Aldrich, G6539, Lot:128M4867V) was added to each tube and incubated for 1 hour on a rotating nutator at 4ºC. Excess anti-GFP was washed off with 200µL TRAP homogenization buffer without RNasin or protease inhibitor and beads were resuspended in a final 100µL volume.) Samples were incubated for 3 hours on a rotating nutator at 4ºC. Beads were washed 3x in 1mL HSWB at 4ºC. After the final wash, the beads were resuspended in 350µL RLT buffer (from Qiagen RNeasy Mini kit #74004) and incubated on a

rotating nutator for 30 minutes at room temperature. Following the incubation, samples were transferred to new 1.5mL tubes and stored at -80ºC until ready for RNA purification.

Separate INTACT Nuclear Isolation

The remaining hippocampal hemisphere from each mouse (not used for TRAP RNA isolation above) was processed for INTACT DNA isolation using methods similar to those described[3,57]. Tissue samples were quickly chopped with a razor blade, added to 1mL of INTACT buffer, and triturated with an 18G needle and syringe 50x on ice. Samples were then added onto 100µm cell strainer caps on 5mL tubes and centrifuged at 1,000rcf for 10 minutes at 4ºC. Cell pellets were resuspended and samples were pipetted onto 40µm cell strainer caps and centrifuged at 1,000rcf for 10 minutes at 4ºC. 100µL of streptavidin coated Dynabeads (washed twice with 1mL INTACT buffer and resuspended to a final 100 µL volume) were added to each sample, and samples were incubated on ice for 20 minutes. After incubation, nuclei bound beads were washed twice with 1mL and resuspended in 100µL INTACT buffer. Bead-bound nuclei were flash frozen on dry ice and stored at -80ºC until ready for CUT&RUN chromatin digestion and DNA purification.

RNA Purification and Sequencing Library Preparation

RNA was purified using the Qiagen RNeasy kit according to the manufacturer's protocol. After purification, RNA quantity and quality were checked using the Qubit RNA High Sensitivity assay and Agilent Bioanalyzer's Eukaryote Total RNA Pico assay, respectively, at the University of California, Irvine Genomics High Throughput Facility (UCI GHTF). Using an input of 15ng of total RNA, mRNA was isolated using NEXTFLEX Poly(A) Beads 2.0, and the

mRNA sequencing libraries were generated using the NEXTFLEX Rapid Directional RNA-Seq Kit 2.0 according to the manufacturer's instructions. Final libraries were sent to the UCI GHTF for Qubit dsDNA High Sensitivity assay and the Agilent Bioanalyzer DNA High Sensitivity assay to determine the quantity and quality of the RNA-seq libraries, respectively. Libraries were sequenced at the UCI GHTF using 100bp paired end reads on a single lane of an Illumina NovaSeq6000 to a minimum sequencing depth of 50 million reads.

Dorsal Hippocampal RNA Isolation

P42 wild type male mice were sacrificed by cervical dislocation. Left dorsal hippocampus was extracted by bisecting the isolated hippocampus. The tissue was homogenized and RNA was extracted using the Qiagen RNeasy kit according to the manufacturer's protocol. Sequencing libraries were prepared from the RNA as described under the section "RNA purification" and the UCI GHTF performed sequencing library preparation, except that ERCC ExFold RNA Spike-In Mixes (ThermoFisher cat. 4465739) were added according to the manufacturer's instructions.

Cleavage Under Target and Release Using Nuclease (CUT&RUN)

For chromatin analysis, CUT&RUN was performed using the EpiCypher CUTANA CUT&RUN protocol with slight modifications similar to what has already been described[40]. Nuclei bound to beads were thawed and pulled down on a magnetic stand. The supernatant was removed and beads were resuspended in 200µL wash buffer (20mM HEPES (pH 7.5); 150mM NaCl; 0.5mM spermidine; 1x Complete EDTA-free protease inhibitor (Roche)). Each sample was divided into three aliquots (50µL for anti-H3K27me3 (Cell Signaling Technologies,

C36B11, Lot: 16), 100µL for anti-H4K8ac (Epicypher, 13-0047, Lot: 20202001-11), and 50µL for anti-IgG control (Rabbit IgG Fisher Scientific, 026102)). Beads were pulled down on a magnetic stand, resuspended in 100µL wash buffer and incubated for 10 minutes at room temperature. After incubation the beads were pulled down, the supernatant was removed, and the beads were resuspended in 50µL ice cold antibody buffer (20mM HEPES (pH 7.5); 150mM NaCl; 0.5mM spermidine; 0.001mM digitonin; 2mM EDTA; 1x Complete EDTA-free protease inhibitor (Roche)). 0.5µL of the appropriate antibody was added to each sample, and the samples were mixed by gentle pipetting prior to overnight incubation at 4ºC on a nutator.

On the second day, the beads were pulled down on a magnetic stand, the supernatant was removed and the beads were washed twice in 250µL ice cold wash buffer with 0.001% digitonin. After the washes, beads were resuspended in 50µL ice cold wash buffer with 0.001% digitonin, and 2.5µL of CUTANA pAG-MNase was added to each sample and mixed by gentle pipetting. Samples were incubated for 10 minutes at room temperature and beads were pulled down on a magnetic stand. The supernatant was removed, and the beads were washed twice in 250µL ice cold wash buffer with 0.001% digitonin and resuspended in 50µL of the same. 1µL of 100mM $CaCl_2$ was added to each sample and mixed by gentle pipetting. Samples were incubated for 2 hours on a nutator at 4ºC. Following the incubation, 33µL of stop buffer (340mM NaCl; 20mM EDTA; 4mM EGTA; 50µg/mL RNase A; 50µg/mL Glycogen) and 1.65µL of Spike-In DNA (Cell Signaling Technology, #40366) was added to each sample. Samples were incubated in a preheated thermocycler for 10 minutes at 37ºC. After incubation, samples were transferred to new 1.5mL tubes and immediately processed for DNA purification.

DNA Purification and Library Preparation

DNA was purified using the Monarch PCR and DNA cleanup kit (New England Biolabs, 13-0041) according to the manufacturer's instructions. After purification, DNA fragments were used to generate sequencing libraries using the NEXTFLEX Rapid DNA-Seq Kit 2.0 according to the manufacturer's instructions. Indices were diluted to a final concentration of 1:1,000 before being added to samples, and a total of 13 PCR cycles was used for DNA amplification of the libraries. Final libraries were sent to the UCI GHTF for Qubit dsDNA High Sensitivity assay and the Agilent Bioanalyzer DNA High Sensitivity assay to determine the quantity and quality of the CUT&RUN-seq libraries, respectively. Libraries were sequenced at the UCI GHTF using 100bp paired end reads on a single lane of an Illumina NovaSeq6000 to a minimum sequencing depth of 10 million reads.

Immunofluoresence

Emx1-NuTRAP mice were anesthetized intraperitoneally with 50mg/kg of sodium pentobarbital and transfused transcardially with 4% paraformaldehyde (PFA) in 1x PBS. After perfusion, whole brains were dissected out and incubated in 4% PFA overnight at 4ºC. After fixation, brains were incubated in 30% sucrose for 72 hours and mounted in optimal cutting temperature (OCT) compound. 50µm coronal sections were sliced through the hippocampus using a microtome, and every tenth section was collected in 1mL of cryoprotectant and stored at -20ºC until ready for immunofluorescent labeling. For immunofluorescence, sections were brought up to room temperature and washed 2x in 1x PBS on a nutator for 5 minutes each. Sections were then washed 3x in 1x PBS with 0.3% triton-X. After washes, sections were

incubated with mCherry polyclonal antibody (ThermoFisher, PA5-34974, Lot: UG2804409F) at a 1:200 dilution in blocking solution (1x PBS with 1% BSA) overnight at 4ºC on a nutator. The following day, sections were washed 3x in 1x PBS. Sections were incubated for two hours at room temperature with goat anti-rabbit Alexa Fluor 594 secondary antibody (Invitrogen, A-11012, Lot: 2119134) at a 1:200 dilution in blocking solution. After incubation, the sections were washed twice in 1x PBS. To label nuclei, sections were incubated with DAPI at a 1:10,000 dilution in 1x PBS for 20 minutes. Sections were then washed 3x in 1x PBS and cover slipped with Vectatshield®. Fluorescent images were acquired using a Keyence BZ-X810 All-in-One Fluorescence microscope using the optical sectioning module.

Fluorescence Activated Cell Sorting

Fluorescence activated cell sorting (FACS) was performed to characterize neuronal and astrocytic NuTRAP cassette expression. Whole hippocampal tissue from Emx1-NuTRAP mice was isolated and single-cell suspensions were immunostained for cytometric analysis, as previously described[58]. We used antibodies for THY-1 (OX7) AlexaFluor™ 647 (Santa Cruz Biotechnology, sc-53116 AF647, Lot: F2716; concentration: 1:50) and S100β (Abcam, ab41548, Lot:GR3326165-1; concentration: 1:200) with an AlexaFluor™ 405 goat anti-rabbit IgG (H+L) (Invitrogen, A31556, Lot: 2273716; concentration:1:800) secondary antibody. FACS analysis was performed using a BD FACSAria™ Fusion Flow Cytometer (BD Biosciences) at the University of California, Irvine Stem Cell Core. Samples and single-stain controls were analyzed using the FlowJo v10.8.1 software (BD Biosciences). Samples and controls were positively gated for live cells (SSC-A and FSC-A) and single cells (FSC-H and FSC-A), and negatively gated for autofluorescence (Comp-Alexa Fluor 647-A (Thy1) and Comp-BV421-A (S100β)). Fraction of

GFP+ neuronal cells was determined using quartile analysis of Thy-1 and Comp-GFP-A (GFP). Fraction of GFP+ astrocytic cells was determined using quartile analysis of S100β and Comp-GFP-A (GFP).

qPCR

cDNA was generated from TRAP-isolated and total input RNA samples (n=2 samples/group) using the Transcriptor First Strand cDNA Synthesis Kit (Roche) following the manufacturer's instructions. Relative gene expression for *Aqp4* (F: 5'-ATCCAGCTCGATCTTTTGGA -3', R: 5'-TGAGCTCCACATCAGGACAG -3'), *Tubb3* (F: 5'-GTCTCTAGCCGCGTGAAGTC -3', R: 5'-GCAGGTCTGAGTCCCCTACA -3'), *Cd11b* (F: 5'-CCCATGACCTTCCAAGAGAA -3', R: 5'-ACACTGGTAGAGGGCACCTG -3'), and *Mog* (F: 5'-AAGAGGCAGCAATGGAGTTG -3', R: 5'-GACCTGCAGGAGGATCGTAG -3') was determined by qPCR using FastStart Essential DNA Green Master Mix (Roche, 06402712001) following the manufacturer's protocol. Cycle counts for mRNA quantification were normalized to *Gapdh* (F: 5'-CGTCCCGTAGACAAAATGGT -3', R: 5'-GAATTTGCCGTGAGTGGAGT -3'). Quantification was performed using the Pfaffl method [59].

Bioinformatics Analysis

Reference assembly: For all sequencing analysis that required it, the primary reference assembly used was Genome Reference Consortium Mouse Build 38 patch release 6 (GRCm38.p6).

RNA-seq analysis: FastQ files were quality checked for sequencing errors using FastQC (version 0.11.9)[60]. No files were found to have sufficient quality errors to discount their use.

Files were aligned using STAR Aligner (version 2.7.3a)[61]. Duplicate reads were removed using Picard Tools (version 1.87)[62]. SAM Tools was used to convert BAM files to SAM files for use in downstream analysis. FastQC, alignment and duplicate removal were all preformed on the High-Powered Compute Cluster (HPC3) operated by The Research Cyberinfrastructure Center (RCIC) at the University of California, Irvine. R (version 4.1.0)[63] was used for differentially expressed genes (DEG) analysis. Genomic Alignments (version 1.28.0)[64] (summarizeOverlaps mode="IntersectionNotEmpty", singleEnd=FALSE, ignore.strand=FALSE, fragments=TRUE), Genomic Features (version 1.44.0) (exons by gene), and R SAM Tools (version 2.8.0)[65] (yieldSize=100000) were used to extract a count matrix and generate a summarized experiment object. DEseq2 (version 1.32.0)[66] was used to perform a DEG analysis. Ensemble IDs were converted to gene symbols using BiomaRt (version 2.48.1)[67,68]. PCA plots using the top 2000 genes were generated using ggplot2 (version 3.3.4)[69]. Samples were determined as outliers if the variability between the samples heavily weighted PC1 to those samples. This excluded 2 sedentary samples and 1 EX sample. Heatmaps were generated using gplots (version 3.1.1)[70] and RColorBrewer (version1.1-2)[71]. Volcano Plots were generated using ggplot2[69]. Venn diagrams were generated using the Venn diagram tool from Bioinformatics and Evolutionary Genomics[72]. Gene ontology analysis was performed using Panther Classification System (version 16.0)[73]. Genes were also categorized and a leading edge heatmap was also generated using Gene Set Enrichment Analysis (version GSEA 4.1.0)[74]. Upstream regulators were identified from the DEGs upregulated by EX using Qiagen's Ingenuity Pathway Analysis (IPA) (Fall 2021 Release)[75].

CUT&RUN-seq analysis: FastQ files were quality checked for sequencing errors using FastQC (version 0.11.9)[60]. No files were found to have sufficient quality errors to discount their

use. FastQ files were aligned using Bowtie2 (version 2.4.1)[76]. Significant peaks were called from these aligned files using SEACR, developed in CUT&Tag for efficient epigenomic profiling of small samples and single cells[76,77], according to CUT&Tag Data Processing and Analysis Tutorial (updated August 12 2020): https://www.protocols.io/view/cut-amp-tag-data-processing-and-analysis-tutorial-bjk2kky. An FDR higher than 0.1 was considered too high for called peaks. This threshold excluded 4 samples (3 EX H4K8ac separate isolation samples and 1 EX H4K8ac SIT sample). Peaks were called using the stringent and 0.01 settings. Significant peaks were annotated using ChIPseeker (version 1.8.6)[78] using TxDb.Mmusculus.UCSC.mm10.knownGene[79] as a reference with the following settings: tssRegion = c(-3000, 3000), TxDb = TxDb.Mmusculus.UCSC.mm10.knownGene, level = "transcript", assignGenomicAnnotation = TRUE, genomicAnnotationPriority = c("Promoter", "5UTR", "3UTR", "Exon", "Intron", "Downstream", "Intergenic"), annoDb = NULL, addFlankGeneInfo = FALSE, flankDistance = 5000, sameStrand = FALSE, ignoreOverlap = FALSE, ignoreUpstream = FALSE, ignoreDownstream = FALSE, overlap = "TSS", verbose = TRUE). This approach annotated peaks to the closest gene by distance from the promoter, except if that peak falls within a gene before the distal intergenic region. Ensemble IDs were converted to gene symbols using BiomaRt[67,68]. Gene lists of peaks present in each condition were used to generate Venn diagrams, as with RNA-seq analysis[72]. Further Venn diagrams were generated comparing DEGs with peak calls. Peaks were visualized using UCSC Genome Browser and Genome Browser in a Box[80-82].

Normalized counts (for read depth) at binned sections of the DNA as well as RNA-seq gene expression count (normalized for read depth) were compared between simultaneous and

separate isolations as well as left and right hemispheres using Spearman's correlations in R with the package ggpubr (version 0.4.0)[83]. Bar plots were generated using Graph Pad 9 PRISM.

Data Availability

RNA-, TRAP- and CUT&RUN-seq have been submitted to GEO. The metadata and processed files are available through GEO and the raw files are available through the SRA database. Accession numbers: Any additional information required to reanalyze the data reported in this dissertation is available from Autumn Skye Ivy MD PhD aivy@uci.edu.

Detailed step by step description of the preparation of the Emx1-NuTRAP mouse

Preparation steps with *step annotations* (Figure 2):

1. Cross female Emx1-IRES-Cre knock-in mice (Jackson Laboratory Stock No: 005628) with male NuTRAP mice (Jackson Laboratory Stock No: 029899). *We do not use male Emx1-IRES-Cre animals in this cross. Emx1 may allow active Cre in Sperm.*
2. Optional: Separate the males from the dams when a pregnancy is noticed. *We have found that this decreases litter cannibalization rate.*
3. Wean pups from their dams at P21. *Earlier weaning may be possible, but qualitatively we observe this to be a weaning time with high pup survival.*
4. At the desired age, sacrifice the mice by cervical dislocation.
5. Dissect the mice to remove the whole hippocampal formation according to Sultan 2013[84].
6. Proceed to Basic Protocol 2 with this tissue.
7. To confirm that the ribosomes and nuclei are being fluorescently labeled specifically in hippocampal neurons, perfuse the mice, remove the brain, section and perform immunofluorescence imaging according to Tu et al. 2021[85]. *We use a traditional immunofluorescent microscope (Keyence BZ-X800), rather than the scanner described in Tu et al. 2021. An mCherry fluorophore could be used to enhance visualization of nuclear labeling.*
8. Conduct experiments and care for the mice according to US National Institutes of Health Guidelines for Animal Care and Use.

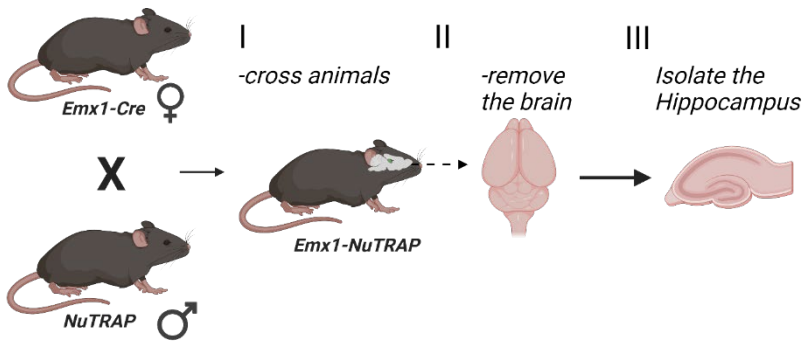

Figure 2: Protocol Diagram: The generation of the Emx1-NuTRAP mouse and the dissection of the hippocampus from those mice.

Detailed step by step description of the preparation of the Emx1-NuTRAP mouse in use with the SIT Protocol

Strategic Planning*:*

This protocol is intensive and has a number of time sensitive steps, especially if RNA integrity is a concern, such as for samples frozen for long periods of time. We recommend at least 2 people proceed with the protocol until the nuclei are isolated. We recommend all buffers be prepared the day before (except for the final addition of DTT and Cycloheximide). It takes approximately 11 hours to complete this protocol if the experimenter chooses to perform a 2-hour TRAP incubation. The alternative is to perform this incubation overnight. If the shorter method is used because of a concern for RNA integrity, that duration of experiment can be accommodated.

Preparation of the protein-G Dynabeads with or without GFP may be done 1 day prior to the protocol and stored overnight at 4°C. The final bead pull-down and elution should be done with freshly prepared buffers. This preparation reduces the number of preparation steps required the day of the protocol.

Reagents and Solutions:

Concentrated TRAP isolation buffer (CTIB)

10mM HEPES pH 7.5; 117mM MgCl2; 1M KCl; 10% IGEPAL CA-630; 100µg/mL cycloheximide; 11mg/mL sodium heparin, 20mM DTT; 2.2units/µl RNasin; 1x Complete EDTA-free protease inhibitor (Roche)

High Salt Wash Buffer (HSWB)

0.05 M Tris pH 7.5, 0.012 M MgCl2, 0.3 M KCl, 1% IGEPAL CA-630, 0.002 M DTT, 100 ug/mL cycloheximide

INTACT Buffer (IB)

10mM HEPES (pH7.5), 1.5mM MgCl2, 10mM KCl, 250mM sucrose, 0.1% IGEPAL CA-630

Nuclear preparation buffer (NPB)

10mM HEPES (pH7.5), 1.5mM MgCl2, 10mM KCl, 250mM sucrose, 0.1% IGEPAL CA-630, 0.2mM DTT, 100µg/mL cycloheximide

Protocol steps with *step annotations:*

Preparation:

This section is critical to smooth and efficient execution of the SIT protocol. It is important enough that we include it here rather than in Strategic planning.

9. Put 1x PBS on ice
10. Thaw cycloheximide and DTT on ice
11. Keep NPB, CTIB, HSWB and IB on ice
12. Prepare appropriate volume of NPB so it's ready immediately after tissue dissection (2mL buffer per animal)
13. Label 5 1.5mL tubes for each sample: 1 for homogenization, 1 for nuclei for INTACT and 1 tube for ribosomal mRNA for TRAP
14. Aliquot 1mL NPB into each of the homogenization tubes
15. For each TRAP isolation, prepare 1 tube of washed protein G Dynabeads for pre-clearing using steps 8-12.
16. Gently resuspend beads by brief vortex and pipette 50 µL of beads into a 1.5mL tube for each sample.
17. Place the tube on the magnetic stand for 1-3 minutes.
18. Slowly pipette off buffer and add 500 µL NPB to each tube.
19. Gently resuspend by inversion and repeat steps 9-10.
20. Place the tube on the magnetic stand for 1-3 minutes and slowly pipette off buffer.
21. Resuspend beads in 50 µL NPB and store on ice or 4°C until ready for use.
22. For each TRAP isolation, prepare 1 tube of washed protein G beads for ribosomal GFP binding.

23. Gently resuspend beads by brief vortex and pipette 100 µL of beads into a 1.5mL tube for each sample.
24. Place the tube on the magnetic stand for 1-3 minutes.
25. Slowly pipette off buffer and add 500 µL NPB to each tube.
26. Gently resuspend by inversion and repeat steps 16-17.
27. Place the tube on the magnetic stand for 1-3 minutes and slowly pipette off buffer.
28. Resuspend beads in 100 µL NPB.
29. Add 2µL anti-GFP antibody
30. Incubate for 1 hour at 4°C on a nutator
31. Centrifuge as above and pipette off buffer
32. Add 200µL NPB and gently resuspend
33. Centrifuge as above, remove buffer, and resuspend in 100µL NPB

Bead washes ensure that the solution that the beads and cells are suspended in is not affected by the buffer that beads are shipped in.

Tissue Homogenization (Figure 3; steps I and II):

1. After tissue dissection add ~700-800 µL of NPB (from the 1mL aliquot) to the tissue and use a razor blade to quickly chop and mince the tissue (we show that hippocampal tissue thawed from flash frozen works well with this protocol. *Caution: Cycloheximide is extremely toxic. Take care not to touch the solution to any part of your body or gloves.*
2. Collect the tissue using a P1000 pipette and place in 1mL (total volume with previously pipetted volume) NPB – Add this to the homogenization tube

3. Homogenize the tissue on ice slowly using 18G needle and syringe 50x. Ensure tissue is thoroughly homogenized. *Sometimes this will not fully homogenize the tissue but have found this amount of homogenization to be sufficient regardless.*

Nuclear Isolation (Figure 3: Steps III, IV, V2):

1. Add homogenized tissue sample to 100 μm cell strainer cap (Yellow) on 5mL tube. *This helps separate the cells and more fully homogenize the sample.*
2. Centrifuge 1,000 rcf for 10 min at 4°C to filter supernatant. During this spin prepare appropriate volume of concentrated TRAP buffer (200μL per animal)
3. Wash streptavidin coated dynabeads (SCD) (Steps 4-9)
4. Resuspend beads by brief vortex and add 100 μL SCD per animal to a 1.7 mL tube.
5. Incubate 3 minutes on a magnetic stand.
6. Remove supernatant.
7. Add 1 mL NPB and vortex briefly.
8. Repeat steps 5-7.
9. Resuspend beads in 100 μL NPB per 100 μL SCD used.
10. Resuspend the cell pellet from step 2 (still in 5 mL tube).
11. Add sample to 40 um cell strainer cap (Blue) on 5mL tube. *This step aims to better lyse the cell membrane and leave only suspended nuclei in the solution.*
12. Centrifuge 1,000 rcf for 10 min at 4°C to filter supernatant.
13. Add 100 μL washed SCD to each tube.

14. Remove tubes from stand, resuspend beads by briefly pipetting up and down. Incubate for 20 minutes on ice, then resuspend, and transfer resuspended beads to a 1mL microcentrifuge tube.
15. Place tubes on magnetic stand for 3-5 minutes to pull down beads (nuclei are bound to these)
16. Slowly collect supernatant with P1000 pipette and save for TRAP Isolation Procedure in mRNA tube (below)
17. Slowly add 1mL IB to beads while still on magnetic stand to wash
18. Pipette off IB slowly
19. Repeat steps 17 and 18.
20. Ensure that the beads do not dry by continuing to a downstream analysis protocol immediately. *At this step the beads will have the isolated nuclei. We use 100µL IB to resuspend the nuclei and beads if we want to freeze for future downstream analysis. We use Zymo Quick-DNA Microprep Plus kit (Zymo D4074) (no modifications to the manufacturer instructions) to isolate genomic DNA for quality control.*

<u>TRAP Isolation Procedure (Figure 3: Steps V1-VIII):</u>

1. Add 100µL concentrated TRAP isolation buffer (CTIB) to each 1mL of supernatant. *This brings the solution concentrations to the concentrations required for a normal TRAP isolation.*
2. Centrifuge 16,000 rcf for 10 min.
3. Collect all clear supernatant and transfer to tube containing 50 µL washed protein G dynabeads (avoid any pellet or top lipid layer). *Optional - Save 50µL of each sample in a*

new tube and keep on ice. RNA from this will be extracted for use as a total RNA input control.

4. Incubate for 30 minutes on nutator at 4°C
5. Incubate 3 min at 4°C on magnetic stand to pellet beads and transfer supernatant to tube containing protein G beads bound to GFP-antibody from the preparation section.
6. Incubate 2 hours (or overnight) on a rotating nutator at 4°C .
7. Slowly pipette off supernatant
8. Wash the beads 3 times by resuspending in 1 mL HSWB incubating at 4°C on the magnetic stand for 3 min and removing supernatant.
9. Pipette off wash buffer and slowly resuspend beads in 350µL RLT buffer (from RNeasy kit) by slowly pipetting up and down. Incubate on nutator for 30 minutes.
10. Proceed to RNA purification. *RLT buffer is necessary as this contains reagent to bind RNA to the column.*

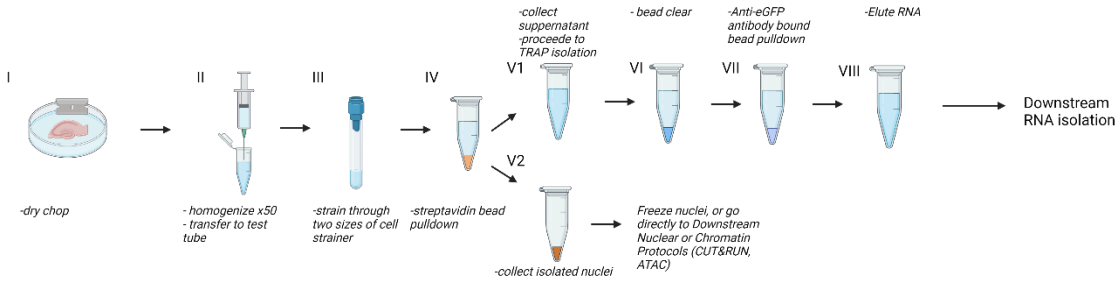

Figure 3: SIT schematic of the major protocol steps.

Results

"Emx1-NuTRAP" mouse allows for simultaneous isolation of nuclear chromatin and translating mRNA from a single population of hippocampal neurons.

We sought to validate neuron-specific expression of the NuTRAP cassette. First, immunohistochemistry of Emx1-NuTRAP hippocampal slices show distinct GFP and mCherry expression in CA1 and CA3 pyramidal neurons (Figure 4A-B) as well as the granule cell layer of the dentate gyrus (DG; Figure 4C). Furthermore, mCherry positive nuclei remained intact and bound to the magnetic beads after our modified nuclear isolation procedure (Figure 4D). As Emx1-expressing neural stem cells can become astrocytes[2], we sought to determine whether a significant number of mature astrocytes were obtained in the population of isolated cells. Flow cytometry experiments using THY-1 as a neuronal marker and S100β as an astrocytic marker revealed a distinct population of cells double positive for GFP and THY-1, whereas a S100β and GFP double positive cell population was absent (Figure 4F and Supplementary Table 1 from Raus et al.[1]).

We performed Simultaneous INTACT & TRAP ("SIT") by dissecting hippocampal tissue from both brain hemispheres, combining, and homogenizing in one sample tube (Figure 3), in order to determine that mRNA from the eGFP tagged cell population was enriched for excitatory neural markers. Using qPCR, we found that TRAP isolated mRNA had significantly reduced expression of *Mog* and *Cd11b* compared to total RNA, suggesting depletion of oligodendrocyte and microglial populations in TRAP mRNA (Figure 4E).

To confirm our TRAP-isolated hippocampal mRNA came primarily from excitatory neurons, we compared RNA-seq data from whole dorsal hippocampal tissue of wild type mice to

our TRAP-isolated RNA-seq data (TRAP-seq) from Emx1-NuTRAP mice to assess for neuronal gene enrichment. We found that TRAP-isolated mRNA had significant enrichment of several neuronal genes, including *Dlg4*, *Thy1*, *Eno2*, and *Syt4*, as well as a significant reduction in astrocytic, microglial, oligodendrocyte, and inhibitory neuronal genes (Figure 4G). There was a relative expression increase of glial fibrillary astrocytic protein (GFAP) in our TRAP samples. This gene can also be expressed in neural stem populations that were present in our whole hippocampus samples, so this finding may be a reflection of the neural stem cell population of the dentate gyrus[86,87]. Overall, these findings suggest that the Emx1-NuTRAP mouse model is a valid tool for neuron-enriched isolation of sequencing-grade, translating mRNA and nuclear chromatin from a single brain tissue homogenate.

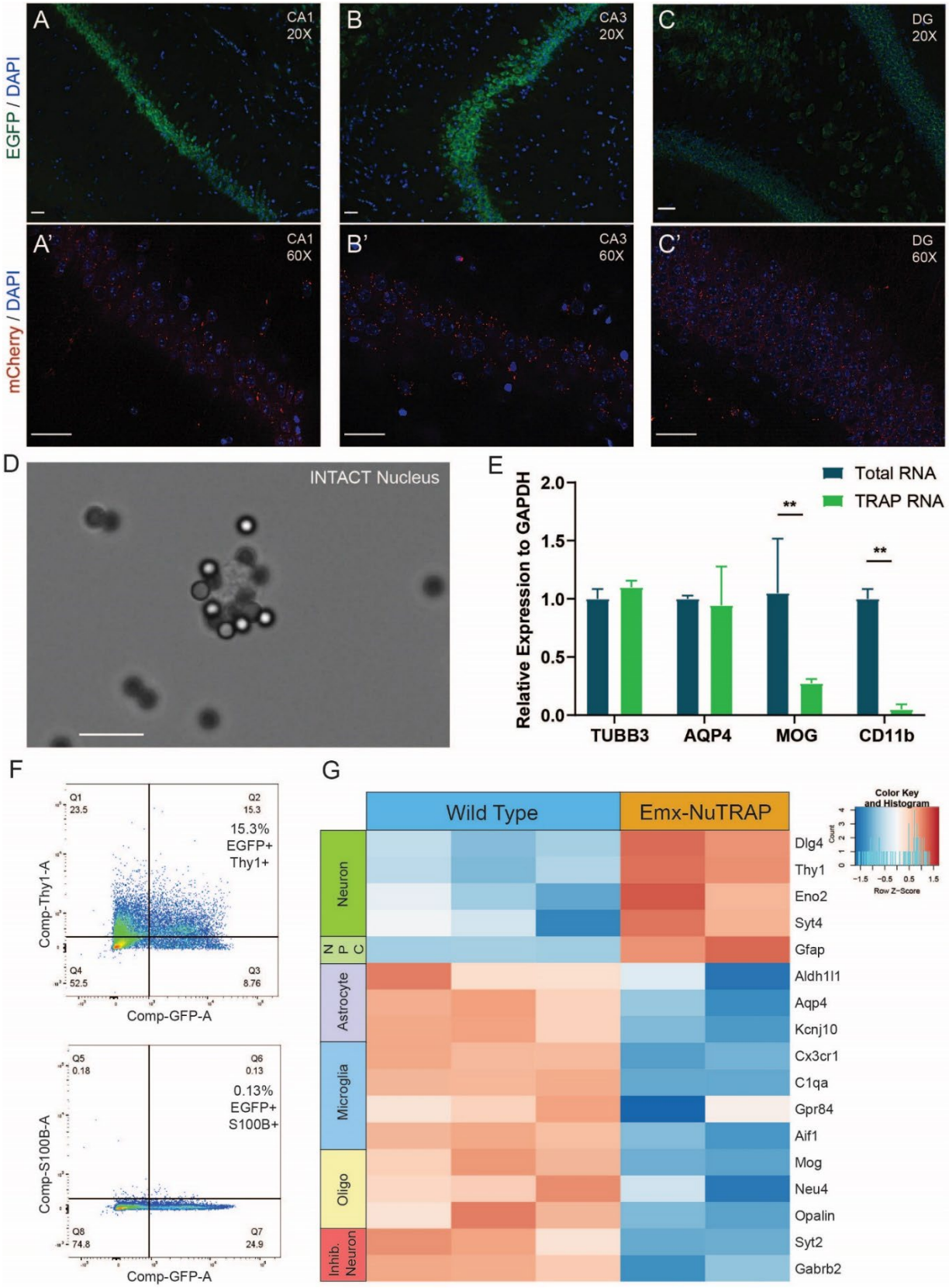

Figure 4: Validation of the Emx1-NuTRAP mouse

Figure 4: Validation of the Emx1-NuTRAP mouse. (A) Immunofluorescence imaging of the CA1 region of the hippocampus at 20x objective and (A') 60x objective after incubation with an mCherry antibody overnight. (B) Immunofluorescence imaging of the CA3 and CA2 region of the hippocampus at 20x objective and (B') 60x objective after incubation with an mCherry antibody overnight. (C) Immunofluorescence imaging of the DG region of the hippocampus at 20x objective and (C') 60x objective after incubation with an mCherry antibody overnight. Scale bars are set to 50μm for all images (A-C). (D) Brightfield microscopy of a neural nucleus bound to streptavidin coated Dynabeads™. The scale bar represents 10μm. (E) qPCR of TRAP isolated RNA compared to total RNA from the simultaneous isolation protocol **$p<0.01$. (F) Flow cytometry for EGFP, THY-1, and S100β (15.3% of cells THY-1+/EGFP+ and 0.13% of cells S100β+/EGFP+). (G) Heatmap of differentially expressed neuronal and other cell type markers from RNA-seq data comparing TRAP-isolated RNA from our Emx1-NuTRAP mice and previously generated dorsal hippocampal tissue RNA from wild type mice.

Performing INTACT/TRAP on the same or separate cell suspensions yields highly comparable TRAP-seq and CUT&RUN-seq results.

We then endeavored to validate our novel SIT technique. We performed SIT on isolated samples by starting the protocol with the beginning steps from the INTACT procedure modified to include cycloheximide. Cycloheximide works rapidly to inhibit protein synthesis and is used for maintaining crosslinks between translating mRNA and ribosomal subunits during purification in the traditional TRAP method. Despite the presence of cycloheximide, nuclear morphology from Emx1-expressing neurons is overall unchanged (Figure 4D). Additionally, a Bioanalyzer was used to determine if there were cycloheximide-induced double-stranded DNA breaks in our nuclear preparation that could interfere with downstream DNA sequencing applications (such as ATAC-, CUT&RUN-, or CUT&Tag-seq). We found no evidence of DNA double strand breaks generating fragments of less than 1kb (Figure 5). Following magnetic purification of biotin-labeled nuclei, the supernatant fraction was removed and taken through TRAP, while the pelleted nuclei were processed through the remaining steps of INTACT (see Methods). Combining bilateral hippocampi from a single mouse yielded TRAP-isolated mRNA of high quality and sufficient concentration for sequencing (RIN > 8 for all samples, average yield RNA = 14.367 ng/ul; Supplementary Table 2 from Raus et al.[1] and Figure 6). INTACT-isolated nuclei were further processed using the CUT&RUN (Cleavage Under Targets and Release Using Nuclease[40]) method to isolate antibody-specific protein-DNA interactions for downstream DNA sequencing. The resulting DNA libraries were of high quality and concentration when using specific antibodies (H4K8ac: average size = 1238 bp, average concentration = 126.8 nM; H3K27me3: average size = 1032 bp, average concentration = 146.5 nM; Supplementary Table 2 from Raus et al.[1]). In contrast, the resulting DNA libraries using the non-specific IgG control had substantially

lower concentrations (IgG: average size = 1035 bp, average concentration = 24.2nM; Supplementary Table 2 from Raus et al.[1]) further indicating that nuclear DNA from both isolations was of high starting quality.

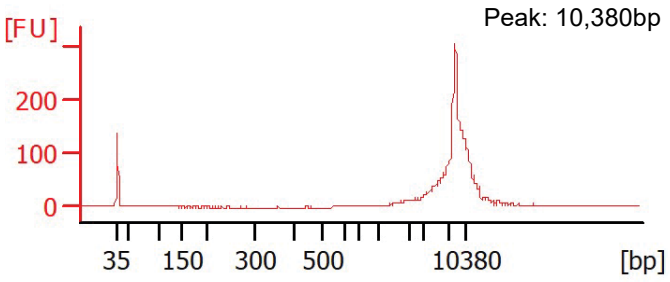

Figure 5: Representative electropherogram of DNA extracted using SIT

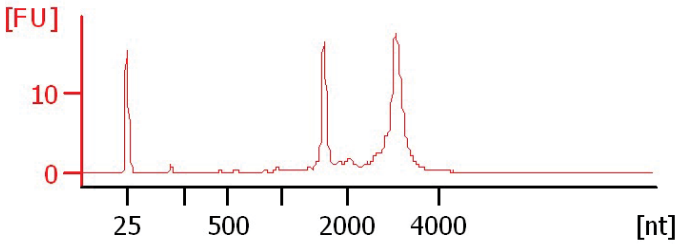

Figure 6: Representative Electropherogram of RNA extracted using SIT (RIN=10)

Previous methods for performing INTACT and TRAP using NuTRAP mice have taken separate tissue homogenates for each procedure[3,88]. In this study, we performed SIT on a single tissue homogenate containing bilateral hippocampi (the products of SIT are referred to as "simultaneous isolations"). To determine if our approach of SIT is comparable to separate INTACT and TRAP procedures, we also performed separate INTACT and TRAP from hippocampal tissue obtained from one brain hemisphere for each method, counterbalancing for left versus right hemispheres (we refer to this protocol as "separate isolations"). A Bioanalyzer was used to determine the amount and quality of the RNA obtained from each type of isolation

(Separate isolations: average RNA concentration = 7.805 ng/ul, average RIN = 9.5; Simultaneous isolations: average RNA concentration = 14.367 ng/ul, average RIN = 9.3; Supplementary Table 2 from Raus et al.[1]). The average RNA yield from the separate isolations (using a unilateral hippocampus) was approximately equal to half of the average yield of the simultaneous isolations (which combined bilateral hippocampi; Supplementary Table 2 from Raus et al.[1]). Similarly, the final library concentrations for the separately isolated IgG CUT&RUN-seq libraries were also approximately half the concentration of the simultaneous isolations (average simultaneous: 24.2nM, average separate: 11nM; Supplementary Table 2 from Raus et al.[1]). We interpret this to mean that nuclear DNA was fully intact in the simultaneous isolation because we did not obtain substantially more than double the concentration in the simultaneous vs separate isolations. Unilateral hippocampal homogenates yielded sufficient sequencing concentrations and quality to allow for library preparations from individual mice (Supplementary Table 2 from Raus et al.[1]).

To determine if normalized TRAP-seq counts were similar between the two isolation methods, we performed a Spearman's correlation between the datasets from sedentary mice. The two TRAP-seq datasets were found to be highly correlated, with R values greater than 0.5 and p value less than 2.2×10^{-16} ($R=1$, $p<2.2\times10^{-16}$; Figure 7A). CUT&RUN-seq was used to identify genomic regions interacting with either H4K8ac, an activating histone post-translational modification (PTM), or H3K27me3, a generally repressive histone PTM. We again applied Spearman's correlation to understand whether the simultaneous vs separate INTACT isolation methods could influence CUT&RUN-seq peak distribution. We compared normalized count data for CUT&RUN-seq peaks across a representative chromosome (chromosome 2). We binned 100bp increments along the entire chromosome from the simultaneous and separate isolations

using datasets generated from sedentary mice. Normalized sequencing counts, which reflected reads assigned to binned genomic regions along chromosome 2, were highly similar between conditions (H4K8ac: $R=0.65$, $p<2.2x10^{-16}$; H3K27me3: $R=0.81$, $p<2.2x10^{-16}$; Figure 7B-C). Taken together, these experiments suggest that translating mRNA and nuclear DNA isolated from hippocampal homogenates using either simultaneous or separate isolation procedures are comparable in terms of quality, concentration, functional characterization, and normalized sequencing reads.

We next wanted to determine if the different isolation methods could bias resulting gene expression on the basis of gene length. When plotting gene length against log fold change of gene expression, we see a similar distribution pattern of EX-induced differentially expressed hippocampal genes (DEGs) between the simultaneous and separate methods (Figure 7D-E). We then compared the biological categories of the EX-induced DEGs obtained using either the separate or the simultaneous isolation methods using Panther Gene Ontology (GO). Although many of the genes did not overlap (Figure 7F-G and Supplementary Table 3 in Raus et al.[1]), most GO terms did (14/20 GO terms for upregulated genes and 15/17 for downregulated genes; Figure 7H-I and Supplementary Table 3 in Raus et al.[1]). Furthermore, there was high similarity between the percentage of genes found in each of the GO categories (Figure 7J-K). Taken together, our results demonstrate that the simultaneous approach for isolating and sequencing mRNA and nuclear chromatin can be performed using a single hippocampal homogenate and can generate highly similar results as more traditional methods using separate cell samples to pair different types of sequencing results.

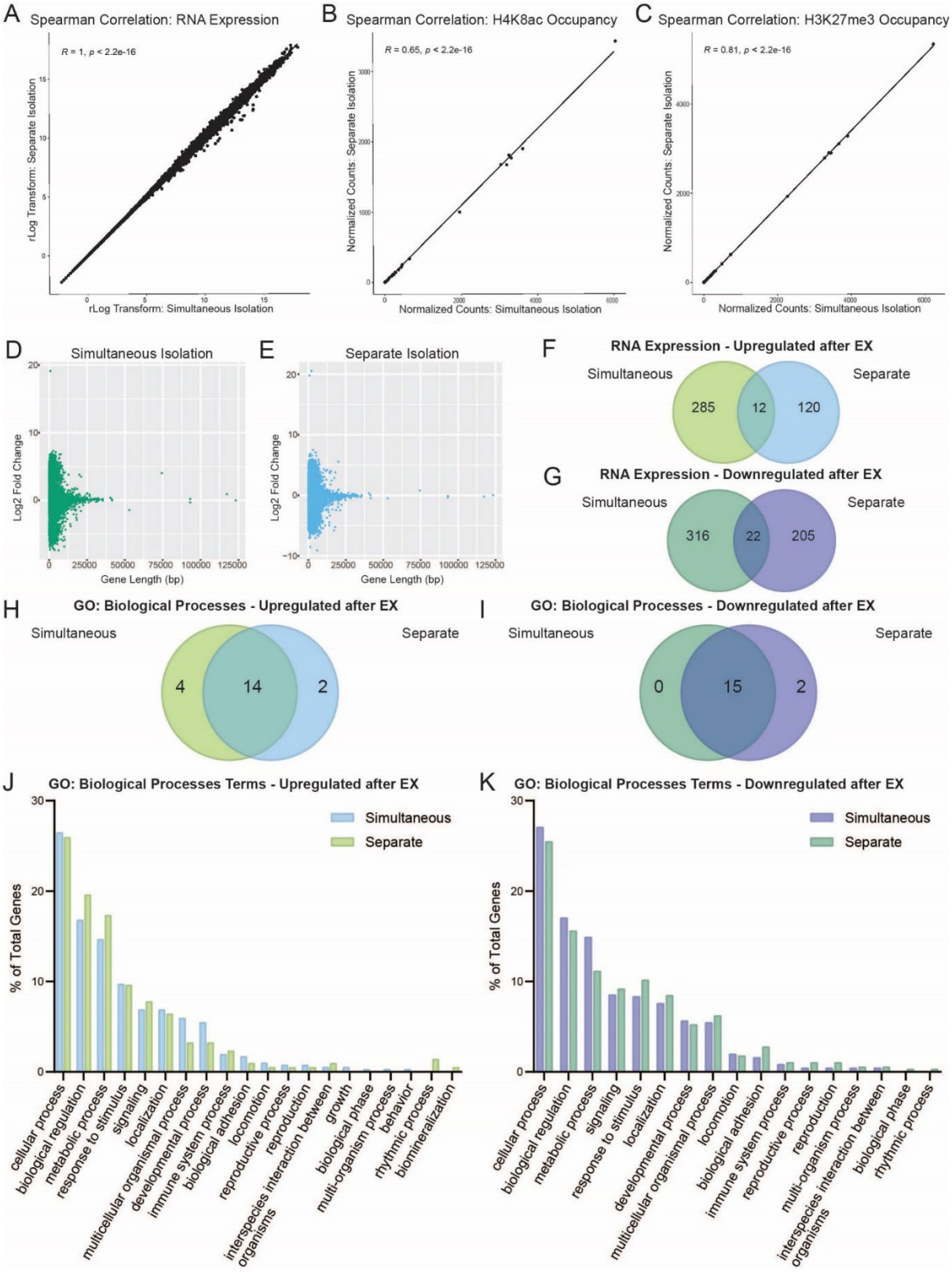

Figure 7: Simultaneous and separate isolations of DNA and RNA from Emx1-NuTRAP mice are comparable.

Figure 7. Simultaneous and separate isolations of DNA and RNA from Emx1-NuTRAP mice are comparable. For Figure 7 A-E, n=2 mice for simultaneous isolations and n=3 mice for separate isolations. (A) Spearman's correlation for RNA expression between separately isolated RNA and simultaneously isolated RNA (R=1, p<2.2x10-16). (B) Spearman's correlation between separate and simultaneously isolated DNA from CUT&RUN-seq for H4K8ac with 100bp chromosome 2 position bins (R=0.65, p<2.2x10-16). (C) Spearman's correlation between separate and simultaneously isolated DNA from CUT&RUN-seq for H3K27me3 with 100bp chromosome 2 position bins (R=0.81, p<2.2x10-16). (D) Gene length versus fold change distribution plot for simultaneously isolated RNA. (E) Gene length versus fold change distribution plot for separately isolated RNA. (F) Genes upregulated in TRAP-seq after EX in either simultaneous (n=2 sedentary mice and n=3 EX mice) or separate isolations (n=3 mice per group). (G) Genes downregulated in TRAP-seq after EX in either simultaneous or separate isolations. (H, I) Panther Gene Ontology: Biological Processes Venn diagram for genes upregulated (H) or downregulated (I) after EX in either separate or simultaneous isolations. (J, K) Panther Gene Ontology: Biological Processes bar graph of gene distributions for genes upregulated (J) and downregulated (K) after EX in either separate or simultaneous isolations.

Demonstrating the efficacy of the Emx1-NuTRAP mouse and the corresponding SIT protocol

The *Emx1*-NuTRAP mouse will express eGFP bound to ribosomes in hippocampal excitatory neurons and mCherry and biotin on the nuclear membranes of those neurons. On coronal brain slices, the eGFP and mCherry can be observed on excitatory pyramidal neurons in the cytoplasm and nuclear membrane respectively. The eGFP should appear diffuse throughout the cytoplasm and the mCherry should appear as puncta on the nuclear membrane. Both can be observed at 20x objective lens (Figure 4A-C) on an epifluorescent microscope but are best observed with the 60x oil immersion objective lens (Figure 4A'-C'). As an example, Figure 4C and 5C' demonstrate the that the NuTRAP cassette is being selectively expressed in hippocampal granule cells with potentially some inclusion of neural progenitor cells in the DG. DAPI is used to stain the nuclear material of all cells with a blue fluorescent signal. Lack of green and red fluorescence in the granule cell layer would indicate that the NuTRAP cassette is not being expressed and would indicate something went wrong with the cross. Low mCherry expression, or low signal, is normal. In these figures presented, we did not have to amplify the signal; however, signal amplification of the mCherry with a fluorescent antibody may be required to visualize the signal in some instances.

The SIT protocol isolates ribosomes by targeting the eGFP-labeled L10a ribosomal subunit and the mRNA bound to those ribosomes. We isolate the RNA with Qiagen's RNeasy kit as described in the protocol. The SIT protocol also isolates biotin labeled nuclei. We use these nuclei directly in our downstream applications, which require intact nuclei (ATAC-seq and CUT&RUN-seq). We occasionally visualize the nuclei before down-stream applications to ensure they are intact (Figure 4D). Here we present a bioanalyzer trace (Figure 6) of DNA

isolated from the Nuclei using Zymo's DNA Miniprep Kit (D3024) for the isolation of genomic DNA. Our trace has no or very little DNA below the peak at the base of the gel indicating that most of the DNA remains intact or genomic (Figure 6). DNA shorter than 1000bp would interfere with our downstream applications. To aid in reproducibility, We check the concentration of the isolated DNA to confirm that we have a sufficient quantity for our downstream applications. We report Quality metrics with a representative bioanalyzer trace and a table of concentrations in your supplemental information. For a method that requires whole nuclei as an input we count nuclei to determine the concentration of the nuclei isolated.

Neuron-specific gene expression and histone PTMs are functionally comparable between left and right hippocampal hemispheres.

We then sought to demonstrate that our novel technique can be used to elucidate differences between similar brain regions because our technique allows corresponding regions from each hemisphere to be analyzed separately. Many studies take advantage of the brain's structural symmetry by using tissue from each hemisphere for separate molecular processing. Prior evidence demonstrates that hippocampal lateralization can influence LTP, hemisphere-specific glutamate receptor density, and performance in certain memory tasks[89]. We wanted to determine if there were differences in transcriptional programs and biological processes resulting from EX in left vs right hippocampi. Using the separate isolation approach described above, we compared EX-induced differential gene expression between left and right hemispheres. We found that although individual gene expression patterns were different between hippocampi originating in the left and right brain hemispheres (Figure 8A-B and Supplementary Table 4 in Raus et al.[1]), the Panther GO: Biological Processes terms were similar, with most categories overlapping (Figure 8C-F and Supplementary Table 4 in Raus et al.[1]). This could suggest spatial or hemispheric assignment of genes with functional similarity.

Finally, we wanted to determine if left and right hippocampal hemispheres had significant differences in DEGs and CUT&RUN-seq peak distributions at baseline (without exercise). We performed Spearman's correlation on the transcript counts from the TRAP-seq data ($R=1$, $p<2.2\times10^{-16}$; Figure 8G), and the CUT&RUN-seq 100 bp binned peak counts along chromosome 2 for H4K8ac ($R=0.59$, $p<2.2\times10^{-16}$; Figure 8H) and for H3K27me3 ($R=0.70$, $p<2.2\times10^{-16}$; Figure 8I). We found that the seq peaks and transcript counts were highly similar with significance considered as R values greater than 0.5 and p value less than 2.2×10^{-16} (Figure

8G-I). Overall, left and right hippocampal hemispheres did not demonstrate significant differences in normalized sequencing counts and peak distributions in the sedentary condition, suggesting that choice of hippocampal hemisphere is a less important factor to consider in obtaining representative data on transcription and transcriptional regulation via histone modifications.

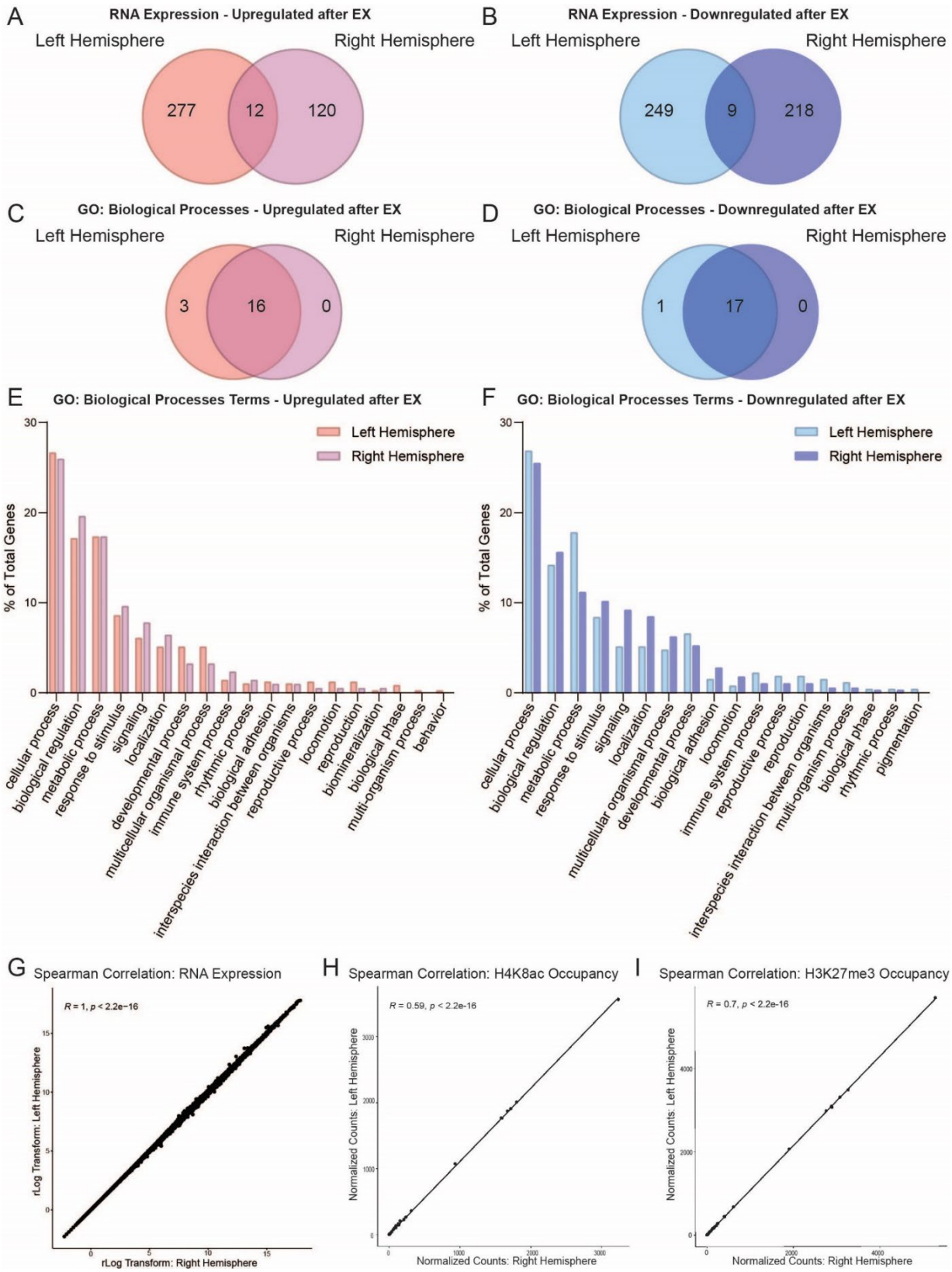

Figure 8: Histone modifications and functional categorizations of gene expression are similar regardless of hemispheric origin of hippocampal tissue.

Figure 8: Histone modifications and functional categorizations of gene expression are similar regardless of hemispheric origin of hippocampal tissue. (A-B) Venn diagram of genes upregulated (A) or downregulated (B) by EX identified between the left and right hemispheres by the separate isolation protocol TRAP-seq (n=3 mice per group). (C-D) Venn diagram of Panther Gene Ontology: Biological Process terms for genes upregulated (C) or downregulated (D) by EX identified between the left and right hemispheres by the separate isolation protocol TRAP-seq. (E-F) Percent of genes fitting into each GO category for the left and right hemisphere for genes upregulated (E) and downregulated (F) by EX by separate isolation TRAP-seq. (G) Spearman's correlation between the left and right hemispheres TRAP-seq data from the separate isolation protocol of sedentary rlog normalized expression ($R=1$, $p<2.2x10^{-16}$). (H) Spearman's correlation between hemispheres for CUT&RUN-seq for H4K8ac normalized count data for chromosome 2 in 100bp bins ($R=0.59$, $p<2.2x10^{-16}$). (I) Spearman's correlation between hemispheres for CUT&RUN-seq for H3K27me3 normalized count data for chromosome 2 in 100bp bins ($R=0.7$, $p<2.2x10^{-16}$).

Discussion

Identifying gene regulatory mechanisms activated by exercise during sensitive developmental periods can aid in understanding how early-life exercise may promote a "molecular memory" of exercise[31,90], via the epigenome, that informs long-term cell function and behavioral outcomes. This chapter presents results demonstrating neuron-specific, simultaneous characterization of translating mRNA and associated histone modifications (validation and method discussed in this chapter) to reveal molecular signatures of the early-life exercise experience (discussed in chapters 3 and 4). To our knowledge, this is the first report describing use of the NuTRAP construct in a predominantly neuronal population. Additionally, our unique experimental approach for simultaneous INTACT and TRAP ("SIT") is a technical advance for NuTRAP applications: by modifying the nuclear chromatin isolation (INTACT) procedure to include cycloheximide, one can obtain both polyribosome-bound mRNA (using TRAP) and nuclear DNA from a single lysate to directly correlate gene expression programs with epigenetic regulatory mechanisms in the same set of cells. The field of neuroepigenetics has been challenged by very limited approaches for coupling cell-type specific transcriptional profiles with chromatin modifications without compromising cell integrity (through flow sorting) or genomic coverage (through single-cell sequencing). Therefore, the NuTRAP model in combination with the "SIT" protocol offers an exciting opportunity to overcome these challenges and perform paired transcriptomic and epigenomic analyses in any brain cell type of interest for which a Cre line exists[3,88].

Traditional epigenetic and gene expression sequencing approaches to bulk tissue samples are confounded by the cellular heterogeneity. Further, current methods for paired analysis of the

epigenome and transcriptome are restricted by the need for multiple transgenic animal models or the use of highly expensive single-cell sequencing technologies. It is critical to obtain epigenomic information in a cell-type specific manner because there are unique epigenetic modifications distinguishing cell subtypes of the central nervous system[91,92]. Roh et al. first developed the NuTRAP mouse to characterize adipocyte-specific and hepatocyte-specific epigenetic and transcriptional profiles[3,38]. The NuTRAP mouse has since been used to perform paired transcriptome and DNA modification analysis in astrocytes and microglia, demonstrating its utility in CNS cell-types[88]. The Emx1-NuTRAP mouse described here provides a rapid, cost-effective means for characterizing neuron-specific changes to epigenetic state and gene expression using whole-tissue homogenates containing multiple cell types. In our technical validation experiments, the "SIT" technique produced high quality RNA and DNA of sufficient concentration for downstream sequencing studies from a single mouse hippocampus. This method effectively increases the total sample size used for each analysis as the tissue sample does not need to be separated for DNA and RNA isolation. CUT&RUN allows for low-input cell-specific chromatin analysis[40,77] further reducing the required amount of starting material. Indeed, the DNA obtained from SIT could be used for other applications for evaluating the chromatin landscape, including ATAC-seq. Presently, the field of neuroepigenetics is shifting to single-cell resolution for sequencing studies. Our study was performed in bulk tissue enriched for neurons. As the goal of this work was to characterize the transcriptional and epigenomic effects of early-life exercise, cell subtype identity (as is often a priority in single-cell approaches) was not necessary for our initial hypotheses but would offer a second layer of complexity to address this study's questions. Single-cell approaches can bias against lowly-expressed genes, which

may present the risk of not capturing small expression changes in rate-limiting genes that may have large changes in function as a result of EX.

In this chapter, we also assessed for hemispheric differences in DEGs and histone modifications using our SIT protocol. A common approach to paired transcriptomic and epigenomic analyses is to use separate brain tissue samples, using one hemisphere for gene expression studies and the other side for epigenetic analyses[93]. A previous study utilizing the NuTRAP allele in non-neuronal brain cells used separate brain hemispheres to perform INTACT and TRAP[88]. However, this assumes that cells of the same type from each half of the tissue will show the same epigenetic and transcriptional profile. This is not necessarily the case for all cell types, especially in the CNS, as structures of the brain can show high degrees of hemispheric specialization[94-98]. To address the degree of transcriptional or epigenetic difference between hippocampi from opposite hemispheres, we performed separate INTACT and TRAP isolations using hippocampal tissue from one hemisphere for DNA isolation and the contralateral hippocampus for mRNA isolation. We found that although DEGs and histone PTMs differed between left and right hippocampi, functional analysis using Panther GO revealed similar biological processes between the two hemispheres. We interpret these data to suggest that hemispheric origin of hippocampal tissue is not a critical contributor to conclusions drawn from these types of sequencing studies.

Chapter 3: Early exercise primes the neuronal genome to promote networks of plasticity-related genes.

Introduction:

Early exercise and the potential role for neural-epigenetic mechanisms underlying enabled memory

Environmental experiences engage epigenetic mechanisms to modulate gene expression and cell function in post-mitotic neurons[41,42]. Histone modifications and DNA methylation are particularly important for neuronal adaptation to environmental signals by altering transcription and synaptic function[22,43]. Behavioral outputs such as stress reactivity, reward seeking, and long-term memory have been shown to result from changes to chromatin accessibility and gene expression in neurons[16,99-102]. In addition to this, the neuronal chromatin landscape undergoes waves of epigenetic modifications as a function of brain maturation itself[91,103,104]. Postnatal periods of heightened sensitivity to environmental stimuli can lead to lasting changes to cellular function and may result from temporally specific epigenetic mechanisms in the developing brain[105,106]. Whether gene regulatory mechanisms in postmitotic neurons are uniquely influenced by early-life experiences to inform long-term function is a question that is just beginning to be explored. Identifying epigenetic processes involved in modulating cell function, particularly during brain development, is critical for understanding how early-life experiences impact long-term behavioral outcomes.

Aerobic exercise enhances performance on cognitive tasks involving the hippocampus in both adult humans and animal models[107,108]. The type, timing, and duration of exercise exposure

matters with regard to whether it has a persistent impact on hippocampal function[11,12,109]. Findings in both adolescent and adult rodents implicate a role for histone modifying enzymes in the mechanisms of exercise-induced benefits to hippocampal memory. Both voluntary exercise or treatment with a HDAC3 inhibitor enable hippocampal memory after a subthreshold learning stimulus, increase brain-derived neurotrophic factor (BDNF), and promote acetylation of H4K8 at the BDNF promoter[20,110,111]. This suggests that exercise engages epigenetic regulatory mechanisms to promote plasticity mechanisms in memory. Adult exercise also opens a temporal window for persistent improvements to memory performance when a reactivating exercise exposure is introduced[31], suggesting a "molecular memory" of the initial exercise[31]. Although the majority of these studies have been performed in adults, more recent work also demonstrates the effects of exercise on hippocampal memory and associated alterations in neurotrophic factor expression, synaptic plasticity, and neurogenesis are similar in juvenile and adolescent periods[12,18,19,26,112]. Previous work in our lab showed that EX for either one week (juvenile period; postnatal days (P) 21-27) or three weeks (juvenile-adolescence; P21-41) facilitated hippocampal long-term memory formation in response to a learning stimulus typically insufficient for forming long-term memory. This finding was associated with increased long-term potentiation (LTP) as well as modulations to synaptic physiology in hippocampal CA1[12]. Using SIT for neuron-specific, paired transcriptomic and epigenomic bulk sequencing, we found hippocampal gene expression programs and associated histone modifications that are driven by EX to promote plasticity. These data reveal an epigenetic signature resulting from EX that may form the basis of persistently enabled hippocampal function.

Materials and Methods

Materials and methods for Chapter 3 are described in Chapter 2 since much of the data presented in Chapter 3 was collected as a direct result of experiments described in Chapter 2.

Results

Early-life exercise promotes expression of plasticity-related genes and is associated with transcriptional regulatory pathways implicated in hippocampal memory.

To identify the transcriptional effects of EX in hippocampal neurons, we performed cell-type specific bulk sequencing on TRAP-isolated mRNA extracted from Emx1-NuTRAP hippocampi using our "SIT" protocol. We compared DEGs from sedentary mice vs EX (running distances shown in Figure 9). Using DESeq2 to assess for DEGs (>30% expression increase with a p value < 0.05), we found that EX alters gene expression in Emx1 expressing neurons (297 upregulated and 338 downregulated genes; Figure 10A and Supplementary Table 3 in Raus et al.[1]). Many of the genes upregulated after EX are known to be involved in exercise and/or hippocampal memory mechanisms, including *Bdnf*[113] and *Nr4a1*[114]. To functionally categorize EX-induced DEGs, we performed a Panther Gene Ontology (GO) analysis[73] focusing on the Molecular Function categorization and separated by upregulated and downregulated genes. Regardless of gene expression directionality, GO term categories with the most genes functionally assigned to them were "binding", "catalytic activity", "molecular function regulator", "transporter activity", "molecular transducer activity", and "structural molecule activity" (Figure 10B). Many of the upregulated genes driving these categories are known to have critical roles in neuronal function (*Kcna1, Slc24a4, Stxbp5l, Gabra2,* and *Camk2n2*), neurodevelopment (*Artn, Kdm7a, Sox21, Gap43,* and *Efna5*), and hippocampal memory (*Bdnf, Nr4a1* and *Dusp5*).

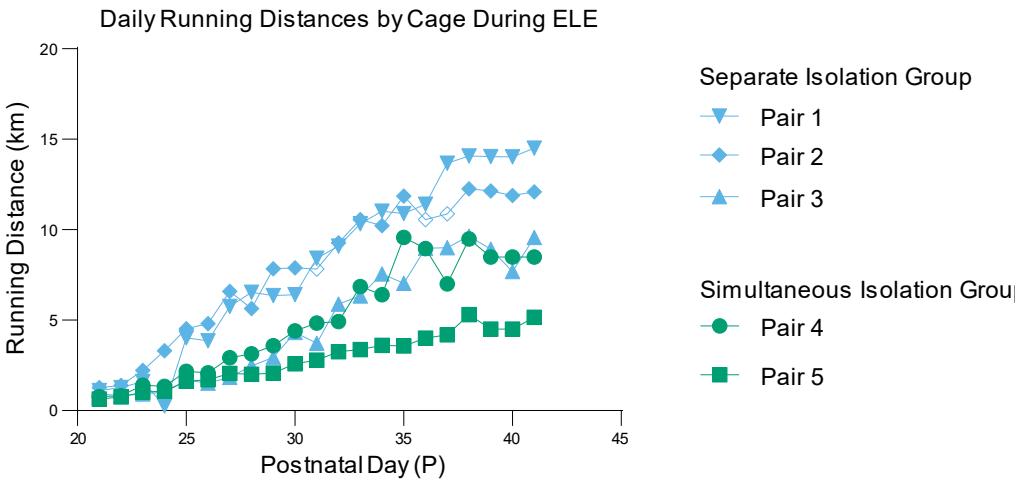

Figure 9: Running Daily running distances of each cage during the EX paradigm.

Figure 9: Running Daily running distances of each cage during the EX paradigm. Values of days missing or low due to software error were imputed by averaging the previous 3 days available. 2 Way Analysis of Variance (ANOVA) reveals that there is significant difference between postnatal days ($p<0.0001$) and cages ($p<0.0001$) but no significant effect of isolation ($p=0.1508$).

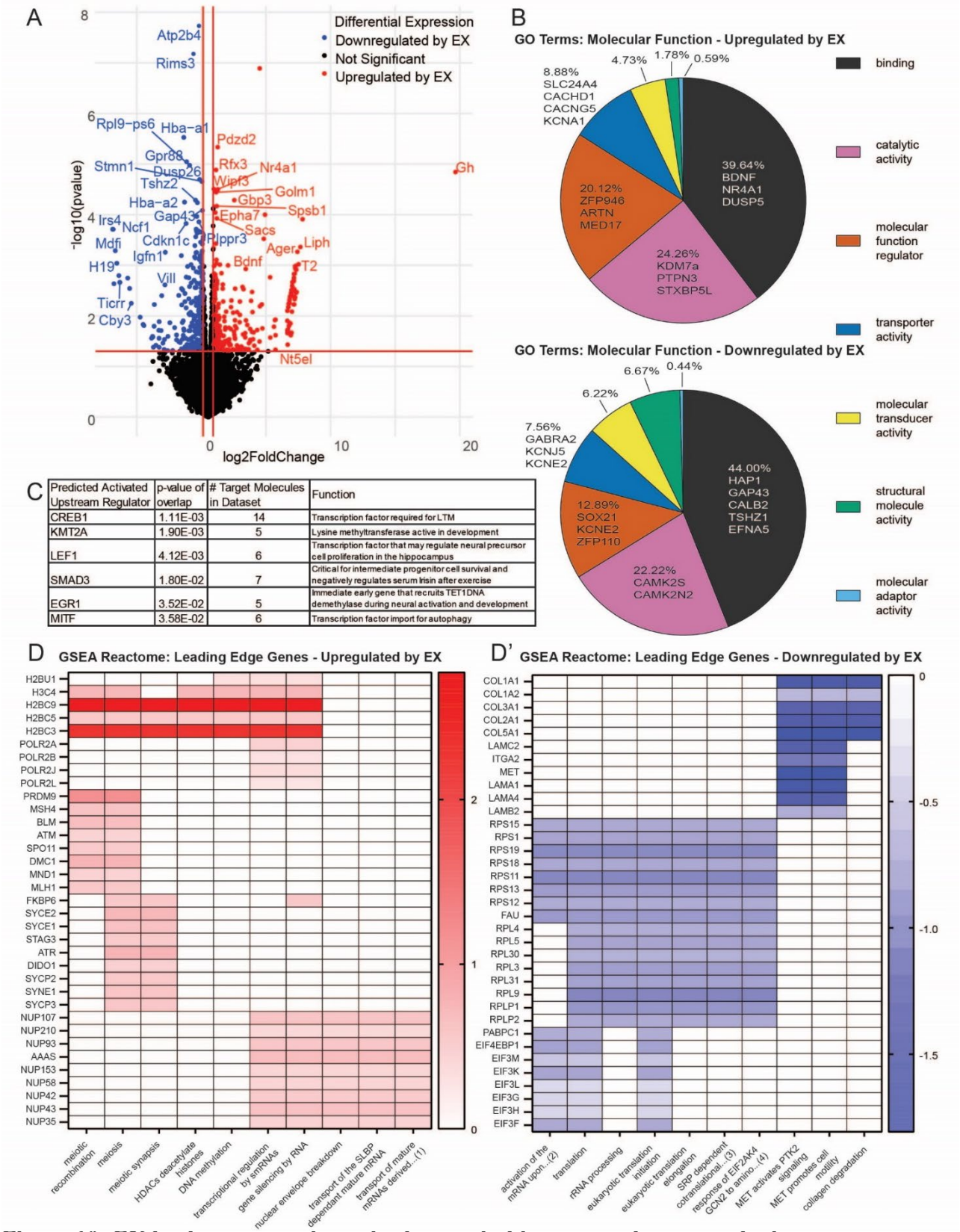

Predicted Activated Upstream Regulator	p-value of overlap	# Target Molecules in Dataset	Function
CREB1	1.11E-03	14	Transcription factor required for LTM
KMT2A	1.90E-03	5	Lysine methyltransferase active in development
LEF1	4.12E-03	6	Transcription factor that may regulate neural precursor cell proliferation in the hippocampus
SMAD3	1.80E-02	7	Critical for intermediate progenitor cell survival and negatively regulates serum Irisin after exercise
EGR1	3.52E-02	5	Immediate early gene that recruits TET1DNA demethylase during neural activation and development
MITF	3.58E-02	6	Transcription factor import for autophagy

Figure 10: EX leads to transcriptomic changes in hippocampal neurons during adolescence.

Figure 10: EX leads to transcriptomic changes in hippocampal neurons during adolescence. (A) Volcano plot of differentially expressed genes reaching significance identified by TRAP-seq on EX versus sedentary (n=2 sedentary mice and n=3 EX mice, absolute value log2 fold change > 0.3785 and p-value < 0.05). (B) Panther Gene Ontology: Molecular Function top terms by most genes assigned. (C) Top 6 "Upstream Regulators" identified by Ingenuity Pathway Analysis (IPA). (D) Representative Gene Set Enrichment Analysis: Reactome leading-edge diagrams showing genes upregulated (D) or downregulated (D') in EX, and their categories of enrichment. *Abbreviated terms in (D): (1) "transport of mature mRNAs derived from intronless transcripts", (D'): (2) "activation of the mRNA upon binding of the cap binding complex and EIFs and subsequent binding to 43S", (3) srp dependent cotranslational protein targeting to membrane, and (4) response of eif2ak4 gcn2 to amino acid deficiency.

To evaluate possible transcription factors and upstream regulators implicated by EX-induced activated gene networks, we applied Qiagen's Ingenuity Pathway Analysis (IPA) to our TRAP-seq dataset[75]. We identified significant canonical signaling pathways implicated in EX effects on hippocampal neuronal function (Figure 11 and Supplementary Table 5 in Raus et al.[1]). Additionally, the top six upstream regulators by significance included CREB1, KMT2A, LEF1, SMAD3, EGR1, and MITF. Each of the top five transcription factors have been implicated in hippocampal development or function (Figure 10C and Supplementary Table 5 in Raus et al.[1])[115-122]. The transcription factors KMT2A and LEF1 have not been previously associated with the effects of exercise on hippocampal function. Interestingly, CREB1 (through its associated CBP[123]) and KMT2A (through its methyltransferase activity[116]) both have histone modifying properties. LEF1 has been shown to regulate neural precursor proliferation in the hippocampus[117]. SMAD3 is critical for intermediate progenitor cell survival and negatively regulates serum insulin after exercise[118,119]. EGR1 is an immediate early gene that recruits TET1 DNA demethylase during neural activation and development[120]. MITF was the sixth upstream regulator identified and is a transcription factor linked to autophagy mechanisms[121]. These specific transcription factors were not significantly differentially expressed in our TRAP-seq dataset; however, their activity may not be linked to a change in their own expression after EX but rather modulated by exercise to influence programs of gene expression.

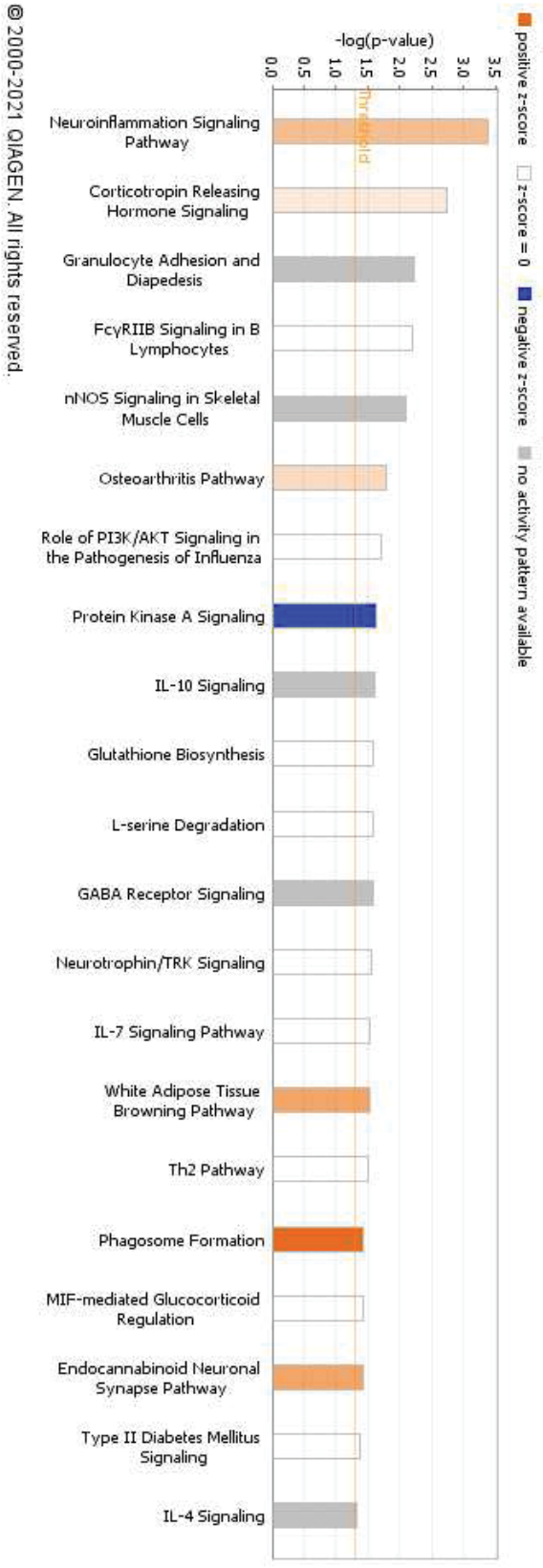

Figure 11: Canonical pathways identified by Qiagen's IPA of genes upregulated by EX.

Figure 11: Canonical pathways identified by Qiagen's IPA of genes upregulated by EX.

Supplementary table 3C and 3D in Raus et al.[1] have the genes identified by the top two pathways listed in this bar chart.

To further understand whether the transcriptional profiles resulting from EX were enriched for specific *a priori* assigned molecular functions, we performed Gene Set Enrichment Analysis (GSEA)[74]. We evaluated the "Reactome" category of functional gene sets followed by a leading-edge analysis to further determine which genes were driving the significant categories (Figure 10D and Supplementary Table 6 in Raus et al.[1]). Of the DEGs upregulated after EX, several interesting categorizations and the genes driving them were revealed. The genes *H3c4*, *H2bc3*, *H2bc5*, and *H2bc9* genes, which encode histone family member proteins, were driving the categories: "DNA methylation", "HDACs deacetylate histones", and "transcriptional regulation by smRNAs". "Meiosis" and "meiotic recombination" also emerged in these results which was unusual; however, leading edge analysis showed many of these genes (*Atm, Blm, Msh4*, and *Mnd1*) to be generally involved in cell-cycling processes. Exercise is well known to increase adult neurogenesis in hippocampal dentate gyrus and can explain cell cycle gene enrichment in our dataset[108]. Several nucleoporin complex genes (*Nup35/ 42/ 43/ 50/ 58/ 62/ 93/ 107/ 153/ 210*) were also identified for their associations with categories such as: "gene silencing by RNA", "nuclear envelope breakdown", and "transport of mature mRNAs derived from intronless transcripts". *Nup* genes form a variety of nuclear pore complexes that play critical roles in cellular processes including cell-cycle regulation, cellular differentiation, and epigenetic control[124].

Of the downregulated pathways identified, translation-associated categories ("translation", "eukaryotic translation initiation/elongation", and "SRP-dependent co-translational protein targeting to membrane") were driven by significant downregulation of ribosomal protein gene families (*Rps*, *Rpl*, *Rplp*) and eukaryotic initiation factor 3 (*eIF3*) subunits. Over-expression of *eIF3* subunits has been linked to neurodegeneration, and altered

expression of *eIF3* has been associated with neurodevelopmental disorders[125]. Additionally, collagen genes (*Col1a1*, *Col1a2*, *Col2a1*, *Col3a1*, and *Col5a1*) were downregulated after EX, leading to the identification of categories including: "MET activates PTK2 signaling", "MET promotes cell motility", and "collagen degradation". *Col1a1* and *Col1a2* have been previously identified as putative aging genes that decrease in their expression after chronic exercise in female adult rodents[126]. By analyzing these enriched pathways and the networks of genes driving them, we were able to identify several expected, as well as unexpected, transcriptional programs activated by EX that could be unique to exercise timing during the juvenile-adolescent period.

Neuronal H4K8ac is enriched and H3K27me3 is reduced at a subset of plasticity genes after EX.

The power of the Emx1-NuTRAP mouse model (coupled with the "SIT" technical approach) is the ability to directly pair differential gene expression with governing epigenetic mechanisms. This is achieved by obtaining both TRAP-seq and epigenomic-sequencing data from the same cell population (Figure 1). To investigate EX-induced changes in histone PTMs across the genome, hippocampal nuclei were obtained from EX and sedentary mice using the INTACT method followed by CUT&RUN-seq for the modifications H3K27me3 and H4K8ac from nuclear chromatin. We chose these two histone PTMs for their previously described functions. H4K8ac is a permissive modification that is enriched at *Bdnf* after adult exercise, and its presence correlates with improved hippocampal memory[20]. H3K27me3 is a repressive histone mark and a common control in CUT&RUN-seq studies[40,127] and is decreased at the *Bdnf* promoter region after contextual fear conditioning training[90]. Peaks were called using SEACR[77] and histone PTM enrichment peaks were overlapped with EX-induced DEGs obtained from our

TRAP-seq experiments described in Chapter 2 (Figure 12A and A'). We evaluated for the presence of H4K8ac and H3K27me3 peaks in union with upregulated and downregulated mRNA as a result of EX. 93 upregulated genes had new H4K8ac peaks, while 35 downregulated genes had new H3K27me3 peaks (Figure 12B and Supplementary Table 7 in Raus et al.[1]). Notably, of those 93 upregulated genes with H4K8ac peaks, 14 also had new H3K27me3 peaks as a result of EX. 17 genes had presence of H3K27me3 in both conditions (ELE and sedentary; Figure 12A). We interpret these results to mean that transcription of these 93 genes was promoted as a result of EX-induced H4K8ac.

The loss of either H3K27me3 or H4K8ac after EX did not substantially correlate with changes in translating mRNA expression (Figure 12B). This result may indicate that EX-induced differential gene expression is associated with the addition, rather than removal, of these two histone modifications. We found one gene that was downregulated and had loss of H4K8ac (*Asphd1*), and two genes downregulated with loss of H3K27me3 (*Fdxr* and *Rtl1*; Figure 12B and Supplementary Table 7 in Raus et al.[1]). Of particular interest, reduced expression of paternally-inherited *Rtl1* is associated with improved hippocampal memory performance, whereas overexpression results in memory deficits[128,129]. Unsurprisingly, the majority of histone PTM peaks newly present as a result of EX did not correlate with gene expression changes. However, notable upregulated genes with new H4K8ac after EX include *Prox1*, *Sntb2*, and *Kptn*. PROX1 is involved governing differentiation, maturation, and DG versus CA3 cell identity in intermediate progenitor cells of the hippocampal DG[130], while SNTB2 is involved in G protein-coupled receptor cell signaling[131]. KPTN encodes a protein involved in cytoskeletal cell structure, and its mutation can cause neurodevelopmental disability and seizures[132]. Interestingly, downregulated genes found to have new H3K27me3 after EX included *Col3a1*, *Efnb2*, *Epop*,

and *Myoc*. COL3A1 and MYOC are structural proteins involved in the extracellular matrix and the cytoskeleton respectively[133-135]. EFNB2 is a signaling molecule involved in cell migration and its haploinsufficiency can cause neurodevelopmental disability[136-138]. EPOP is a known editor of the chromatin landscape by altering H2Bub and H3K4me3 distributions[139,140].

Although changes in gene expression associated with H3K27me3 peaks were less numerous than those associated with H4K8ac, we noticed a striking difference in the distribution of peaks across the genome (Figure 12C). After EX, the distribution of H3K27me3 decreases in the promoter region and increases in the distal intergenic and intronic regions (Figure 12C). To investigate how EX-induced changes to histone PTM distribution might alter gene expression, we looked at the distribution of peaks around *Prox1* (Figure 12D). Most apparent changes in histone PTM peaks occurred in regions annotated as regulatory regions, rather than the promoter region, which is concordant with our data showing that most histone PTM changes happen outside of the promoter region. Taken together, these results suggest that EX promotes the new addition of H4K8ac and H3K27me3 PTMs to regulate gene expression. Given that most identified peaks did not correlate with DEGs, they may instead implicate regions of interest that are "primed" for facilitated gene expression following future stimuli, such as learning.

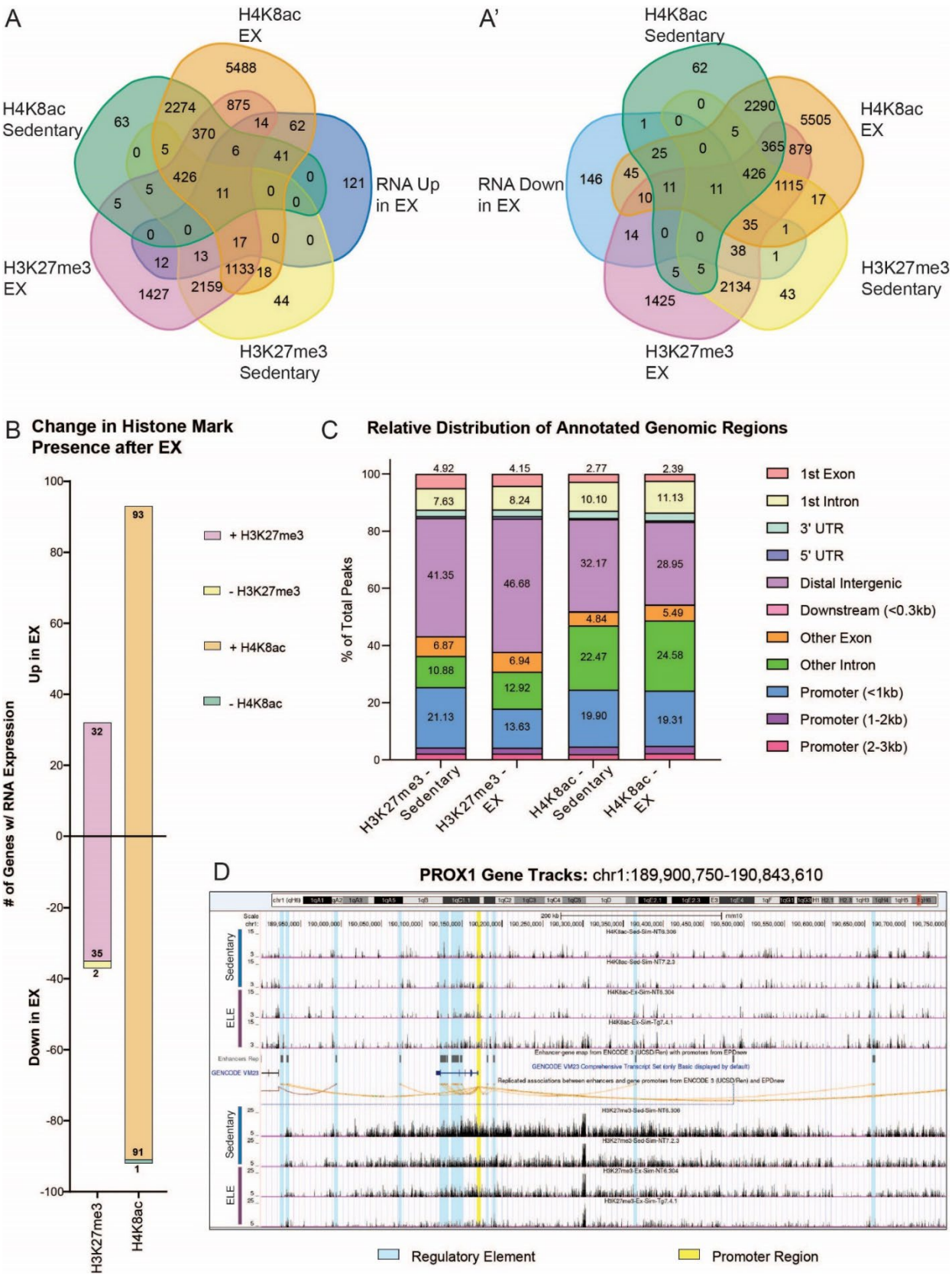

Figure 12: EX alters H4K8ac and H3K27me3 occupancy.

Figure 12: EX alters H4K8ac and H3K27me3 occupancy. (A) Venn diagram of gene peaks identified in CUT&RUN-seq for H4K8ac and H3K27me3 by SEACR (top 1% of peaks FDR<0.1) overlapped with genes upregulated (A) and downregulated (A') in RNA by EX (n=2 sedentary mice and n=3 EX mice). (B) CUT&RUN-seq SEACR peak calls at genes that overlap with genes differentially expressed by EX as determined by TRAP-seq. (C) Stacked bar of the relative distribution of peak calls at various genomic regions identified by CUT&RUN-seq called using SEACR. (D) Representative track of CUT&RUN-seq data around *Prox1* showing differential peak height between EX and sedentary conditions for H4K8ac (top) and H3K27me3 (bottom).

Discussion

This chapter focuses on the impact of exercise on hippocampal gene expression and associated epigenetic modifications specifically during juvenile-adolescent periods (the fourth through sixth postnatal weeks of life in mice). We discovered gene expression programs, and alterations in the histone modifications H4K8ac and H3K27me3, that may be unique to this early-life period. Recently published reports have investigated the effects of voluntary exercise on adolescent and adult hippocampal gene expression and epigenetic modifications through RNA and DNA sequencing methods from heterogenous cell populations[109,110]. Our data revealed several notable genes with either chromatin-modifying or neurogenesis-regulating properties were either upregulated with new H4K8ac (*Prox1*, *Sntb2*, and *Kptn*), or downregulated with new H3K27me3 (*Col3a1*, *Efnb2*, *Epop*, and *Myoc*). One could consider the mechanistic implications for these genes: for example, EX could "prime" the expression of *Prox1* by the addition of H4K8ac, and in turn, subsequent *Prox1* expression can promote neurogenic fate and cell location assignment[141]. EX was also found to alter the expression of *Kptn,* which encodes a protein involved in actin dynamics and neuromorphogenesis[132]. Increased *Kptn* expression could promote cytoskeletal changes occurring with altered synaptic plasticity after exercise. Overall, the differentially expressed genes and their associated chromatin states occurring after EX provide molecular candidates involved in the effects of EX on hippocampal function.

Chapter 4: Early exercise engages histone PTMS to facilitate gene expression and memory consolidation.

Introduction:

Early exercise may "prime" the epigenome to enable memory

The hippocampal memory effects of juvenile exercise (P21-27) demonstrated by our lab[12] persisted two weeks after exercise cessation, which is potentially longer than the effect of exercise on adult hippocampal function[31]. Given Ivy et al.'s previous finding that EX can facilitate long-term memory and increase LTP[12], we hypothesize that this may be due to altering the epigenomic landscape, to ultimately promote a transcriptional state supporting hippocampal memory consolidation. Transcription is required for both hippocampal long-term memory and LTP. LTP is defined as a synaptic plasticity response considered the cellular correlate of learning and memory[142].. The hypothesis that epigenetic mechanisms underlie enabled long-term memory is supported by the finding that in adult rodents, long-term memory is formed in response to a subthreshold learning event after exercise or HDAC3 inhibition and involves increased acetylation of neuroplasticity gene promoters[20]. It is possible that exercise (whether in early life or adulthood) may "prime" hippocampal function for response to future experiences (such as future exercise bouts or hippocampal learning events). Epigenetic mechanisms are strong candidates for the priming effects of exercise: the epigenome could harbor a "molecular memory" of the exercise experience by readying the chromatin landscape for efficient gene expression, thereby modulating neuronal function and behavioral output [20,31]. The specific mechanisms underlying sustained electrophysiological and behavioral effects observed in our

studies of EX have not been assessed from the perspective of a potential molecular memory of EX within the epigenome. In this Chapter, we compare our epigenomic and translatomic EX data from Chapter 3 with gene expression data acquired during hippocampal memory consolidation (and after EX). We identified a network of genes that may underly this primed enabling effect of EX on memory.

Materials and Methods

Much of the materials and methods for Chapter 4 are described in Chapter 2 since much of the data presented in Chapter 4 was collected as a direct result of experiments described in Chapter 2. The exception to that is the behavior paradigm described here.

Behavior

Wild type mice were habituated, handled and then underwent OLM training[143] for either three or ten minutes at P41 as described previously[12]. On postnatal day 36, mice were brought into a testing room with reduced room brightness. Mice were handled for approximately 2 min each, for a total of 5 consecutive days prior to the OLM training session (twice a day for the first 2 days followed by once a day for the next 3 days). Habituation sessions were 5 min, twice per day for 3 days (P39-P41) and occurred within chambers containing four unique spatial cues on each wall of the chamber (horizontal lines, black X, vertical strip, and blank wall). Habituation overlapped with the last 3 days of handling. During the training phase (P42), mice were placed into the same chambers with two identical objects and exposed to either a subthreshold (3 min) or threshold (10 min) training period. Mice were sacrificed for consolidation experiments 1 hour later.

Results

ELE alters H4K8ac and H3K27me3 occupancy at regulatory regions of genes involved in hippocampal memory consolidation.

Prior work from our lab and others has found that both EX and adult exercise can facilitate hippocampal long-term memory formation in mice exposed to a typically sub-threshold learning event (3 minutes of object location memory (OLM) training, which is normally insufficient for LTM formation in sedentary mice)[12,20]. These findings suggest that EX may "prime" neuronal function to facilitate hippocampal learning. In this experiment, we investigate whether EX-enabled hippocampal memory is associated with altered presence of histone PTMs H4K8ac and H3K27me3 in regulatory regions of genes associated with learning and hippocampal plasticity; the prediction being that alterations of histone PTM occupancy as a result of EX could promote gene expression programs necessary for facilitating memory consolidation. Wild type animals underwent EX followed by OLM training on P42 and were sacrificed 60 minutes later (Figure 13A). Dorsal hippocampi were dissected, and tissue was homogenized and processed for bulk RNA-seq. These data were compared to the EX-induced DEGs, H4K8ac, and H3K27me3 occupancy occurring without learning (generated from Emx1-NuTRAP mice TRAP-seq and CUT&RUN-seq). We categorized DEGs based on the experimental group: EX alone, EX+3 min learning stimulus, Sedentary+3 min learning stimulus, and Sedentary+10 min learning stimulus. To discover EX-induced genes "primed" for regulation during memory consolidation, we focused specifically on candidate genes associated with memory after exercise (cGAME), candidate genes associated with memory after exercise or sedentary (cGAMES), and candidate genes associated with memory after sedentary (cGAMS)

conditions (Figure 13B-C and Supplementary Table 8 in Raus et al.[1]). We then evaluated cGAME and cGAMES groups of genes for the new presence or absence of histone modifications H4K8ac and H3K27me3 after EX, suggesting addition or removal of these histone marks denoting a permissive (increased gene expression) or repressive (reduced gene expression) chromatin state, respectively (Figure 13B'-C' and Supplementary Table 9 in Raus et al.[1]).

In the cGAMES group, there were 145 genes found to be significantly increased in the mice that underwent a threshold learning event (3 min for EX; 10 min for sedentary mice). Of these 145 genes, 40% of them (58) had new H4K8ac following EX, whereas 87 genes had no change in the histone PTMs evaluated in this study (Figure 13B-B'). We consider the group of 58 genes to potentially be "primed," or readied, by EX for rapid transcription to support hippocampal memory consolidation at 3 min OLM training, while also being involved in memory consolidation mechanisms in the threshold learning of sedentary mice (10 min OLM training). The cGAME group of genes are those which significantly increased in the EX mice that underwent a threshold learning event but were not increased in any of the other groups (including the sedentary, threshold learning event / cGAMS group and cGAMES group). These genes may be of unique importance for memory consolidation specifically occurring after EX given their absence in sedentary learners. We found that the cGAME group had significant upregulation of 256 genes, with approximately 30% (76) of those genes receiving new H4K8ac following EX alone (Figure 13B-B'). We also evaluated the cGAMES and cGAME that were significantly downregulated during memory consolidation. We found 304 cGAMES and 361 cGAME genes (Figure 13C). In both of these groups, a small minority of down-regulated genes had altered H3K27me3 after EX, and this was mostly gain of H3K27me3 (cGAMES: 6.3%; cGAME: 6.4%) (Figure 13C'). Notably, we did not find any genes that were upregulated during

memory consolidation and had new H3K27me3 in the cGAME and cGAMES groups and no genes that were downregulated had new H4K8ac in the cGAME and cGAMES groups

We next wanted to determine how EX "priming" directed gene expression during memory consolidation that occurs after exercise (ELE 3min OLM) relative to sedentary memory consolidation (Sed 10min OLM). We compared these to the group that experienced the sub-threshold learning event (Sed 3min OLM). We compared the relative log2 fold changes (LFCs) of the genes in cGAME and cGAMES using z-scores for each group across the genes (Figure 13D). In the vast majority of these primed genes, the EX drove gene expression during 3 min of OLM training in the same direction as 10 minutes of OLM training in sedentary animals (Figure 13D). In some cases, the gene expression changes after EX were more exaggerated in the same direction as a sedentary threshold event (Figure 13D). We interpret this to indicate that EX enables a 3min consolidation event to be threshold (when 10 minutes is required for a sedentary mouse) by priming these genes for altered gene expression in the same direction as a sedentary threshold event.

We next identified upstream regulators of cGAME and cGAMES genes with EX-induced histone modifications, as these mediators are likely involved in long-term memory formation of a subthreshold learning event following EX. The cGAMES and cGAME lists were evaluated using Qiagen's Ingenuity Pathway Analysis (IPA). First, candidate regulators were identified for the cGAME and cGAMES groups that have histone PTM changes as a result of EX that we measured (Figure 13E and Supplementary Table 10 in Raus et al.[1]). Inhibition of MECP2 may indicate a reduction in DNA methylation. CREB1 is required for LTM[115,144]. SNCA may play a role in neuroplasticity by modulating synaptic vesicle transport[145].

Next, we wanted to identify gene networks that might be at play that are not just regulated by the histone PTMs we selected. Many more histone modifications exist and may regulate gene expression during consolidation in addition to those we selected. We investigated the genes in cGAME and cGAMES using IPA and identified a set of likely upstream regulators for these genes taken together (Figure 13E'' and Supplementary Table 10 in Raus et al.[1]). Once again MECP2 inhibition and CREB1 activation appear to be indicated validating their presence in the previous IPA. Notably new to this group are inhibition of FMR1, KMT2D, and TCF20, along with activation of FASN, CTNNB1, and MKNK1. Next, we interrogated what networks might be unique to exercise-enabled consolidation by running the cGAME list through IPA analysis (Figure 13E' and Supplementary Table 10 in Raus et al.[1]). Unique to this group, RTN4, an inhibitor of neurite outgrowth[146], was predicted to trend towards inhibition. GRIN3A, a glutamatergic NMDA receptor important to synaptic development and refinement[147], was predicted activated in this group. These findings suggest that EX may enable consolidation by increasing neurite and synapse growth and development. TCF7L2 is also predicted to be activated. Given that this transcription factor is involved in Wnt signaling, and neurogenesis[148], and activated CTNNB1 is also predicted to be associated with threshold consolidation generally, altered Wnt signaling may be critical for EX enabled consolidation.

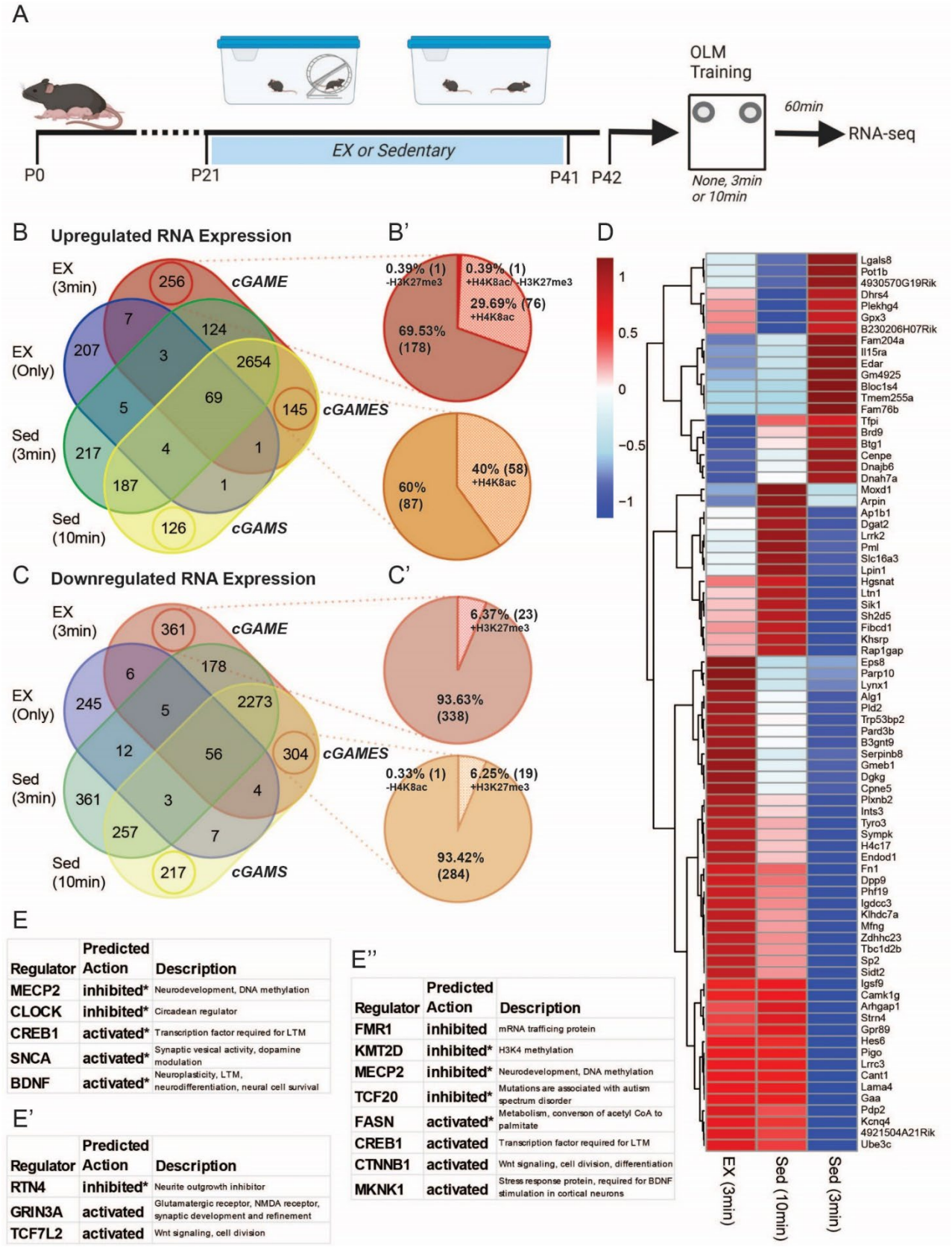

E

Regulator	Predicted Action	Description
MECP2	inhibited*	Neurodevelopment, DNA methylation
CLOCK	inhibited*	Circadean regulator
CREB1	activated*	Transcription factor required for LTM
SNCA	activated*	Synaptic vesical activity, dopamine modulation
BDNF	activated*	Neuroplasticity, LTM, neurodifferentiation, neural cell survival

E'

Regulator	Predicted Action	Description
RTN4	inhibited*	Neurite outgrowth inhibitor
GRIN3A	activated	Glutamatergic receptor, NMDA receptor, synaptic development and refinement
TCF7L2	activated	Wnt signaling, cell division

E''

Regulator	Predicted Action	Description
FMR1	inhibited	mRNA trafficing protein
KMT2D	inhibited*	H3K4 methylation
MECP2	inhibited*	Neurodevelopment, DNA methylation
TCF20	inhibited*	Mutations are associated with autism spectrum disorder
FASN	activated*	Metabolism, converson of acetyl CoA to palmitate
CREB1	activated	Transcription factor required for LTM
CTNNB1	activated	Wnt signaling, cell division, differentiation
MKNK1	activated	Stress response protein, required for BDNF stimulation in cortical neurons

Figure 13: EX may prime consolidation-induced gene expression.

Figure 13: EX may prime consolidation-induced gene expression. (A) Experimental design diagram. (B) Venn diagram representing upregulated genes relative to mice without EX or learning in either EX, EX and 3 min OLM training, Sed and 3 min OLM training, and Sed and 10 min OLM training. (B') Pie chart showing the relative percentage of genes that have new H4K8ac presence or H3K27me3 loss as a result of EX in specific groups identified in the Figure 13B labeled cGAME and cGAMES. (C) Same as Figure 13B but for downregulated genes relative to mice without EX. (C') Pie chart of downregulated genes in the cGAME or cGAMES groups that have new H3K27me3 or new loss of H4K8ac as a result of EX. (D) Z-score based heatmap of genes in the cGAMES and cGAME groups that have new H4K8ac or H3K27me3 presence or loss as a result of EX. Expression values used to calculate the Z-scores were relative to mice that did not experience OLM training or EX. (E) Upstream regulators identified by IPA of the genes represented by Figure 13D. (E') Upstream regulators identified by IPA of the genes in the cGAME (up and downregulated) group that are unique to that when only those are included in the IPA analysis. (E'') Upstream regulators identified by IPA of the genes in the cGAME and cGAMES (up and downregulated) group when the genes in those groups are put through IPA together. (* indicates that the activated or inhibited indicator is registered from the IPAs based on the z-score for that regulator's expression and not directly indicated based on software prediction).

Discussion

This chapter identified, for the first time, novel gene expression networks and their epigenetic regulation that may be involved in the hippocampal memory benefits of EX. We also identified a group of genes that are altered in their gene expression only in sedentary animals undergoing a threshold learning event ("cGAMS" group). The separation of this group from the cGAME and cGAMES groups indicates that EX may engage a separate, perhaps complementary network of genes to promote memory consolidation. We also identify a subset of cGAME and cGAMES genes that appears to support a "priming" model of EX induced epigenetic changes and their impact on memory. Genes that have altered hPTMs after EX and underwent 3min training have gene expression driven in the same direction as sedentary animals undergoing a ten min learning event. 3 min of training is on average insufficient to encode a long-term memory in a sedentary mouse but sufficient for anEX mouse whereas 10 min of training is on average sufficient[12,20]. A next step of this work will be to test the necessity and sufficiency of identified genes and gene networks, their histone modifications, and/or their upstream regulators mediating the effects of EX on hippocampal memory performance. Another unanswered question is how long the memory-promoting effects of EX last after exercise cessation, and whether there is stability of EX-induced epigenetic modifications to allow for the persistence of EX effects.

Chapter 5: Developing a method for individual tracking of group housed juvenile mice.

Introduction:

The need for a method for individually tracking voluntary wheel running of pair housed juvenile mice

The lack of techniques to monitor exercise in group-housed mice has also been a major gap in the field of exercise research and a particular impediment to investigation into the effects of exercise in early-life time points. Because studies involving voluntary exercise usually require comparison of individual running amounts, the traditional approach is to individually housed and track mice[149,150]. However, mice are social animals and solitary housing could increase the stress of the mice[151,152]. Since stress has a major impact on the cognitive development of rodents in early life[153], investigating the effects of exercise in this way could complicate interpretation of results. To address this difficulty, I helped develop a novel method for tracking voluntary wheel running in group-housed juvenile mice[154]. This method will allow for studying the effects of exercise, as well as exercise amount, in early life without the possible confound of isolation stress.

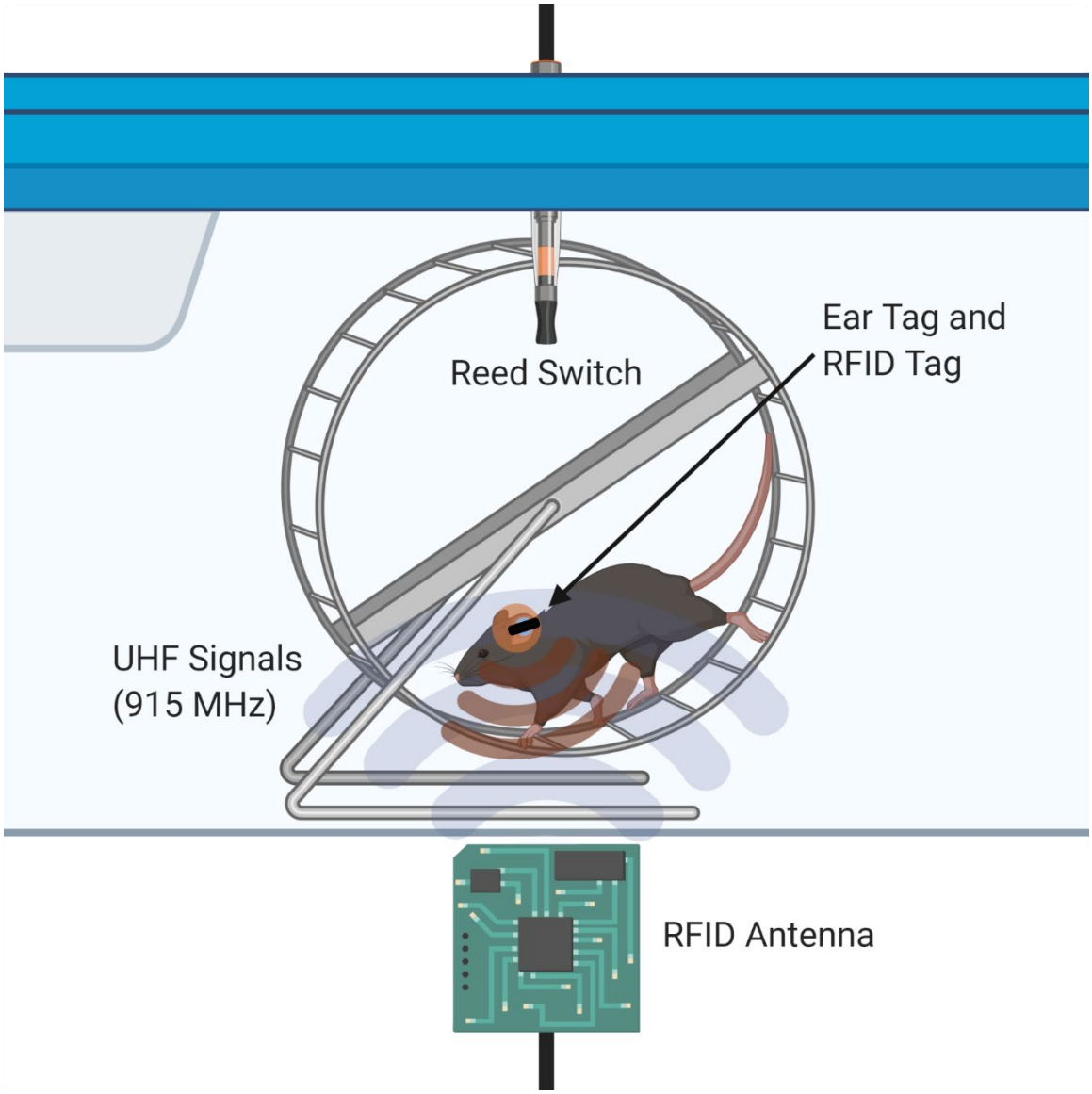

Figure 14: Illustration of dual RFID and Vital View system for individual mouse running in pair-housed cage.

Materials and Methods

Animals

Mice were progeny of C57Bl6J dams obtained from Jackson Laboratories and were bred, born, and reared in our vivarium. Mice had free access to food and water and lights were maintained on a 12-hour light/dark cycle. Upon weaning on postnatal day (P) 21, mice were pair-housed in standard cages with free access to an in-cage stainless steel running wheel equipped with a plastic net fitted around the rim for the safety of the juvenile mice. All mice are typically 6g-9g at time of weaning. Tracking was conducted continuously 24 hours a day for three weeks from P21-41. All experiments were conducted according to US National Institutes of Health guidelines for animal care and use and were approved by the Institutional Animal Care and Use Committee of the University of California, Irvine.

Materials and Reagents

1. UHF RFID Tag for Metal Product Management (Murata Manufacturing Co: LXTBKZMCMG-010)
2. Command™ Small Poster Strips (3M Company: 17024ES)
3. Pegboard, 5/32” thickness, holes spaced 1” apart
4. LOCTITE® SUPER GLUE PRECISION PEN (Henkel Corp: 2066118)
5. Netting material (Industrial Netting: Vexar: NG3060-164)
6. Ear Tag, Mouse, Light Blue, 1-100 (Stoelting Co: 56782)
7. Ear Tag, Backing only, Pk/100 (Stoelting Co: 56792)
8. Etching Engraver Pen (Porsin: LX1323)

9. Jackson mice WT C57Bl6J (Jackson Laboratories: 000664)
10. Teklad 1/8” Corncob Bedding (Envigo, Teklad: 7092A)
11. Cotton Nestlets (Ancare nestlets)
12. Teklad Global Soy Protein-Free Extruded Rodent Diet (Envigo, Teklad: 2020X)

Equipment

1. RFID Passive Antenna (Abracon LLC: ARRAN5-915.000MHz)
2. L-Size Mouse Cage Body – 36.5 x 20.7 x 14.0 cm - Polycarbonate (Tecniplast Group: 1284L001; sourced from Starr Life Sciences)
3. Autoclavable Filter Top (Tecniplast Group: 1284L-400SU; sourced from Starr Life Sciences)
4. 4.5" Running wheel with reed switch (Bio-Lynx scientific equipment, Inc.: 610-0003-00; sourced from Starr Life Sciences)
5. MMCX (J)-LL100HF-RPTNC (M) 60" Cables (Federal Custom Cable, LLC: SCA1086-60)
6. Ear Tag, Applicator (Stoelting Co: 56791)
7. Keonn AdvanReader-160 UHF RFID Reader (4-Port) (Keonn Technologies: ADRD-M4-ESMA-160.01)
8. AdvanMux-8 UHF RFID Multiplexer (8-Port) (Keonn Technologies: ADMX-8-e-110.04)
9. CAT5 Ethernet Cable
10. USB 3.0-to-Gigabit Ethernet Adapter (Best Buy Co., Inc., Insignia: NS-PU98635-C)

11. Power Over Ethernet Injector (Phihong: PSA16U-480(POE); sourced from Keonn Technologies)
12. SMA Male to SMA Male 24" Cable (Bracke Manufacturing, LLC: BM92046.24)
13. Data Port 24 channel box (Starr Life Sciences)
14. Data Port USB Cable (Starr Life Sciences)
15. Electric Drill
16. Table Saw
17. 5/32", 3/16" Drill Bits
18. Two Laptops (one for each software program) with the following requirements:
    i. Minimum Requirements for VitalView®: Windows PC (Windows XP or newer), 2 GHz Processor, 2 GB Ram, 800 MG Free Hard Disk space, USB port.
    ii. Minimum Requirements AdvanNet™ Software: Firefox or Chrome browser, Internet connection, USB port.
19. Computer (for IndividualRFIDELEMus program)
    i. Minimum Requirements: Windows 10, 12 GB of RAM

Software

1. AdvanNet™ Software (Keonn Technologies, S.L.)
2. VitalView® Activity Data Acquisition Software (Starr Life Sciences Corp)
3. IndividualRFIDELEMus program (IndividualRFIDELEMus)

Procedure

A. RFID Antenna Setup (Figure 2)

1. Cut 2” x 2” pegboard squares for each cage with two holes inside each square: Take the pegboard and draw lines to make cuts orthogonally such that:
    a. One set of lines runs across every other hole.
    b. The other set of lines runs ½” between every other hole.
    c. Using a table saw, carefully cut through the lines (Figure 15A).
2. Place the pegboard square white-side-up. Using a drill and a 3/16” drill bit, drill diagonally through one of the holes such that the angled hole points away from the center of the square (distal end on the bottom). Repeat this process for every square. *Note: The purpose of this step is to make the existing pegboard hole wider for the antenna head lie flat on the pegboard, once the antenna wire is thread through.*
3. Thread the wire of an antenna through the angled hole of a pegboard square such that the wire comes out the bottom (brown side). Have the base of the antenna cover both holes as much as possible.
4. Place a double-sided Command™ strip on the surface of the pegboard, covering the hole opposite to the hole that the antenna wire is threaded through. Affix the base of the antenna to the top (white side) of the pegboard square to the double-sided Command™ strip (Figure 15B).

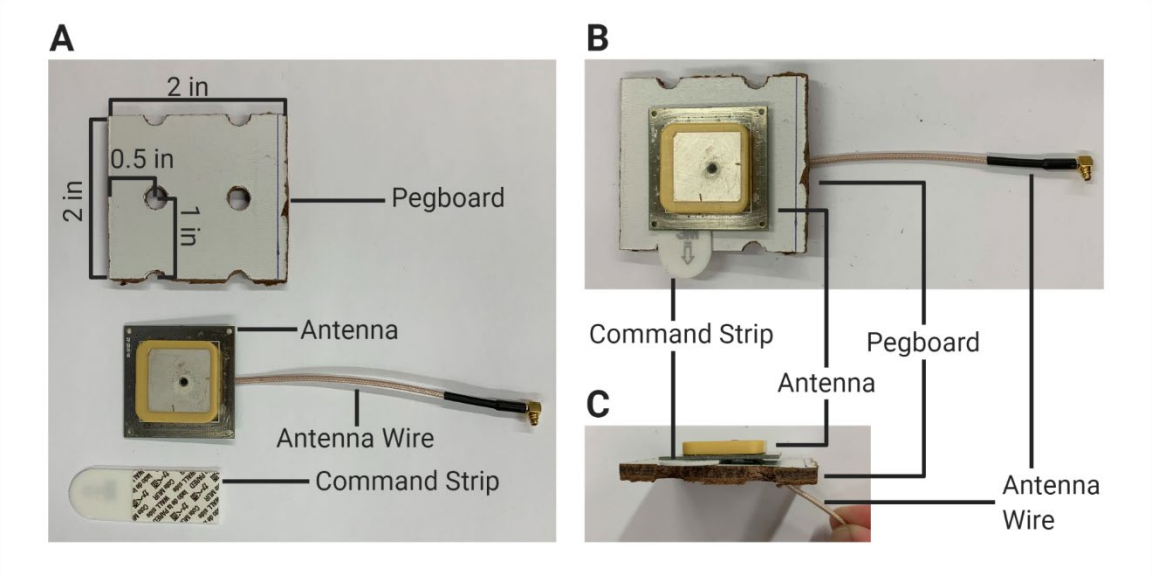

Figure 15. RFID antenna setup.

Figure 15. RFID antenna setup. A) Proper dimensions of the pegboard square in relation to the antenna and Command™ strip. B,C) Proper assembly of the antenna + pegboard square in top-down (B) and side profile (C) views.

B. Cage Setup (Figure 16)

1. Pre-determine and assign two mice of the same sex for each running cage. Plan to construct RFID-compatible running cages based on number of mouse pairs for your study.
2. Position the wheel housing on the underside of wire lid adjacent to the food hopper of the Techniplast cage so that:
    a. The wheel is in front of and to the left of the food and water area.
    b. The left edge of the wheel housing is three slots away from the left edge of the cage.
    c. The screw of the housing is flush with the crossbar closest to the hopper.
    d. The slot for the reed switch faces toward nearest wall of the cage.
    e. Then screw the washer and wingnut onto the screw to affix the housing to the wire lid (Figure 16A).
3. Using scissors, cut a strip of netting material the width of the running wheel such that the mesh fits around the outer rim of the wheel. This is used so the limbs of the small juvenile mice do not fall through rungs of wheels. *CAUTION: Ensure that this fit is precise. Improperly fit netting (when cut too narrow) can slide on wheel and potentially injure the mouse tail*.
4. Unscrew the axle of the wheel housing, place the wheel inside the housing with the wheel magnet facing outward, and thread the axle through the housing and the wheel, screwing the axle cap back on.
5. Place the assembled RFID antenna + pegboard square directly underneath the wheel in its cage (aim the wire end of the antenna toward the back wall of the cage) and secure

the antenna + pegboard square into place with a double-sided Command™ strip. Mark a circle with the diamond-tipped pen next to where the hole with the wire is (Figure 16B). Take away the antenna-pegboard square by pulling out the Command™ strip laterally.

6. Flip over the cage such that the base is on top. Using the drill and a 5/32” drill bit, drill the spot that was marked. When a complete hole has been made, use the 3/16” drill bit to widen the hole. Drill diagonally through the hole such that the hole exit on the bottom of the cage points toward the back wall. *Note: steps 1-6 only need to be performed once for each cage.*
7. Flip over the cage to an upright position. Place the antenna + pegboard square back into the cage. Thread the antenna wire through the hole such that the wire points out of the bottom of the back wall. Readjust the antenna + pegboard square until it is squarely under the wheel. Affix the bottom of the pegboard to the cage bottom using a double-sided Command™ strip (Figure 16C). *Note: In subsequent assemblies using pre-drilled cages, the orientation of the antenna can be modified to a non-orthogonal position with respect to the cage base. It is crucial to ensure the center of the antenna is directly under the center of the wheel*.
8. Add a thin layer of bedding to the cage bottom until the bedding submerges the pegboard but not the antenna. Add two nesting squares into the bottom of the cage, away from the wheel. Place the wire lid with wheel over the cage such that the wheel lies above the antenna with adequate clearance (Figure 16D). Cover the cage with the filtered cage top.

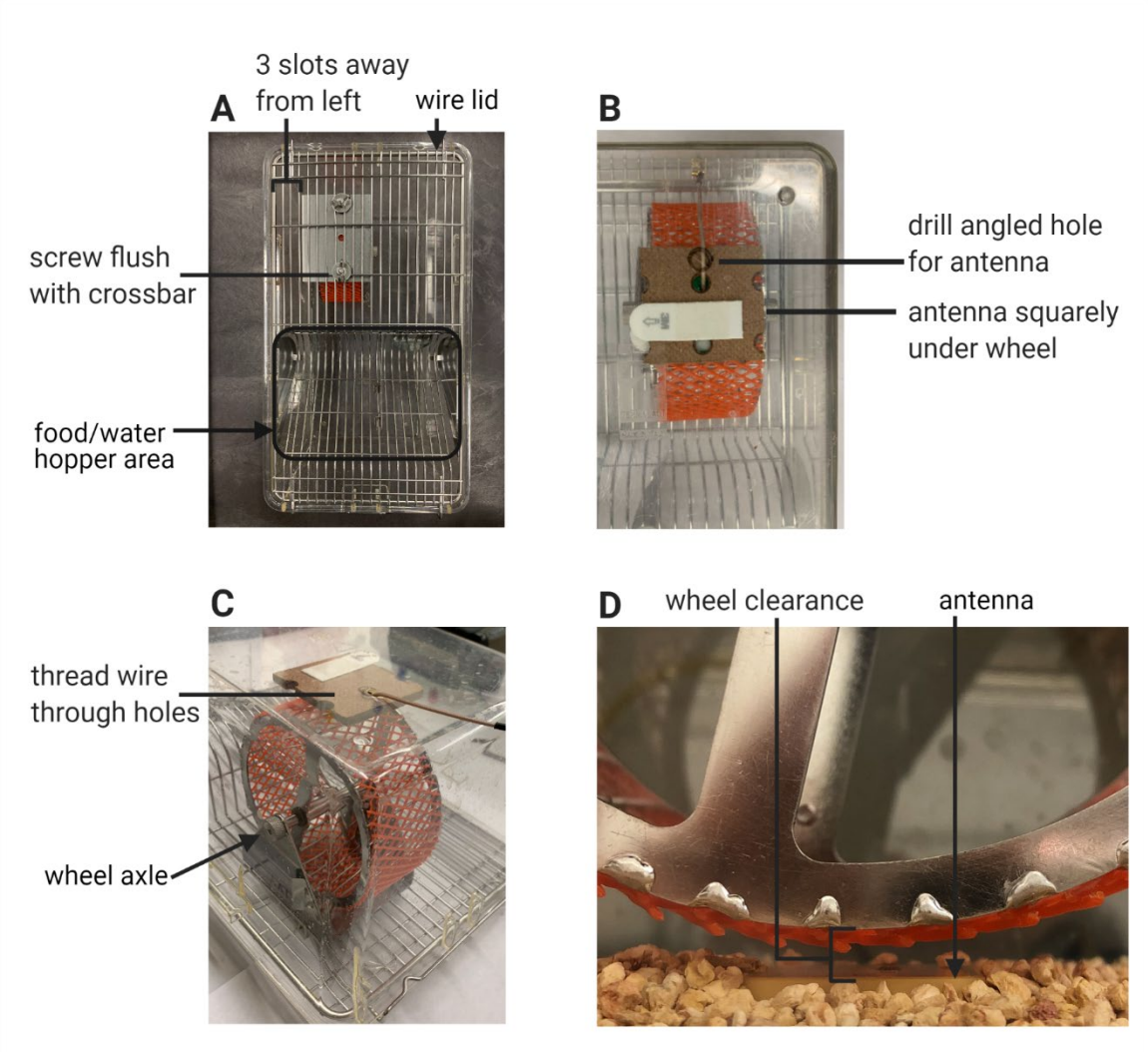

Figure 16. Individual RFID tracking cage setup.

Figure 16. Individual RFID tracking cage setup. A) Proper assembly of the wheel housing in relation to the wire lid and cage layout. B) Bottom-up view of the Techniplast cage showing the area under the wheel. Proper placement of the antenna + pegboard square under the wheel. The drill site is adjacent to the wire exit hole of the pegboard, and is indicated by the black circle drawn on the cage bottom. C) Threading of the antenna wire through the cage hole. D) Clearance between the antenna and the wheel.

C. RFID + VV System Setup (Figure 17)

1. Set up the VitalView® system and RFID reader system per the manufacturer's instructions. Initialize as many VitalView® channels and RFID antennas as you anticipate possibly needing at one time. Keep the data recording configurations for each system default such that recording intervals for VitalView® are less than or equal to 1 minute, and the channel names remain numeric and sequential (1-24). Using one VitalView® system (24-port), one RFID Reader (4-port), and three RFID Multiplexers (8-port), a maximum of 24 cages can be equipped for individual tracking.
2. Connect one antenna wire to one port on the RFID reader or multiplexer using the 60" LMR 100 cables (Figure 17).
3. Thread one reed switch into the reed switch slot in each running cage. Plug the other end of the reed switch cable into the port on the VitalView® box (Figure 17). Test your wheel setup by spinning the running wheel and adjust the depth of insertion of the reed switch until wheel revolutions are recorded by the VitalView® system.

Note: The configuration with one RFID reader and one multiplexer can track 11 cages at a time with two mice in each cage. Additional multiplexers can be added to increase the capacity of simultaneously recording cages.

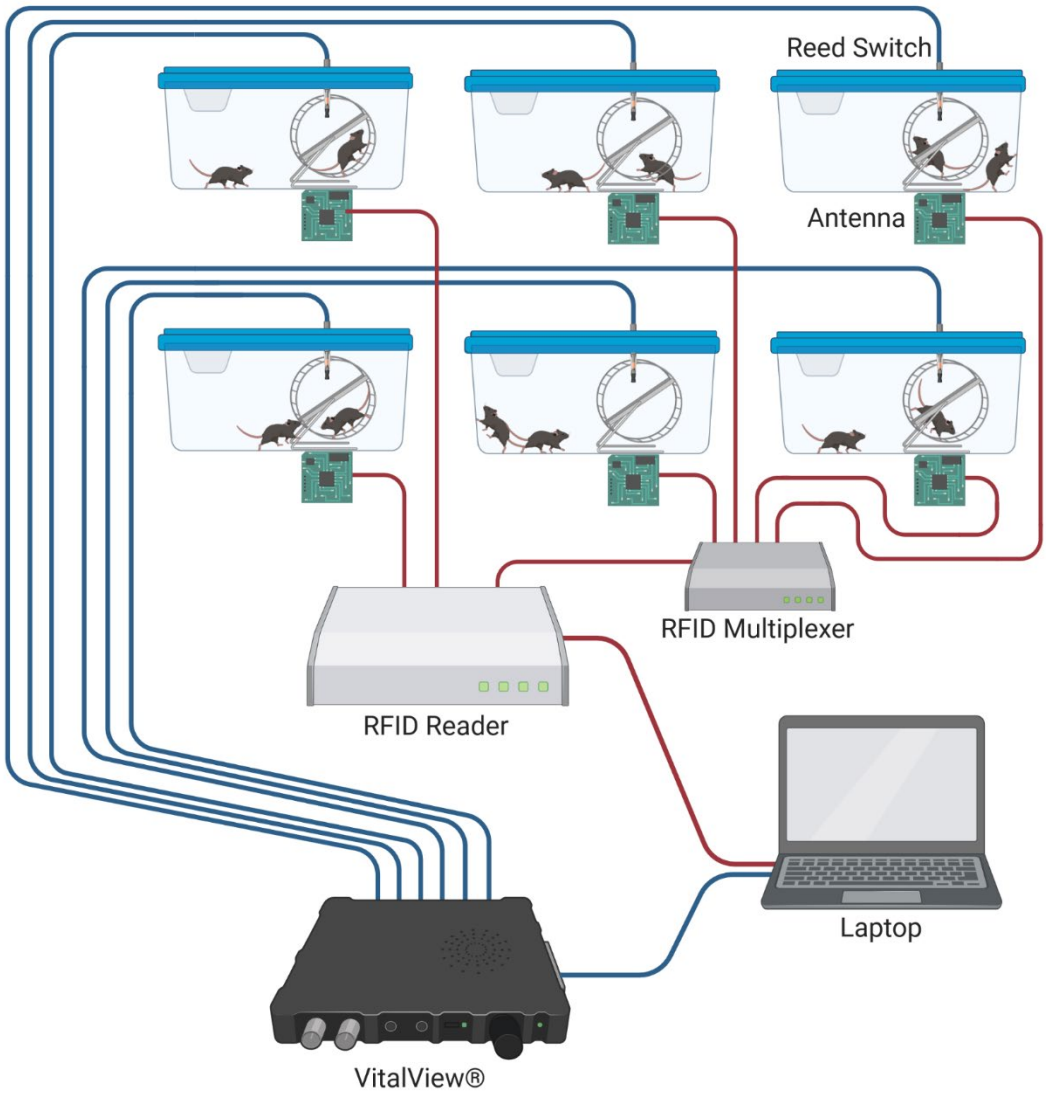

Figure 17. RFID + VitalView® system setup.

Figure 17. RFID + VitalView® system setup. Schematic of data feeds from parallel RFID and VitalView® systems. RFID reader connections can be expanded to multiple cages using an RFID multiplexer. Each RFID antenna is connected to the reader or multiplexer via a 60” LMR 100 cable. We typically use separate computers for VitalView® and RFID reader software (AdvanNet™ Software) programs.

D. Mouse Tagging (Figure 18)

1. Etch each RFID tag based on cage number (e.g. 1,2, …) and animal ID within a cage (e.g. A, B) using the diamond-tipped pen.
2. On the laptop using the RFID software (instructions in AdvanNet™ User Guide), change an RFID tag's EPC code to e00000000000000000001A, e00000000000000000001B, e…2A, e…2B, etc. based on the tag number that was etched into it (Figure 18A). Assign these numbers, as well as the mice, so that they match the channel names 1-24 from the VitalView® channels; e.g., mice tagged 1A and 1B must be in the cage connected to VitalView® channel 1, and so forth.
3. Scruff the P21 mouse. Using the Stoelting ear tags and ear tag applicator, tag each mouse on one ear (Figure 18B). Alternate ears (left vs right), if possible, for easy visual identification of pair-housed mice.
4. Place a small drop of super glue on the green base of an RFID tag (Figure 18C). Using the tweezers, carefully affix the glued side of the RFID tag onto the Stoelting tag on the mouse ear. Holding the RFID tag and ear tag in place between the tweezer tips, let the glue dry for approximately 30 seconds (Figure 18D).
5. Place the mice in the cage. Ensure that mice 1A and 1B, indicated by the EPC code of the RFID tag affixed to them, are in the cage connected to VitalView® port 1. Repeat with other cages.

Note: It is recommended that daily in-person monitoring is performed to identify and prevent the possibility of jammed wheels or insecure or fallen tags. These are infrequent occurrences in our experience, however they can introduce error in the data collected if

not addressed quickly. These issues can be easily remedied with proper supervision of the apparatus to maintain high data accuracy.

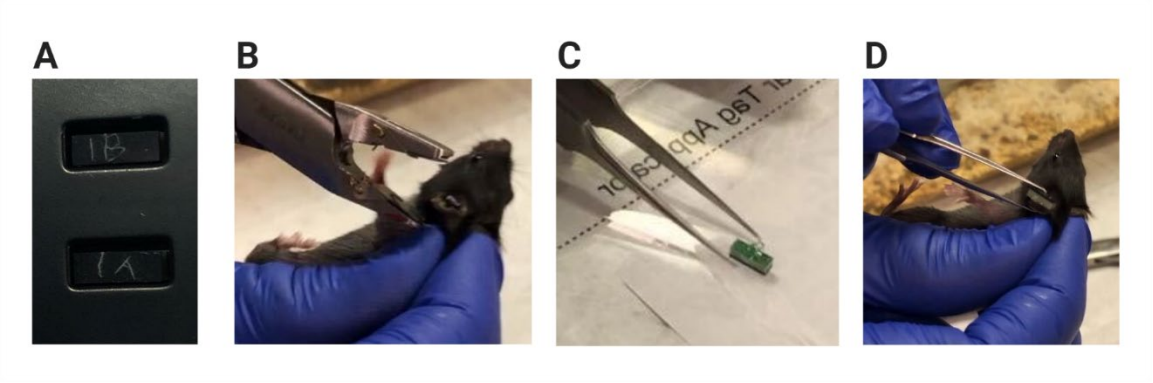

Figure 18. RFID mouse tagging.

Figure 18. RFID mouse tagging. A) Example of RFID tags etched with their new EPC designation. B) The mouse is scruffed and an ear tag is attached to mouse's left ear. C) Super glue has been added to the base of the RFID tag and the RFID tag can be picked up with the tweezers. Only a minimal amount of super glue is needed to affix the RFID tag to the ear tag. D) The RFID tag is applied to the ear tag and held in place for about 30 seconds to allow for the glue to dry.

E. RFID Cage and Antenna Reuse

1. Once experiment is completed, unplug the antenna from the LMR100 cable. Remove the antenna + pegboard square by pulling the Command™ strips laterally. Dispose of the pegboard. Save the antenna and wash carefully with a water and sponge.
2. Pre-drilled cages and washed antennae may be reused for future experiments. A new pegboard square must be used for each cage.

Data Analysis

A. Aligning VitalView® and RFID raw data to generate individual running distances (Figure 19,21)

Note: Wheel revolutions are determined minute-by-minute per cage by the VitalView® Activity Software and exported as a .csv file. For each RFID-tagged mouse, individual tag reads are logged by the RFID reader and exported as a .csv file via the AdvanNet™ Software.

1. Per manufacturers' instructions, export data from the VitalView® system and AdvanNet™ Software. The AdvanNet™ Software automatically names the file "data.csv". The VitalView software is named according to user designation.
2. Make six new directories (folders) for holding your files during processing. These directories will accept and store files for (suggested names): 1) VV Input 2) RFID Input, 3) VV Output, 4) RFID Output, 5) Distances, and 6) Stats.
3. Place the Vital View export .csv file(s) into the "VV Input" directory.
4. "Preprocess" the RFID data file before proceeding: The RFID export .csv data file needs to be reformatted (preprocessed) in order for the program to align it with VV data. Open

the RFID export .csv file in Microsoft Excel (Figure 20A). Locate the time stamp column (in our case, column L). Convert the number format of the column to "MM/DD/YY HH:MM" (use a 24-hour clock). Select and cut the whole timestamp column and paste it into column B to the left of the EPC column (in our case, column C). Delete all columns except the timestamp and EPC columns such that the timestamp column is column A and the EPC column is column B. Select the whole timestamp column, sort by oldest to newest, and expand the selection. Insert a new row 1. In cell 1A, write "TIME_STAMP" and in cell 1B, write "HEX_EPC" (Figure 20B). If these words appear anywhere else in the document, delete those rows and keep only the words written into row 1. Save the excel sheet as a new "preprocessed" export .csv file and place it in the "RFID input" directory.

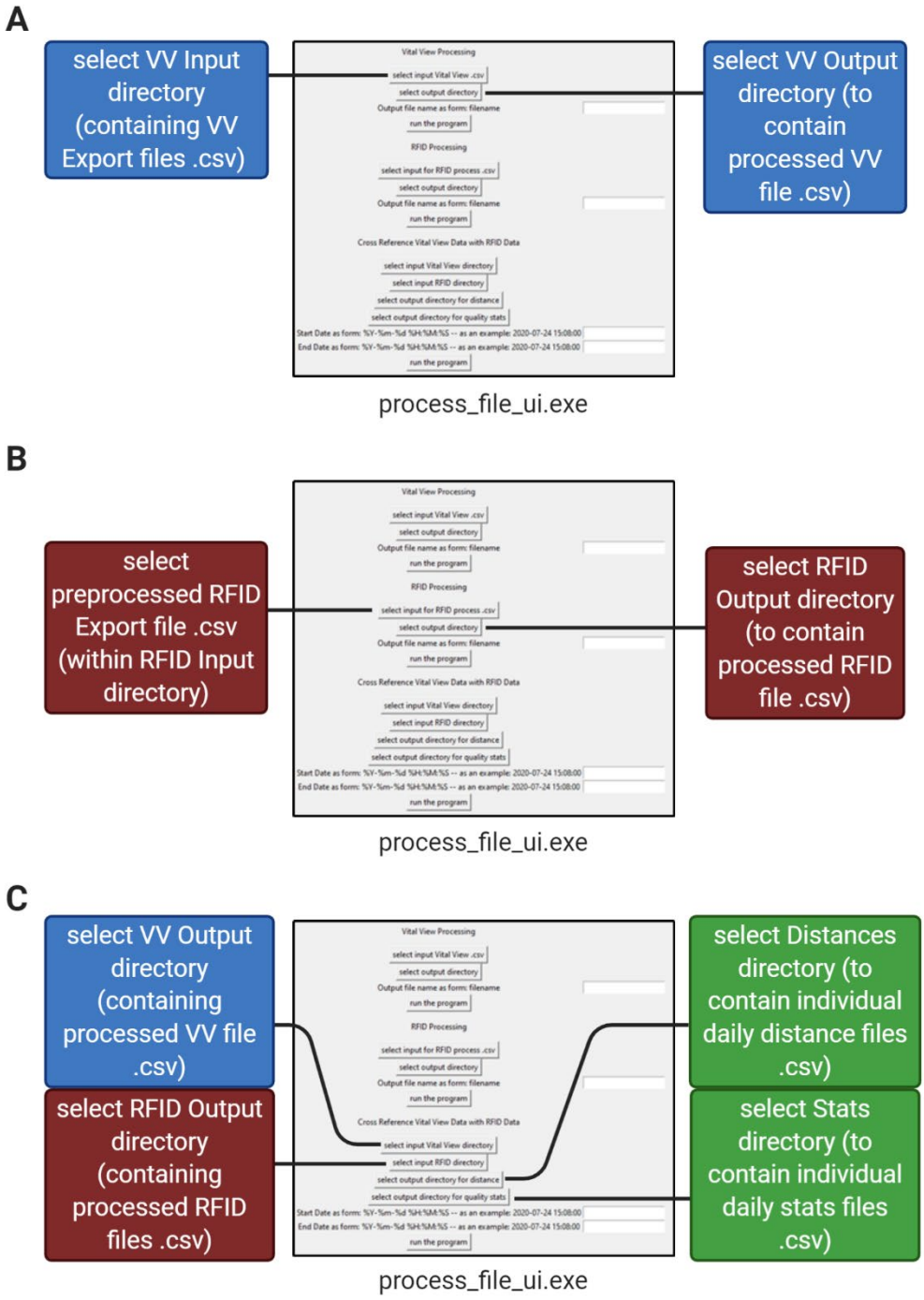

Figure 19: Individual tracking data processing pipeline in 3 steps.

Figure 19. Individual tracking data processing pipeline in 3 steps. Illustration of the pipeline processing RFID export and VV export files using the *process_file_ui.exe* program. A) Step 1: Processing of Vital View files from input directory. B) Step 2: Processing of RFID export data. C) Step 3: Cross-referencing of RFID and Vital View files into individual daily distances and daily error rates.

5. Open the project “Individual RFIDELEMus” on GitHub (downloadable link can be found in the above “Software” section). Use the RFID code program, *process_file_ui.exe*, to process the data in three steps:
    a. The **“Vital View Processing”** section of the *process_file_ui.exe* program collects one or multiple Vital View export files in the VV input directory and combines them into one processed file. The Program then resamples the data over 1 minute time intervals so that the data can be directly compared to the RFID data. *Ensure the VV input directory only contains Vital View export files.* Select the “VV input” directory as your input and select the “VV output” directory as your output. Type in a name for your output VV file and run this section of the program (Figure 19A). The output file will be written to the “VV output” directory (Figure 20C).
    b. The **“RFID Processing”** section of the *process_file_ui.exe* program accepts a preprocessed RFID file .csv and bins its tag reads into rows of minutes for each mouse (each mouse has its own column) based on their unique EPC code. Select the preprocessed RFID data file in the “RFID Input” directory as your input and select the “RFID Output” directory as your output (Figure 19B). Type in a name for your output RFID file and run this section of the program. The output file will appear in the “RFID Output” directory (Figure 20D).
    c. The **“Cross Reference Vital View Data with RFID Data”** section of the process_file_ui.exe program assigns the sum of the number of wheel revolutions within each 1-minute interval to the mouse in the cage with the most tag reads during that minute. It then converts wheel revolutions to distances ran (using our running wheel diameter of 4.5 inches), and outputs individual running distances as one .csv

file per day (for example, if you recorded for seven days, there will be seven separate files in the output directory) (Figure 20E). Select the “VV Output” directory (containing the file from step 1) as your VV input to the program and select the “RFID Output” directory (containing the file from step 2) as your RFID input to the program. Select the “Distances” directory as your Distances output and select the “Stats” directory as your Stats output. Provide dates and times in “YYYY-MM-DD HH:MM:SS” (24-hour) format for the start and end of the desired data processing and run this section of the program (Figure 19C, 22A, 22B).

A

	A	B	C	D	E	F	G	H	I	J	K	L	M
1	TAG_READ		e0000000000000000000003b			AdvanReader-m4-160	192.168.1.123	4	0	0		20:00.7	-70
2	TAG_READ		e0000000000000000000003b			AdvanReader-m4-160	192.168.1.123	4	0	0		20:02.0	-61
3	TAG_READ		e0000000000000000000003b			AdvanReader-m4-160	192.168.1.123	4	0	0		20:03.5	-62
4	TAG_READ		e0000000000000000000003b			AdvanReader-m4-160	192.168.1.123	4	0	0		20:04.8	-72
5	TAG_READ		e0000000000000000000003b			AdvanReader-m4-160	192.168.1.123	4	0	0		20:05.9	-67
6	TAG_READ		e0000000000000000000003b			AdvanReader-m4-160	192.168.1.123	4	0	0		20:07.0	-61
7	TAG_READ		e0000000000000000000003b			AdvanReader-m4-160	192.168.1.123	4	0	0		20:08.1	-62
8	TAG_READ		e0000000000000000000003b			AdvanReader-m4-160	192.168.1.123	4	0	0		20:10.6	-62
9	TAG_READ		e0000000000000000000003b			AdvanReader-m4-160	192.168.1.123	4	0	0		20:11.7	-70
10	TAG_READ		e0000000000000000000003b			AdvanReader-m4-160	192.168.1.123	4	0	0		20:13.0	-66

B

	A	B	C	D
1	TIME_STAMP	HEX_EPC		
2	8/31/2020 21:41	e0000000000000000000004a		
3	8/31/2020 22:06	e0000000000000000000003b		
4	8/31/2020 22:07	e0000000000000000000003b		
5	8/31/2020 22:07	e0000000000000000000003b		
6	8/31/2020 22:07	e0000000000000000000003b		
7	8/31/2020 22:07	e0000000000000000000003b		
8	8/31/2020 22:07	e0000000000000000000003b		
9	8/31/2020 22:07	e0000000000000000000003b		
10	8/31/2020 22:07	e0000000000000000000003b		

C

	A	B	C	D	E	F	G	H	I	J	K	L	M
1	Channel_Name	1	2	3	4	5	6	7	8	9	10	11	12
2	12/20/2020 14:08	0	0	0	0	0	1	0	0	0	0	0	0
3	12/20/2020 14:09	0	0	0	0	0	0	0	0	0	0	0	0
4	12/20/2020 14:10	0	0	0	0	0	0	0	0	0	0	0	0
5	12/20/2020 14:11	0	0	0	0	0	1	0	0	0	0	0	0
6	12/20/2020 14:12	0	0	0	0	0	0	0	0	0	0	0	0
7	12/20/2020 14:13	0	0	0	0	0	0	0	0	0	0	0	0
8	12/20/2020 14:14	0	0	0	0	0	0	0	0	0	0	0	0
9	12/20/2020 14:15	0	0	0	0	0	0	0	0	0	0	0	0
10	12/20/2020 14:16	0	0	0	0	0	0	0	0	0	0	0	0

D

	A	B	C	D	E	F	G	H	I	J	K	L	M
1	TS	1a	1b	2a	2b	3a	3b	4a	4b	5a	5b	6a	6b
2	12/20/2020 14:25	0	0	0	0	5	0	0	0	0	0	0	0
3	12/20/2020 14:26	0	0	0	0	0	3	0	0	0	0	0	0
4	12/20/2020 14:27	0	0	2	0	0	0	0	0	0	0	0	0
5	12/20/2020 14:28	3	4	0	0	0	0	0	0	0	0	0	0
6	12/20/2020 14:29	0	0	0	0	0	0	0	0	0	0	0	0
7	12/20/2020 14:30	0	0	0	4	0	0	0	0	0	0	0	0
8	12/20/2020 14:31	0	0	0	0	0	0	0	0	0	0	0	0
9	12/20/2020 14:32	0	0	0	0	0	0	0	0	0	0	0	0
10	12/20/2020 14:33	0	0	0	0	0	0	0	0	0	0	0	0

E

	A	B	C	D	E	F	G	H	I	J	K	L	M
1		Description	1a	1b	2a	2b	3a	3b	4a	4b	5a	5b	6a
2	0	distance in km	0.204678	0.155842	0.003232	0.000359	0	0	0	0	0	0	0
3													
4													

F

	A	B	C	D	E	F	G	H	I	J	K	L	M
1		Description	1	2	3	4	5	6	7	8	9	10	11
2	0	total vv counts	174	4	1	0	0	1	0	0	0	0	0
3	1	vv counts without RFID	52	1	1	0	0	1	0	0	0	0	0
4													

Figure 20. VV data preprocessing input, output and RFID + VV processing outputs.

Figure 20. VV data preprocessing input, output and RFID + VV processing outputs. A) Excerpt of raw RFID export file format before reformatting (preprocessing). B) Excerpt of final reformatted (preprocessed) RFID export file, ready for use in RFID processing. C) Excerpt of VV output file of "Vital View Processing" step. D) Excerpt of RFID output file of "RFID Processing" step. E) Excerpt of Distances output file for one day of "Cross Reference Vital View Data with RFID Data" step. When cross-referencing multiple days, each day will produce one output file in the "Distances" directory. F) Excerpt of Stats output file for one day of "Cross Reference Vital View Data with RFID Data" step. When cross-referencing multiple days, each day will produce one output file in the "Stats" directory.

B. Data Validation (Figure 21)

Note: Running distances are assigned and compiled on a minute-by-minute basis. The process_file_ui.exe program provides separate .csv files logging a) the number of minutes with at least one wheel revolution, or "total vv counts", and b) the number of minutes with a wheel revolution but without a tag read, or "vv counts without RFID". These files are in the "Stats" folder. One Stats file is produced per day (Figure 20F).

1. Divide b) by a) to yield the proportion (error rate) of running minutes that were not captured by the RFID system (Figure 21C).

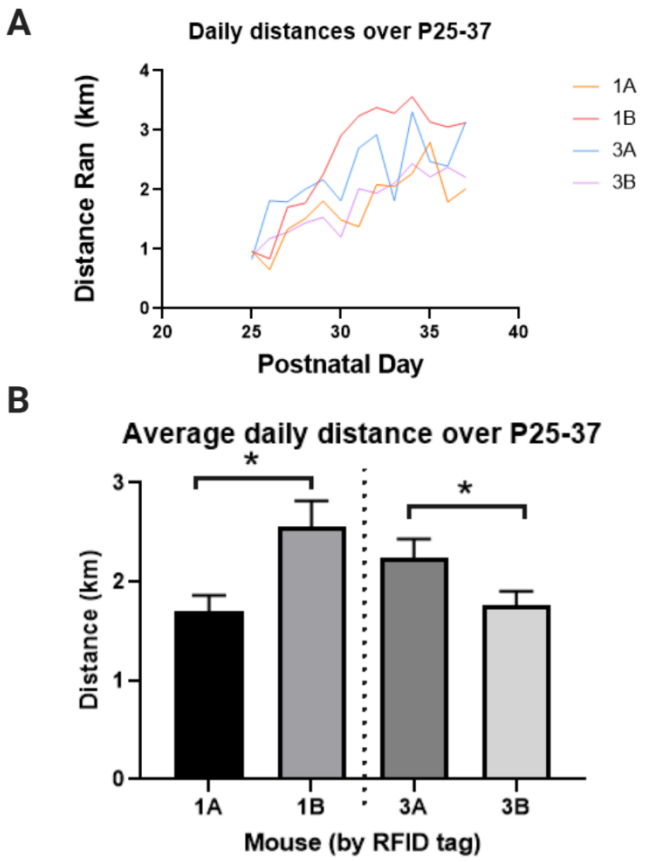

C

	Description	Cage 1	Cage 3
9/4/20 12:00	total vv counts	260	198
P25	vv counts without RFID	26	10
	error rate	10.000%	5.051%
9/5/20 12:00	total vv counts	187	339
P26	vv counts without RFID	8	20
	error rate	4.278%	5.900%
9/6/20 12:00	total vv counts	379	360
P27	vv counts without RFID	29	15
	error rate	7.652%	4.167%
9/7/20 12:00	total vv counts	407	435
P28	vv counts without RFID	25	29
	error rate	6.143%	6.667%
9/8/20 12:00	total vv counts	417	471
P29	vv counts without RFID	19	39
	error rate	4.556%	8.280%
9/9/20 12:00	total vv counts	453	300
P30	vv counts without RFID	26	13
	error rate	5.740%	4.333%
9/10/20 12:00	total vv counts	464	504
P31	vv counts without RFID	25	32
	error rate	5.388%	6.349%
9/11/20 12:00	total vv counts	510	486
P32	vv counts without RFID	21	26
	error rate	4.118%	5.350%
9/12/20 12:00	total vv counts	500	376
P33	vv counts without RFID	22	12
	error rate	4.400%	3.191%
9/13/20 12:00	total vv counts	511	549
P34	vv counts without RFID	20	21
	error rate	3.914%	3.825%
9/14/20 12:00	total vv counts	542	424
P35	vv counts without RFID	28	11
	error rate	5.166%	2.594%
9/15/20 12:00	total vv counts	452	399
P36	vv counts without RFID	22	18
	error rate	4.867%	4.511%
9/16/20 12:00	total vv counts	506	495
P37	vv counts without RFID	20	14
	error rate	3.953%	2.828%
P25-37 Overall	**Average error rate**	**5.398%**	**4.850%**

Figure 21. Representative individual running tracking data.

Figure 21. Representative individual running tracking data. A) Individual running distances of male mice per day recorded for 13 consecutive days (between postnatal days 25 – 37) in two cages, Cage 1 and Cage 3. Mice 1A and 1B were pair-housed together and mice 3A and 3b were pair-housed together. Mice acclimated to the running wheel during P21-24 (data not shown). B) Average distance ran per day, demonstrating a significant intra-cage difference in average running volume (unpaired t-test, *$p < 0.05$). C) Total number of minutes with wheel revolutions (as recorded by VitalView®) and total minutes of running without an accompanying RFID tag read (as recorded by the RFID reader) per day, per cage. $\textbf{Error Rate}\ (\%) = \frac{\boldsymbol{VV\ counts\ without\ RFID}}{\boldsymbol{Total\ VV\ counts}} \times \mathbf{100}\%$.

Notes

A. System Monitoring

1. RFID-equipped cages must be routinely monitored for wheel obstructions from nesting material or excessive bedding under the wheel. This can be determined by daily visual inspection or by viewing Vital View software recordings.
2. Check the RFID export files regularly to make sure tags are still being detected as expected. Check the Vital View data exports regularly to ensure mouse running is being recorded as expected. We monitor these exports every other day.
3. Monitor the mice daily for any disruptions in the RFID tag and/or ear tag attached to their ear. A separated ear tag and RFID tag from a mouse has only occurred twice in our experiments. If a mouse is missing an RFID tag or ear tag, give the mouse a new set, making sure the EPC of the new RFID tag is the same as that of the tag that has fallen off.

B. Mouse Running

1. Tracking is conducted continuously over 24 hours a day, through the light and dark cycle, and may start as soon as pups are weaned from their mother (postnatal day 21).
2. Mice were not given a stationary wheel acclimation period and were instead allowed to run on the running wheel from the time they are weaned. The plastic netting fitted around the rim of the wheel ensures the wheel is safe for juvenile mice to run on, so an acclimation period is not necessary to guarantee safety. Our data showed juvenile mice gradually increase their running over time post-weaning. The first few days of acclimation may be removed during data analysis if need be.

Discussion

Studies utilizing in-cage voluntary running wheels have traditionally housed rodents individually to generate accurate running distances and capture individual variations in exercise amounts[150]. Individual running data can then be correlated with other intra-individual data sets. For example, total distance run over a 2-6 hour period positively correlates with brain-derived neurotrophic factor (BDNF) gene expression in the hippocampus[155]. However, a disadvantage to individual housing is the potential for stress induced by social isolation. As mice are social animals, their innate social behaviors (whether in wild or captive environments) develop most naturally in social arrangements similar to those found in wild colonies[156]. The controlled laboratory environments required for accurate data collection frequently result in housing conditions that challenge the formation of natural social structures. The lack of social environment when mice are individually housed must be considered not only for rodent welfare but also for its impact on the quality of data produced and interpretation of findings [151,152].

Prior research has demonstrated that individual housing of mice can impact brain function in a number of ways. It can alter hypothalamic-pituitary-adrenocortical (HPA) axis function, specifically glucocorticoid regulation and feedback[157]. Individual housing can also confound performance on various behavioral tests, including those assessing anxiety[158] and learning and memory[159]. Finally, single housing can lower expression of neuroplasticity-related genes in hippocampus and prefrontal cortex[160]. Social isolation stress in singly-housed rodents is therefore an important variable to consider when interpreting studies assessing the neurobiological effects of voluntary exercise.

On the other hand, group housing of mice can invoke male-on-male aggression. This usually emerges in rodents after the onset of puberty and tends not to be present during juvenile and adolescent developmental stages[161]. Female mice have a lower tendency to exhibit this aggression, even post-puberty[162]. Social isolation in juvenile rodents adversely impacts myelination in the medial prefrontal cortex[163], whereas social play in juveniles can enhance neural plasticity in this region[164]. Moreover, juvenile mice use the body temperature of cage mates for thermoregulation[165]. This underscores the importance of paired or grouped housing for maintaining basal body temperature, particularly in the setting of shifting metabolic demands with exercise. Therefore, in studies linking juvenile voluntary wheel running with neural function and behavior, a group-housing based approach will eliminate isolation stress and reduce likelihood of thermal dysregulation.

Individual home cage rodent tracking has been accomplished through the use of video[166-168], subcutaneously implanted RFID microchips[169,170], a combination of the two, or passive infrared sensors[171]. Current protocols utilizing subcutaneously implanted RFID microchips require prolonged restraint and anesthesia, which may produce undesired stress and pain. Unified Information Devices (UID) details a protocol that describes safely implanting a mouse RFID microchip (UID UC-1485) without anesthesia on postnatal day 12. This approach is used primarily for mouse identification at single point in time, such as for taking rapid mouse inventory within a group housed cage, but its use has not been demonstrated for live, continuous tracking. Another factor is the size of the RFID chip, which must be large enough to be detected by the antenna. For juvenile mice typically weighing 6-9 grams, this size requirement prohibits administration without the use of anesthesia. In video tracking, wire cage tops obstruct continuous top-down video recording but are required for many home cage running wheel

systems. Finally, existing home cage RFID activity-tracking systems currently on the market use a matrix of RFID antennae arranged throughout the base of the cage or in strategic locations to monitor baseline ambulatory activity[172]. However, if the objective of the experiment is to track voluntary wheel-running, only one antenna with a read range precisely limited to the area inside the wheel is required.

This chapter discussed our apparatus which uses strong, low-profile RFID ear tags and one RFID antenna at the base of each cage to present a minimally invasive alternative to existing video-based and implantation-based tracking systems. The major advantage of our protocol is the ability to individually track running wheel activity of pair-housed juvenile mice starting at the age of weaning (postnatal day 21). We eliminate isolation stress and reduce issues with thermoregulation by pair housing the mice. Indeed, this model can be scaled up to >2 mice per cage if preferred. A limitation of this apparatus is that in our hands, about 5-10% of running activity is unable to be reconciled. However, we believe that our 90-95% accuracy of allocating individual running data in group housed environments is a very acceptable yield. Although this method does not encounter the same issues with accuracy-diminishing antenna cross-talk as observed in RFID antenna matrices[172] the metal wheel in very close proximity to the antenna may have the same interfering effect (thus necessitating a large ear tag). Our design effectively limits the read range of the antenna to the wheel area only.

This procedure has been tested in pair housed cages containing mice of the same sex, but we did not investigate mixed-sex population effects on individual running activity. Our experimental design allows for the comparison of individual running distances between female and male pairs of mice within the same cage. Although there may be territorial issues once social hierarchy is established in cages housing two or more male mice, a precise quantity of exercise

from each individual mouse in a group housed cage can be correlated with any desired experimental readout.

Investigating the effects of voluntary physical activity has numerous implications for increasing our understanding of its benefits towards brain function and behavior. Determining individualized amounts of exercise for specific outcomes or targets requires accurate monitoring of running distances, which can now be performed as described in this protocol. Our approach can track individual mice by recognizing the unique RFID tags of pair-housed mice coupled with time-stamped data obtained from a magnetic sensor on a home-cage running wheel. Importantly, the procedure can be scaled up to tracking running distances of multiple mice in a cage sharing access to one running wheel. Our method brings RFID applications to juvenile mouse exercise studies while minimizing stress from isolation and restraint, eliminating the need for anesthesia, and producing highly precise and individualized running data.

Chapter 6: Summary, Conclusions, and Discussion

Overview

Early-life experiences such as exercise can profoundly impact learning and memory[12,18,19,26,173,174]. The Ivy laboratory at the University of California Irvine demonstrated in 2020 that EX beginning during the 4th postnatal week of life in mice enables hippocampal memory for at least two weeks after the exercise has ended[12]. Although the effect on memory and cognition of negative early life experiences such as stress have been studied on the molecular level, a large gap in research exists in positive experience in early life such as exercise. The goal of my dissertation project was to lay the foundations for the study of the neuro-epigenetic mechanisms of EX. We developed tools for the study of neuro-epigenetic mechanisms and applied them to discover epigenetic and translational signatures of EX on the hippocampus and used that to understand the transcriptional signature underlying EX-enabled memory performance. We also developed a tool that can be used to determine an exercise dose required for the observed enabling effect of EX on memory.

Chapter 2

Chapter 2 describes the approaches we developed for the study of the neuro-epigenetic mechanisms of EX. First, we generated a transgenic mouse line by crossing Emx1-Cre mice (Emx1 is a gene primarily expressed in excitatory cortical neurons) with NuTRAP mice (which allow for labeling with biotin and mCherry on the nucleus and eGFP on the ribosomes). We name the offspring of this cross Emx1-NuTRAP mice. The use of this transgenic mouse line led to the development of the protocol we name SIT. We used this protocol to isolate chromatin and

translating mRNA specifically from excitatory *Emx1*-expressing neurons in the mouse hippocampus from the same cell homogenate. Chapter 2 goes on to detail the validation of both the mouse line and the protocol. We demonstrated that the mouse's hippocampal neuronal labeling was successful and that the SIT protocol produces results comparable to previous methods but with the distinct advantage of being able to derive both data sets from the same homogenate. We demonstrate the power of this advantage by comparing the left and right hippocampal hemisphere response to EX using previously established techniques. We ultimately conclude that although there are differences in gene expression resulting from EX between the hippocampal hemispheres, many of these differences fall into the same functional categories. Likely, this indicates that there is shared function but with lateralization of specific gene assignments. Lateralization adds utility to the SIT method which can derive both translating mRNA and chromatin from the same mouse hippocampal hemisphere. Our Emx1-NuTRAP model has the limitation that the Cre-recombinase in Emx1 expressing cells is constitutively expressed, and this may present off-target effects when present during development. Despite this, our mouse and technique offer a previously undescribed approach in the field of neuro-epigenetics to pair transcriptomic and epigenomic sequencing results from a population of hippocampal neurons. The SIT method in union with the Emx1-NuTRAP mouse are powerful tools for the study of the neuro-epigenetic mechanisms of the enabling of memory by EX.

Chapter 3

Chapter 3 describes the use of the Emx1-NuTRAP mouse and the SIT method to reveal EX-induced transcriptomic and epigenomic signatures in hippocampal neurons. We revealed new molecular epigenetic candidates for further mechanistic studies to examine the effects of

early-life exercise on hippocampal function. Several upstream regulators identified by the translatomic study, like LEF1 and KMT2a, are particularly important in development. These developmentally significant pathways could indicate a potential mechanism for the developmental-timepoint specific effects of exercise on memory. Many of the genes that we identified as differentially regulated had new H4K8ac or new H3K27me3 strongly implicating these histone PTMs, and likely other epigenetic mechanisms, as playing a critical role in the differential regulation of gene expression as a result of EX. Curiously, many of the genes that we found had new H4K8ac or H3K27me3 as a result of EX did not have changed expression levels after EX. This led us to consider a possible epigenetic "priming" mechanism for the effect of EX on memory in adolescence. We investigated such a potential and discuss our findings in the following chapter. Future studies will determine the necessity or sufficiency of the upstream regulators we identified for the effect of EX on memory in adolescence.

Chapter 4

Chapter 4 presents evidence for an epigenetic "priming" mechanism for the effect of EX on memory in adolescence. We compared the gene expression during consolidation (defined here as one hour after an OLM training event) of mice exposed to EX versus sedentary mice. When considering genes that had new epigenetic marks present as a result of EX (see Chapter 3), we found that EX mice with only 3 min of training (sufficient for a EX mouse to encode a long-term memory but insufficient for sedentary mice) have differential gene expression driven in the same direction as 10 min trained sedentary animals (sufficient training for a sedentary mouse to encode a long-term memory) when compared to 3 min trained sedentary animals . These genes were not differentially expressed by exercise alone. Only during consolidation were these

differences observed between EX and sedentary animals. It appears these genes were readied, or primed, for gene expression by the epigenetic signature of EX we identified. This is powerful evidence for the epigenetic "priming" effect of experience. Future studies will be aimed at determining which of the regulatory networks implicated by these primed genes are necessary for EX enabled memory. Additionally, it will be critical to determine the necessity and sufficiency of the epigenetic priming of these genes for the effect of EX-enabled memory. Such data could confirm or refute the epigenetic priming hypothesis for EX-enabled memory.

Chapter 5

Although we identified an epigenetic and translational signature of EX and a signature of EX-enabled consolidation associated transcription, we have yet to determine a dose of EX required for this enabling of memory observed previously by the Ivy laboratory[12]. Chapter 5 lays the foundation for addressing that gap. We present a method for individual tracking of running by pair housed mice. Such a procedure is necessary because cognition is significantly impacted by stress in early life and isolation, the traditional method for tracking individual running of mice, is stressful. Individually tracking pair housed animals eliminates this confound. Our method, described in chapter 5, uses RFID tags, a VitalView® running tracking system, and a software to compare the data to individually track juvenile mouse running in a minimally stressful way. Future studies could use this tool to determine the dose of exercise required for enabling memory in adolescence by EX.

Closing Remarks

This dissertation presents foundational work for the study of the neuro-epigenetic mechanisms of EX-enabled memory. It describes the development of the tools necessary for the study of these mechanisms and the use of those tools to identify a novel epigenetic and translatomic signature of EX. It then connects this information with memory consolidation to implicate an epigenetic priming mechanism. Together, these data suggest key candidate regulatory networks and epigenetic marks for future study to determine exactly what is necessary or sufficient for the memory enabling effect of EX. We then present a way to determine what dose is required for this enabling effect in future studies.

Our new techniques are significant advances not only for our own field but have broad applications. SIT is a technical advance for NuTRAP applications that could be used in any cell type for which a Cre line exists. It allows for more coordinated data and the use of less biological material per experiment potentially even reducing the amount of animals required for studies making use of the NuTRAP cassette. Our individual tracking of juvenile group housed mouse running is a significant advance for exercise studies. It's lower cost and stress impact makes group housed monitoring more accessible in general and eliminates isolation stress as a confound in juvenile exercise studies.

Our findings are foundational for research the positive impact early life environmental experiences can have on the epigenome and memory function. No prior study to our knowledge has examined the effects of early exercise on the epigenome especially with this level of detail and on this scale. It adds to the growing body of work supporting the long term regulatory role of epigenetic changes in post mitotic cells especially neurons.

Understanding how exercise uniquely impacts neuronal function during juvenile-adolescent developmental periods could provide insights into an early-life epigenetic memory of the EX experience and how much EX is required for this induction. Ultimately, future studies could use these potential targets we identified for improving memory function or mitigating memory deficits in the setting of early-life cognitive and neurodevelopmental disorders[12]. With our research, we lay the groundwork for mechanistic study of EX enabled memory. This knowledge will have enormous potential for medical future medical treatments.

References

1 Raus, A. *et al.* Early life exercise primes the neural epigenome to facilitate gene expression and hippocampal memory consolidation. *bioRxiv*, 2021.2012.2023.473936 (2022). https://doi.org:10.1101/2021.12.23.473936

2 Gorski, J. A. *et al.* Cortical excitatory neurons and glia, but not GABAergic neurons, are produced in the Emx1-expressing lineage. *The Journal of neuroscience : the official journal of the Society for Neuroscience* **22**, 6309-6314 (2002). https://doi.org:10.1523/jneurosci.22-15-06309.2002

3 Roh, H. C. *et al.* Simultaneous Transcriptional and Epigenomic Profiling from Specific Cell Types within Heterogeneous Tissues In Vivo. *Cell reports* **18**, 1048-1061 (2017). https://doi.org:10.1016/j.celrep.2016.12.087

4 Jenks, K. M., de Moor, J. & van Lieshout, E. C. Arithmetic difficulties in children with cerebral palsy are related to executive function and working memory. *J Child Psychol Psychiatry* **50**, 824-833 (2009). https://doi.org:10.1111/j.1469-7610.2008.02031.x

5 Helmstaedter, C. & Witt, J. A. Epilepsy and cognition - A bidirectional relationship? *Seizure* **49**, 83-89 (2017). https://doi.org:10.1016/j.seizure.2017.02.017

6 Zhang, M. *et al.* Exploring the spatial working memory and visual perception in children with autism spectrum disorder and general population with high autism-like traits. *PLoS One* **15**, e0235552 (2020). https://doi.org:10.1371/journal.pone.0235552

7 Oswald, K. A., Fosco, W. D., Sarver, D. E. & Karlson, C. W. Psychometric evaluation of the pediatric applied cognition scale in pediatric hematology/oncology. *Child Neuropsychol* **26**, 1047-1064 (2020). https://doi.org:10.1080/09297049.2020.1752368

8 Crawford, C. Learning Disabilities in Canada: Economic Costs to Individuals, Families and Society. (Roeher Institute Learning Disabilities Association of Canada, 2007).

9 Erickson, K. I. *et al.* Exercise training increases size of hippocampus and improves memory. *Proceedings of the National Academy of Sciences of the United States of America* **108**, 3017-3022 (2011). https://doi.org:10.1073/pnas.1015950108

10 Xu, L. *et al.* Moderate Exercise Combined with Enriched Environment Enhances Learning and Memory through BDNF/TrkB Signaling Pathway in Rats. *Int J Environ Res Public Health* **18** (2021). https://doi.org:10.3390/ijerph18168283

11 Berchtold, N. C., Castello, N. & Cotman, C. W. Exercise and time-dependent benefits to learning and memory. *Neuroscience* **167**, 588-597 (2010). https://doi.org:10.1016/j.neuroscience.2010.02.050

12 Ivy, A. S. *et al.* A Unique Mouse Model of Early Life Exercise Enables Hippocampal Memory and Synaptic Plasticity. *Scientific Reports* **10**, 9174 (2020). https://doi.org:10.1038/s41598-020-66116-4

13 Roth, T. L., Lubin, F. D., Funk, A. J. & Sweatt, J. D. Lasting epigenetic influence of early-life adversity on the BDNF gene. *Biol Psychiatry* **65**, 760-769 (2009). https://doi.org:10.1016/j.biopsych.2008.11.028

14 Krugers, H. J. *et al.* Early life adversity: Lasting consequences for emotional learning. *Neurobiol Stress* **6**, 14-21 (2017). https://doi.org:10.1016/j.ynstr.2016.11.005

15 Walker, C. D. *et al.* Chronic early life stress induced by limited bedding and nesting (LBN) material in rodents: critical considerations of methodology, outcomes and translational potential. *Stress* **20**, 421-448 (2017). https://doi.org:10.1080/10253890.2017.1343296

16 Kronman, H. *et al.* Long-term behavioral and cell-type-specific molecular effects of early life stress are mediated by H3K79me2 dynamics in medium spiny neurons. *Nat Neurosci* **24**, 667-676 (2021). https://doi.org:10.1038/s41593-021-00814-8
17 Yang, X. D. *et al.* Stress during a critical postnatal period induces region-specific structural abnormalities and dysfunction of the prefrontal cortex via CRF1. *Neuropsychopharmacology* **40**, 1203-1215 (2015). https://doi.org:10.1038/npp.2014.304
18 Gomes da Silva, S. & Arida, R. M. Physical activity and brain development. *Expert Rev Neurother* **15**, 1041-1051 (2015). https://doi.org:10.1586/14737175.2015.1077115
19 Gomes da Silva, S. *et al.* Early exercise promotes positive hippocampal plasticity and improves spatial memory in the adult life of rats. *Hippocampus* **22**, 347-358 (2012). https://doi.org:10.1002/hipo.20903
20 Intlekofer, K. A. *et al.* Exercise and Sodium Butyrate Transform a Subthreshold Learning Event into Long-Term Memory via a Brain-Derived Neurotrophic factor-Dependent Mechanism. *Neuropsychopharmacology* **38**, 2027-2034 (2013). https://doi.org:10.1038/npp.2013.104
21 Marano, D., Fioriniello, S., D'Esposito, M. & Della Ragione, F. Transcriptomic and Epigenomic Landscape in Rett Syndrome. *Biomolecules* **11** (2021). https://doi.org:10.3390/biom11070967
22 Campbell, R. R. & Wood, M. A. How the epigenome integrates information and reshapes the synapse. *Nature reviews. Neuroscience* **20**, 133-147 (2019). https://doi.org:10.1038/s41583-019-0121-9
23 Malvaez, M. *et al.* HDAC3-selective inhibitor enhances extinction of cocaine-seeking behavior in a persistent manner. *Proceedings of the National Academy of Sciences of the United States of America* **110**, 2647-2652 (2013). https://doi.org:10.1073/pnas.1213364110
24 Sultan, F. A. & Day, J. J. Epigenetic mechanisms in memory and synaptic function. *Epigenomics* **3**, 157-181 (2011). https://doi.org:10.2217/epi.11.6
25 Lopez-Atalaya, J. P. & Barco, A. Can changes in histone acetylation contribute to memory formation? *Trends Genet* **30**, 529-539 (2014). https://doi.org:10.1016/j.tig.2014.09.003
26 Fernandes, J., Arida, R. M. & Gomez-Pinilla, F. Physical exercise as an epigenetic modulator of brain plasticity and cognition. *Neurosci Biobehav Rev* **80**, 443-456 (2017). https://doi.org:10.1016/j.neubiorev.2017.06.012
27 Lindholm, M. E. *et al.* An integrative analysis reveals coordinated reprogramming of the epigenome and the transcriptome in human skeletal muscle after training. *Epigenetics* **9**, 1557-1569 (2014). https://doi.org:10.4161/15592294.2014.982445
28 McGee, S. L. & Hargreaves, M. Epigenetics and Exercise. *Trends Endocrinol Metab* **30**, 636-645 (2019). https://doi.org:10.1016/j.tem.2019.06.002
29 Cotman, C. W. & Berchtold, N. C. Exercise: a behavioral intervention to enhance brain health and plasticity. *Trends Neurosci* **25**, 295-301 (2002). https://doi.org:10.1016/s0166-2236(02)02143-4
30 Meireles, A. L. F. *et al.* Maternal resistance exercise promotes changes in neuroplastic and epigenetic marks of offspring's hippocampus during adult life. *Physiol Behav* **230**, 113306 (2021). https://doi.org:10.1016/j.physbeh.2020.113306

31 Butler, C. W. *et al.* Exercise opens a temporal window for enhanced cognitive improvement from subsequent physical activity. *Learning & memory (Cold Spring Harbor, N.Y.)* **26**, 485-492 (2019). https://doi.org:10.1101/lm.050278.119
32 Avishai-Eliner, S., Brunson, K. L., Sandman, C. A. & Baram, T. Z. Stressed-out, or in (utero)? *Trends Neurosci* **25**, 518-524 (2002). https://doi.org:10.1016/s0166-2236(02)02241-5
33 Mody, M. *et al.* Genome-wide gene expression profiles of the developing mouse hippocampus. *Proceedings of the National Academy of Sciences of the United States of America* **98**, 8862-8867 (2001). https://doi.org:10.1073/pnas.141244998
34 Dabrowski, A., Johnson-Venkatesh, E. & Umemori, H. in *Conn's Translational Neuroscience* (ed P. Michael Conn) 89-111 (Academic Press, 2017).
35 Rice, D. & Barone, S., Jr. Critical periods of vulnerability for the developing nervous system: evidence from humans and animal models. *Environ Health Perspect* **108 Suppl 3**, 511-533 (2000). https://doi.org:10.1289/ehp.00108s3511
36 Azevedo, F. A. *et al.* Equal numbers of neuronal and nonneuronal cells make the human brain an isometrically scaled-up primate brain. *The Journal of comparative neurology* **513**, 532-541 (2009). https://doi.org:10.1002/cne.21974
37 Ivy, A. S. & Standridge, S. M. Rett Syndrome: A Timely Review From Recognition to Current Clinical Approaches and Clinical Study Updates. *Semin Pediatr Neurol* **37**, 100881 (2021). https://doi.org:10.1016/j.spen.2021.100881
38 Deal, R. B. & Henikoff, S. The INTACT method for cell type-specific gene expression and chromatin profiling in Arabidopsis thaliana. *Nature protocols* **6**, 56-68 (2011). https://doi.org:10.1038/nprot.2010.175
39 Heiman, M. *et al.* A translational profiling approach for the molecular characterization of CNS cell types. *Cell* **135**, 738-748 (2008). https://doi.org:10.1016/j.cell.2008.10.028
40 Skene, P. J., Henikoff, J. G. & Henikoff, S. Targeted in situ genome-wide profiling with high efficiency for low cell numbers. *Nature protocols* **13**, 1006-1019 (2018). https://doi.org:10.1038/nprot.2018.015
41 Bedrosian, T. A., Quayle, C., Novaresi, N. & Gage, F. H. Early life experience drives structural variation of neural genomes in mice. *Science (New York, N.Y.)* **359**, 1395-1399 (2018). https://doi.org:10.1126/science.aah3378
42 Stroud, H. *et al.* Early-Life Gene Expression in Neurons Modulates Lasting Epigenetic States. *Cell* **171**, 1151-1164.e1116 (2017). https://doi.org:https://doi.org/10.1016/j.cell.2017.09.047
43 Herre, M. & Korb, E. The chromatin landscape of neuronal plasticity. *Curr Opin Neurobiol* **59**, 79-86 (2019). https://doi.org:10.1016/j.conb.2019.04.006
44 Wang, J. *et al.* Effect of exercise on microglial activation and transcriptome of hippocampus in fluorosis mice. *Sci Total Environ* **760**, 143376 (2021). https://doi.org:10.1016/j.scitotenv.2020.143376
45 Yamada, T. *et al.* Sensory experience remodels genome architecture in neural circuit to drive motor learning. *Nature* **569**, 708-713 (2019). https://doi.org:10.1038/s41586-019-1190-7
46 Tonn Eisinger, K. R. & West, A. E. Transcribing Memories in Genome Architecture. *Trends Neurosci* **42**, 565-566 (2019). https://doi.org:10.1016/j.tins.2019.06.002

47 Gao, Y. *et al.* RGS6 Mediates Effects of Voluntary Running on Adult Hippocampal Neurogenesis. *Cell reports* **32**, 107997 (2020). https://doi.org:10.1016/j.celrep.2020.107997
48 Richardson, G. M., Lannigan, J. & Macara, I. G. Does FACS perturb gene expression? *Cytometry. Part A : the journal of the International Society for Analytical Cytology* **87**, 166-175 (2015). https://doi.org:10.1002/cyto.a.22608
49 Alberini, C. M. & Kandel, E. R. The regulation of transcription in memory consolidation. *Cold Spring Harb Perspect Biol* **7**, a021741 (2014). https://doi.org:10.1101/cshperspect.a021741
50 Mou, T., Deng, W., Gu, F., Pawitan, Y. & Vu, T. N. Reproducibility of Methods to Detect Differentially Expressed Genes from Single-Cell RNA Sequencing. *Front Genet* **10**, 1331 (2019). https://doi.org:10.3389/fgene.2019.01331
51 Chan, C. H. *et al.* Emx1 is a marker for pyramidal neurons of the cerebral cortex. *Cerebral cortex (New York, N.Y. : 1991)* **11**, 1191-1198 (2001). https://doi.org:10.1093/cercor/11.12.1191
52 Hong, S. M. *et al.* Reduced hippocampal neurogenesis and skill reaching performance in adult Emx1 mutant mice. *Experimental neurology* **206**, 24-32 (2007). https://doi.org:10.1016/j.expneurol.2007.03.028
53 Willaime-Morawek, S. & van der Kooy, D. Cortex- and striatum- derived neural stem cells produce distinct progeny in the olfactory bulb and striatum. *The European journal of neuroscience* **27**, 2354-2362 (2008). https://doi.org:10.1111/j.1460-9568.2008.06206.x
54 Luo, L. *et al.* Optimizing Nervous System-Specific Gene Targeting with Cre Driver Lines: Prevalence of Germline Recombination and Influencing Factors. *Neuron* **106**, 37-65.e35 (2020). https://doi.org:10.1016/j.neuron.2020.01.008
55 David A Valientes, A. M. R., Autumn S Ivy. An Improved Method for Individual Tracking of Voluntary Wheel Running in Pair-housed Juvenile Mice. *BIO-PROTOCOL* **11** (2021). https://doi.org:10.21769/bioprotoc.4071
56 Long, J. Z. *et al.* A smooth muscle-like origin for beige adipocytes. *Cell metabolism* **19**, 810-820 (2014). https://doi.org:10.1016/j.cmet.2014.03.025
57 Deal, R. B. & Henikoff, S. A simple method for gene expression and chromatin profiling of individual cell types within a tissue. *Developmental cell* **18**, 1030-1040 (2010). https://doi.org:10.1016/j.devcel.2010.05.013
58 Schwarz, J. M. Using fluorescence activated cell sorting to examine cell-type-specific gene expression in rat brain tissue. *Journal of visualized experiments : JoVE*, e52537 (2015). https://doi.org:10.3791/52537
59 Pfaffl, M. W. A new mathematical model for relative quantification in real-time RT-PCR. *Nucleic Acids Res* **29**, e45 (2001). https://doi.org:10.1093/nar/29.9.e45
60 FastQC v. 0.11.9 (Babraham Bioinformatics, 2005).
61 Dobin, A. *et al.* STAR: ultrafast universal RNA-seq aligner. *Bioinformatics* **29**, 15-21 (2013). https://doi.org:10.1093/bioinformatics/bts635
62 Picard v. 1.87 (Broad Institute, 2013).
63 R (R Foundation for statistical Computing, Vienna, Austria, 2010).
64 Lawrence, M. *et al.* Software for Computing and Annotating Genomic Ranges. *PLoS Computational Biology* **9**, e1003118 (2013). https://doi.org:10.1371/journal.pcbi.1003118
65 Rsamtools: Binary alignment (BAM), FASTA, variant call (BCF), and tabix file import (Bioconductor Bioconductor 2021).

66 Love, M. I., Huber, W. & Anders, S. Moderated estimation of fold change and dispersion for RNA-seq data with DESeq2. *Genome Biology* **15** (2014). https://doi.org:10.1186/s13059-014-0550-8
67 Durinck, S. *et al.* BioMart and Bioconductor: a powerful link between biological databases and microarray data analysis. *Bioinformatics* **21**, 3439-3440 (2005). https://doi.org:10.1093/bioinformatics/bti525
68 Durinck, S., Spellman, P. T., Birney, E. & Huber, W. Mapping identifiers for the integration of genomic datasets with the R/Bioconductor package biomaRt. *Nature protocols* **4**, 1184-1191 (2009). https://doi.org:10.1038/nprot.2009.97
69 Ggplot2: Elegant graphics for data analysis v. 3.3.4 (Springer International Publishing, Cham, Switzerland, 2016).
70 gplots: Various R Programming Tools for Plotting Data v. 3.1.1 (Tal Galili 2020).
71 RColorBrewer: ColorBrewer Palettes (Erich Neuwirth, CRAN, 2014).
72 Venn Diagram: Calculate and draw custom Venn diagrams (BELGIUM, 2021).
73 Mi, H. & Thomas, P. 123-140 (Humana Press, 2009).
74 Subramanian, A. *et al.* Gene set enrichment analysis: A knowledge-based approach for interpreting genome-wide expression profiles. *Proceedings of the National Academy of Sciences* **102**, 15545-15550 (2005). https://doi.org:10.1073/pnas.0506580102
75 Krämer, A., Green, J., Pollard, J. & Tugendreich, S. Causal analysis approaches in Ingenuity Pathway Analysis. *Bioinformatics* **30**, 523-530 (2014). https://doi.org:10.1093/bioinformatics/btt703
76 Langmead, B. & Salzberg, S. L. Fast gapped-read alignment with Bowtie 2. *Nature Methods* **9**, 357-359 (2012). https://doi.org:10.1038/nmeth.1923
77 Kaya-Okur, H. S. *et al.* CUT&Tag for efficient epigenomic profiling of small samples and single cells. *Nature Communications* **10** (2019). https://doi.org:10.1038/s41467-019-09982-5
78 Humburg, P., Helliwell, C. A., Bulger, D. & Stone, G. ChIPseqR: analysis of ChIP-seq experiments. *BMC Bioinformatics* **12**, 39 (2011). https://doi.org:10.1186/1471-2105-12-39
79 TxDb.Mmusculus.UCSC.mm10.knownGene: Annotation package for TxDb object(s) v. 3.4.7 (Bioconductor 2019).
80 Kent, W. J. *et al.* The Human Genome Browser at UCSC. *Genome Research* **12**, 996-1006 (2002). https://doi.org:10.1101/gr.229102
81 Rosenbloom, K. R. *et al.* ENCODE whole-genome data in the UCSC Genome Browser. *Nucleic Acids Research* **38**, D620-D625 (2010). https://doi.org:10.1093/nar/gkp961
82 Haeussler, M. *et al.* Navigating protected genomics data with UCSC Genome Browser in a Box. *Bioinformatics* **31**, 764-766 (2014). https://doi.org:10.1093/bioinformatics/btu712
83 ggpubr: 'ggplot2' Based Publication Ready Plots (CRAN, 2020).
84 Sultan, F. A. Dissection of Different Areas from Mouse Hippocampus. *Bio Protoc* **3** (2013). https://doi.org:10.21769/bioprotoc.955
85 Tu, L. *et al.* Free-floating Immunostaining of Mouse Brains. *Journal of Visualized Experiments* (2021). https://doi.org:10.3791/62876
86 Liu, Y. *et al.* Glial fibrillary acidic protein-expressing neural progenitors give rise to immature neurons via early intermediate progenitors expressing both glial fibrillary acidic protein and neuronal markers in the adult hippocampus. *Neuroscience* **166**, 241-251 (2010). https://doi.org:10.1016/j.neuroscience.2009.12.026

87 Garcia, A. D. R., Doan, N. B., Imura, T., Bush, T. G. & Sofroniew, M. V. GFAP-expressing progenitors are the principal source of constitutive neurogenesis in adult mouse forebrain. *Nature Neuroscience* **7**, 1233-1241 (2004). https://doi.org:10.1038/nn1340

88 Chucair-Elliott, A. J. *et al.* Inducible cell-specific mouse models for paired epigenetic and transcriptomic studies of microglia and astroglia. *Commun Biol* **3**, 693 (2020). https://doi.org:10.1038/s42003-020-01418-x

89 Jordan, J. T. The rodent hippocampus as a bilateral structure: A review of hemispheric lateralization. *Hippocampus* **30**, 278-292 (2020). https://doi.org:https://doi.org/10.1002/hipo.23188

90 Butler, A. A., Sanchez, R. G., Jarome, T. J., Webb, W. M. & Lubin, F. D. O-GlcNAc and EZH2-mediated epigenetic regulation of gene expression during consolidation of fear memories. *Learning & memory (Cold Spring Harbor, N.Y.)* **26**, 373-379 (2019). https://doi.org:10.1101/lm.049023.118

91 Lister, R. *et al.* Global Epigenomic Reconfiguration During Mammalian Brain Development. *Science* **341**, 1237905 (2013). https://doi.org:10.1126/science.1237905

92 Luo, C. *et al.* Single-cell methylomes identify neuronal subtypes and regulatory elements in mammalian cortex. *Science* **357**, 600-604 (2017). https://doi.org:10.1126/science.aan3351

93 Helbling, J.-C., Kinouchi, K., Trifilieff, P., Sassone-Corsi, P. & Moisan, M.-P. Combined Gene Expression and Chromatin Immunoprecipitation From a Single Mouse Hippocampus. *Current Protocols* **1**, e33 (2021). https://doi.org:https://doi.org/10.1002/cpz1.33

94 Doty, R. W., Fei, R., Hu, S. & Kavcic, V. Long-term reversal of hemispheric specialization for visual memory in a split-brain macaque. *Behavioural brain research* **102**, 99-113 (1999). https://doi.org:10.1016/s0166-4328(99)00006-6

95 Duboc, V., Dufourcq, P., Blader, P. & Roussigné, M. Asymmetry of the Brain: Development and Implications. *Annual review of genetics* **49**, 647-672 (2015). https://doi.org:10.1146/annurev-genet-112414-055322

96 Güntürkün, O., Ströckens, F. & Ocklenburg, S. Brain Lateralization: A Comparative Perspective. *Physiological reviews* **100**, 1019-1063 (2020). https://doi.org:10.1152/physrev.00006.2019

97 Hubel, D. H. & Wiesel, T. N. Receptive fields, binocular interaction and functional architecture in the cat's visual cortex. *The Journal of Physiology* **160**, 106-154 (1962). https://doi.org:https://doi.org/10.1113/jphysiol.1962.sp006837

98 Spiers, H. J. *et al.* Unilateral temporal lobectomy patients show lateralized topographical and episodic memory deficits in a virtual town. *Brain : a journal of neurology* **124**, 2476-2489 (2001). https://doi.org:10.1093/brain/124.12.2476

99 Sagarkar, S. *et al.* LSD1-BDNF activity in lateral hypothalamus-medial forebrain bundle area is essential for reward seeking behavior. *Progress in neurobiology* **202**, 102048 (2021). https://doi.org:10.1016/j.pneurobio.2021.102048

100 Webb, W. M. *et al.* The SETD6 Methyltransferase Plays an Essential Role in Hippocampus-Dependent Memory Formation. *Biological psychiatry* **87**, 577-587 (2020). https://doi.org:10.1016/j.biopsych.2019.05.022

101 Bolton, J. L. *et al.* Unexpected Transcriptional Programs Contribute to Hippocampal Memory Deficits and Neuronal Stunting after Early-Life Adversity. *Cell Rep* **33**, 108511 (2020). https://doi.org:10.1016/j.celrep.2020.108511
102 Campbell, R. R. *et al.* HDAC3 Activity within the Nucleus Accumbens Regulates Cocaine-Induced Plasticity and Behavior in a Cell-Type-Specific Manner. *The Journal of neuroscience : the official journal of the Society for Neuroscience* **41**, 2814-2827 (2021). https://doi.org:10.1523/JNEUROSCI.2829-20.2021
103 Lavery, L. A. & Zoghbi, H. Y. The distinct methylation landscape of maturing neurons and its role in Rett syndrome pathogenesis. *Current opinion in neurobiology* **59**, 180-188 (2019). https://doi.org:10.1016/j.conb.2019.08.001
104 Aguilar, R., Bustos, F. J., Nardocci, G., van Zundert, B. & Montecino, M. Epigenetic silencing of the osteoblast-lineage gene program during hippocampal maturation. *Journal of cellular biochemistry* **122**, 367-384 (2021). https://doi.org:10.1002/jcb.29865
105 West, A. E. & Greenberg, M. E. Neuronal activity-regulated gene transcription in synapse development and cognitive function. *Cold Spring Harbor perspectives in biology* **3** (2011). https://doi.org:10.1101/cshperspect.a005744
106 Bale, T. L. *et al.* Early life programming and neurodevelopmental disorders. *Biological psychiatry* **68**, 314-319 (2010). https://doi.org:10.1016/j.biopsych.2010.05.028
107 Cotman, C. W., Berchtold, N. C. & Christie, L.-A. Exercise builds brain health: key roles of growth factor cascades and inflammation. *Trends in Neurosciences* **30**, 464-472 (2007). https://doi.org:https://doi.org/10.1016/j.tins.2007.06.011
108 Voss, M. W., Vivar, C., Kramer, A. F. & van Praag, H. Bridging animal and human models of exercise-induced brain plasticity. *Trends in cognitive sciences* **17**, 525-544 (2013). https://doi.org:10.1016/j.tics.2013.08.001
109 Urdinguio, R. G. *et al.* Physical exercise shapes the mouse brain epigenome. *Mol Metab* **54**, 101398 (2021). https://doi.org:10.1016/j.molmet.2021.101398
110 Abel, J. L. & Rissman, E. F. Running-induced epigenetic and gene expression changes in the adolescent brain. *International journal of developmental neuroscience : the official journal of the International Society for Developmental Neuroscience* **31**, 382-390 (2013). https://doi.org:10.1016/j.ijdevneu.2012.11.002
111 Ieraci, A., Mallei, A., Musazzi, L. & Popoli, M. Physical exercise and acute restraint stress differentially modulate hippocampal brain-derived neurotrophic factor transcripts and epigenetic mechanisms in mice. *Hippocampus* **25**, 1380-1392 (2015). https://doi.org:10.1002/hipo.22458
112 Titterness, A. K., Wiebe, E., Kwasnica, A., Keyes, G. & Christie, B. R. Voluntary exercise does not enhance long-term potentiation in the adolescent female dentate gyrus. *Neuroscience* **183**, 25-31 (2011). https://doi.org:10.1016/j.neuroscience.2011.03.050
113 Berchtold, N. C., Chinn, G., Chou, M., Kesslak, J. P. & Cotman, C. W. Exercise primes a molecular memory for brain-derived neurotrophic factor protein induction in the rat hippocampus. *Neuroscience* **133**, 853-861 (2005). https://doi.org:10.1016/j.neuroscience.2005.03.026
114 McNulty, S. E. *et al.* Differential roles for Nr4a1 and Nr4a2 in object location vs. object recognition long-term memory. *Learning & memory (Cold Spring Harbor, N.Y.)* **19**, 588-592 (2012). https://doi.org:10.1101/lm.026385.112
115 Kandel, E. R. The molecular biology of memory: cAMP, PKA, CRE, CREB-1, CREB-2, and CPEB. *Molecular brain* **5**, 14 (2012). https://doi.org:10.1186/1756-6606-5-14

116 Kerimoglu, C. *et al.* KMT2A and KMT2B Mediate Memory Function by Affecting Distinct Genomic Regions. *Cell reports* **20**, 538-548 (2017). https://doi.org:10.1016/j.celrep.2017.06.072
117 Ashbrook, D. G. *et al.* Transcript co-variance with Nestin in two mouse genetic reference populations identifies Lef1 as a novel candidate regulator of neural precursor cell proliferation in the adult hippocampus. *Front Neurosci* **8**, 418 (2014). https://doi.org:10.3389/fnins.2014.00418
118 Tapia-González, S., Muñoz, M., Cuartero, M. & Sánchez-Capelo, A. Smad3 is required for the survival of proliferative intermediate progenitor cells in the dentate gyrus of adult mice. *Cell Communication and Signaling* **11**, 93 (2013). https://doi.org:10.1186/1478-811x-11-93
119 Tiano, J. P., Springer, D. A. & Rane, S. G. SMAD3 Negatively Regulates Serum Irisin and Skeletal Muscle FNDC5 and Peroxisome Proliferator-activated Receptor γ Coactivator 1-α (PGC-1α) during Exercise. *Journal of Biological Chemistry* **290**, 7671-7684 (2015). https://doi.org:10.1074/jbc.m114.617399
120 Sun, Z. *et al.* EGR1 recruits TET1 to shape the brain methylome during development and upon neuronal activity. *Nature Communications* **10** (2019). https://doi.org:10.1038/s41467-019-11905-3
121 Bouché, V. *et al.* Drosophila Mitf regulates the V-ATPase and the lysosomal-autophagic pathway. *Autophagy* **12**, 484-498 (2016). https://doi.org:10.1080/15548627.2015.1134081
122 Guan, Z. *et al.* Integration of long-term-memory-related synaptic plasticity involves bidirectional regulation of gene expression and chromatin structure. *Cell* **111**, 483-493 (2002). https://doi.org:10.1016/s0092-8674(02)01074-7
123 Korzus, E., Rosenfeld, M. G. & Mayford, M. CBP Histone Acetyltransferase Activity Is a Critical Component of Memory Consolidation. *Neuron* **42**, 961-972 (2004). https://doi.org:10.1016/j.neuron.2004.06.002
124 Nofrini, V., Di Giacomo, D. & Mecucci, C. Nucleoporin genes in human diseases. *European Journal of Human Genetics* **24**, 1388-1395 (2016). https://doi.org:10.1038/ejhg.2016.25
125 Gomes-Duarte, A., Lacerda, R., Menezes, J. & Romão, L. eIF3: a factor for human health and disease. *RNA Biol* **15**, 26-34 (2018). https://doi.org:10.1080/15476286.2017.1391437
126 Alvarez-López, M. J. *et al.* Long-term exercise modulates hippocampal gene expression in senescent female mice. *J Alzheimers Dis* **33**, 1177-1190 (2013). https://doi.org:10.3233/jad-121264
127 Butler, A. A., Sanchez, R. G., Jarome, T. J., Webb, W. M. & Lubin, F. D. O-GlcNAc and EZH2-mediated epigenetic regulation of gene expression during consolidation of fear memories. *Learning & memory (Cold Spring Harbor, N.Y.)* **26**, 373-379 (2019). https://doi.org:10.1101/lm.049023.118
128 Chou, M.-Y. *et al.* RTL1/PEG11 imprinted in human and mouse brain mediates anxiety-like and social behaviors and regulates neuronal excitability in the locus coeruleus. *Human Molecular Genetics* (2022). https://doi.org:10.1093/hmg/ddac110
129 Kitazawa, M., Sutani, A., Kaneko-Ishino, T. & Ishino, F. The role of eutherian-specific RTL1 in the nervous system and its implications for the Kagami-Ogata and Temple syndromes. *Genes to Cells* **26**, 165-179 (2021). https://doi.org:https://doi.org/10.1111/gtc.12830

130 Stergiopoulos, A., Elkouris, M. & Politis, P. K. Prospero-related homeobox 1 (Prox1) at the crossroads of diverse pathways during adult neural fate specification. *Front Cell Neurosci* **8**, 454 (2014). https://doi.org:10.3389/fncel.2014.00454
131 Camp, N. D. *et al.* Individual protomers of a G protein-coupled receptor dimer integrate distinct functional modules. *Cell Discov* **1**, 15011- (2015). https://doi.org:10.1038/celldisc.2015.11
132 Baple, E. L. *et al.* Mutations in KPTN cause macrocephaly, neurodevelopmental delay, and seizures. *Am J Hum Genet* **94**, 87-94 (2014). https://doi.org:10.1016/j.ajhg.2013.10.001
133 Peterson, M. D. & Titus, M. A. F-actin distribution of Dictyostelium myosin I double mutants. *J Eukaryot Microbiol* **41**, 652-657 (1994). https://doi.org:10.1111/j.1550-7408.1994.tb01529.x
134 Johnson Chacko, L. *et al.* Transcriptome-Wide Analysis Reveals a Role for Extracellular Matrix and Integrin Receptor Genes in Otic Neurosensory Differentiation from Human iPSCs. *Int J Mol Sci* **22** (2021). https://doi.org:10.3390/ijms221910849
135 Truter, S., Andrikopoulos, K., Di Liberto, M., Womack, L. & Ramirez, F. Pro-alpha 2(V) collagen gene; pairwise analysis of the amino-propeptide coding domain, and cross-species comparison of the promoter sequence. *Connect Tissue Res* **29**, 51-59 (1993). https://doi.org:10.3109/03008209309061966
136 Lévy, J. *et al.* EFNB2 haploinsufficiency causes a syndromic neurodevelopmental disorder. *Clin Genet* **93**, 1141-1147 (2018). https://doi.org:10.1111/cge.13234
137 Xiong, C. *et al.* Targeting Forward and Reverse EphB4/EFNB2 Signaling by a Peptide with Dual Functions. *Sci Rep* **10**, 520 (2020). https://doi.org:10.1038/s41598-020-57477-x
138 Zhu, F. *et al.* EFNB2 facilitates cell proliferation, migration, and invasion in pancreatic ductal adenocarcinoma via the p53/p21 pathway and EMT. *Biomed Pharmacother* **125**, 109972 (2020). https://doi.org:10.1016/j.biopha.2020.109972
139 Ferrari, K. J., Lavarone, E. & Pasini, D. The Dual Role of EPOP and Elongin BC in Controlling Transcriptional Activity. *Mol Cell* **64**, 637-638 (2016). https://doi.org:10.1016/j.molcel.2016.11.009
140 Liefke, R., Karwacki-Neisius, V. & Shi, Y. EPOP Interacts with Elongin BC and USP7 to Modulate the Chromatin Landscape. *Mol Cell* **64**, 659-672 (2016). https://doi.org:10.1016/j.molcel.2016.10.019
141 Iwano, T., Masuda, A., Kiyonari, H., Enomoto, H. & Matsuzaki, F. Prox1 postmitotically defines dentate gyrus cells by specifying granule cell identity over CA3 pyramidal cell fate in the hippocampus. *Development (Cambridge, England)* **139**, 3051-3062 (2012). https://doi.org:10.1242/dev.080002
142 Lynch, M. A. Long-term potentiation and memory. *Physiological reviews* **84**, 87-136 (2004). https://doi.org:10.1152/physrev.00014.2003
143 Kwapis, J. L. *et al.* Epigenetic regulation of the circadian gene Per1 contributes to age-related changes in hippocampal memory. *Nat Commun* **9**, 3323 (2018). https://doi.org:10.1038/s41467-018-05868-0
144 Warburton, E. C. *et al.* cAMP responsive element-binding protein phosphorylation is necessary for perirhinal long-term potentiation and recognition memory. *J Neurosci* **25**, 6296-6303 (2005). https://doi.org:10.1523/jneurosci.0506-05.2005

145 Logan, T., Bendor, J., Toupin, C., Thorn, K. & Edwards, R. H. α-Synuclein promotes dilation of the exocytotic fusion pore. *Nat Neurosci* **20**, 681-689 (2017). https://doi.org:10.1038/nn.4529
146 Fournier, A. E., GrandPre, T. & Strittmatter, S. M. Identification of a receptor mediating Nogo-66 inhibition of axonal regeneration. *Nature* **409**, 341-346 (2001). https://doi.org:10.1038/35053072
147 Pérez-Otaño, I., Larsen, R. S. & Wesseling, J. F. Emerging roles of GluN3-containing NMDA receptors in the CNS. *Nat Rev Neurosci* **17**, 623-635 (2016). https://doi.org:10.1038/nrn.2016.92
148 Chodelkova, O., Masek, J., Korinek, V., Kozmik, Z. & Machon, O. Tcf7L2 is essential for neurogenesis in the developing mouse neocortex. *Neural Dev* **13**, 8 (2018). https://doi.org:10.1186/s13064-018-0107-8
149 Liu, Y. *et al.* The beneficial effects of physical exercise in the brain and related pathophysiological mechanisms in neurodegenerative diseases. *Lab Invest* **99**, 943-957 (2019). https://doi.org:10.1038/s41374-019-0232-y
150 Goh, J. & Ladiges, W. Voluntary Wheel Running in Mice. *Curr Protoc Mouse Biol* **5**, 283-290 (2015). https://doi.org:10.1002/9780470942390.mo140295
151 Kappel, S., Hawkins, P. & Mendl, M. T. To Group or Not to Group? Good Practice for Housing Male Laboratory Mice. *Animals (Basel)* **7** (2017). https://doi.org:10.3390/ani7120088
152 Arakawa, H. Ethological approach to social isolation effects in behavioral studies of laboratory rodents. *Behavioural brain research* **341**, 98-108 (2018). https://doi.org:10.1016/j.bbr.2017.12.022
153 Ivy, A. S. *et al.* Hippocampal dysfunction and cognitive impairments provoked by chronic early-life stress involve excessive activation of CRH receptors. *The Journal of neuroscience : the official journal of the Society for Neuroscience* **30**, 13005-13015 (2010). https://doi.org:10.1523/jneurosci.1784-10.2010
154 Valientes, D. A., Raus, A. M. & Ivy, A. S. An Improved Method for Individual Tracking of Voluntary Wheel Running in Pair-housed Juvenile Mice. *Bio-protocol* **11**, e4071 (2021). https://doi.org:10.21769/BioProtoc.4071
155 Oliff, H. S., Berchtold, N. C., Isackson, P. & Cotman, C. W. Exercise-induced regulation of brain-derived neurotrophic factor (BDNF) transcripts in the rat hippocampus. *Brain Res Mol Brain Res* **61**, 147-153 (1998). https://doi.org:10.1016/s0169-328x(98)00222-8
156 Reimer, J. D. & Petras, M. L. Breeding structure of the house mouse, Mus musculus, in a population cage. *J Mammal* **48**, 88-99 (1967).
157 Hawkley, L. C., Cole, S. W., Capitanio, J. P., Norman, G. J. & Cacioppo, J. T. Effects of social isolation on glucocorticoid regulation in social mammals. *Hormones and Behavior* **62**, 314-323 (2012). https://doi.org:https://doi.org/10.1016/j.yhbeh.2012.05.011
158 Koike, H. *et al.* Behavioral abnormality and pharmacologic response in social isolation-reared mice. *Behavioural brain research* **202**, 114-121 (2009). https://doi.org:10.1016/j.bbr.2009.03.028
159 Okada, R. *et al.* Involvement of dopaminergic and cholinergic systems in social isolation-induced deficits in social affiliation and conditional fear memory in mice. *Neuroscience* **299**, 134-145 (2015). https://doi.org:10.1016/j.neuroscience.2015.04.064

160 Ieraci, A., Mallei, A. & Popoli, M. Social Isolation Stress Induces Anxious-Depressive-Like Behavior and Alterations of Neuroplasticity-Related Genes in Adult Male Mice. *Neural Plast* **2016**, 6212983 (2016). https://doi.org:10.1155/2016/6212983
161 Terranova, M. L., Laviola, G., de Acetis, L. & Alleva, E. A description of the ontogeny of mouse agonistic behavior. *J Comp Psychol* **112**, 3-12 (1998). https://doi.org:10.1037/0735-7036.112.1.3
162 Hayes, L. D. To nest communally or not to nest communally: a review of rodent communal nesting and nursing. *Anim Behav* **59**, 677-688 (2000). https://doi.org:10.1006/anbe.1999.1390
163 Makinodan, M., Rosen, K. M., Ito, S. & Corfas, G. A critical period for social experience-dependent oligodendrocyte maturation and myelination. *Science* **337**, 1357-1360 (2012). https://doi.org:10.1126/science.1220845
164 Himmler, B. T., Pellis, S. M. & Kolb, B. Juvenile play experience primes neurons in the medial prefrontal cortex to be more responsive to later experiences. *Neuroscience letters* **556**, 42-45 (2013). https://doi.org:10.1016/j.neulet.2013.09.061
165 Batchelder, P., Kinney, R. O., Demlow, L. & Lynch, C. B. Effects of temperature and social interactions on huddling behavior in Mus musculus. *Physiol Behav* **31**, 97-102 (1983). https://doi.org:10.1016/0031-9384(83)90102-6
166 Krynitsky, J. *et al.* Rodent Arena Tracker (RAT): A Machine Vision Rodent Tracking Camera and Closed Loop Control System. *eNeuro* **7** (2020). https://doi.org:10.1523/ENEURO.0485-19.2020
167 Poffe, C., Dalle, S., Kainz, H., Berardi, E. & Hespel, P. A noninterfering system to measure in-cage spontaneous physical activity in mice. *J Appl Physiol (1985)* **125**, 263-270 (2018). https://doi.org:10.1152/japplphysiol.00058.2018
168 Wang, Z., Mirbozorgi, S. A. & Ghovanloo, M. An automated behavior analysis system for freely moving rodents using depth image. *Med Biol Eng Comput* **56**, 1807-1821 (2018). https://doi.org:10.1007/s11517-018-1816-1
169 Peleh, T., Bai, X., Kas, M. J. H. & Hengerer, B. RFID-supported video tracking for automated analysis of social behaviour in groups of mice. *J Neurosci Methods* **325**, 108323 (2019). https://doi.org:10.1016/j.jneumeth.2019.108323
170 Frahm, S. *et al.* Alpha-Synuclein transgenic mice, h-α-SynL62, display α-Syn aggregation and a dopaminergic phenotype reminiscent of Parkinson's disease. *Behavioural brain research* **339**, 153-168 (2018). https://doi.org:https://doi.org/10.1016/j.bbr.2017.11.025
171 Matikainen-Ankney, B. A. *et al.* Rodent Activity Detector (RAD), an Open Source Device for Measuring Activity in Rodent Home Cages. *eNeuro* **6** (2019). https://doi.org:10.1523/ENEURO.0160-19.2019
172 Voikar, V. & Gaburro, S. Three Pillars of Automated Home-Cage Phenotyping of Mice: Novel Findings, Refinement, and Reproducibility Based on Literature and Experience. *Front Behav Neurosci* **14**, 575434 (2020). https://doi.org:10.3389/fnbeh.2020.575434
173 Serra, F. T. *et al.* Early exercise induces long-lasting morphological changes in cortical and hippocampal neurons throughout of a sedentary period of rats. *Scientific Reports* **9**, 13684 (2019). https://doi.org:10.1038/s41598-019-50218-9
174 Gomes, F. G., Gomes Da Silva, S., Cavalheiro, E. A. & Arida, R. M. Beneficial influence of physical exercise following status epilepticus in the immature brain of rats. *Neuroscience* **274**, 69-81 (2014). https://doi.org:10.1016/j.neuroscience.2014.05.024